Volume 9, No. 4
September, 1961

THE SOVIET JOURNAL OF

ATOMIC ENERGY

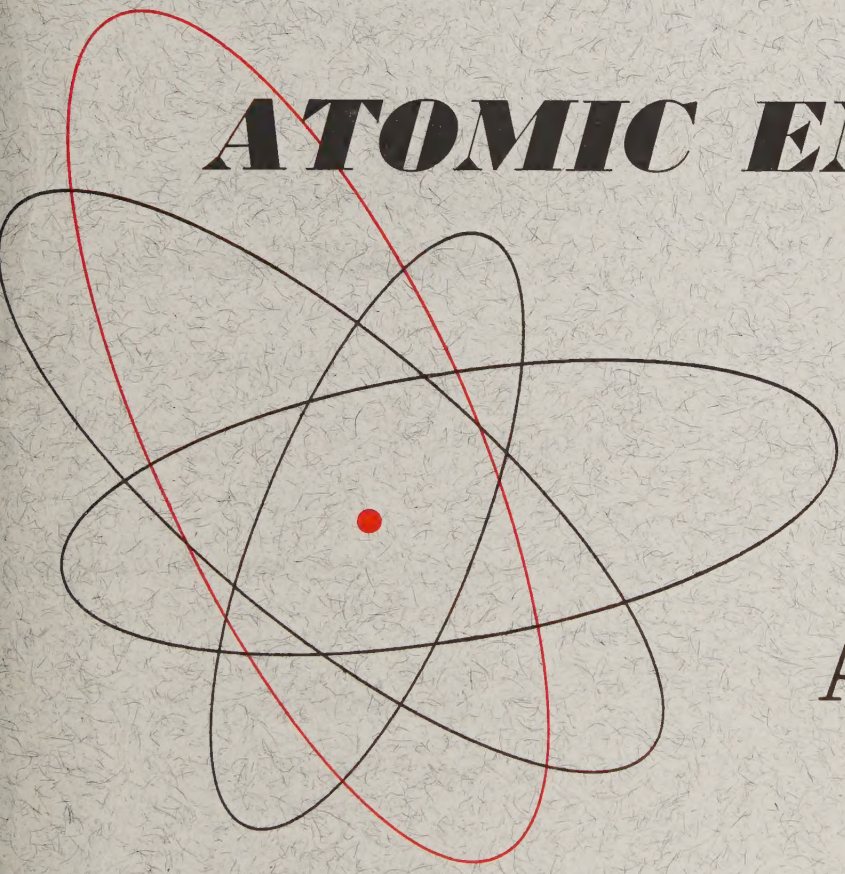

Атомная энергия

TRANSLATED FROM RUSSIAN

CONSULTANTS BUREAU

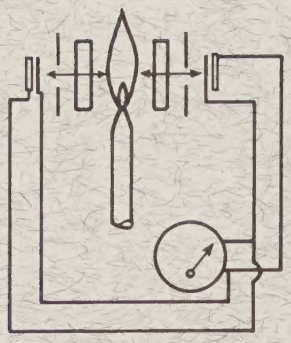

TECHNIQUES IN FLAME PHOTOMETRIC ANALYSIS

by N. S. Poluéktov

TRANSLATED FROM RUSSIAN

Original published by the
State Scientific-Technical Press
for Chemical Literature, Moscow

This volume contains a practical and comprehensive survey of the techniques employed and the instruments required for this important rapid analysis method, as well as a brief account of the theoretical principles involved. Experimental procedures and the design of apparatus are discussed at length, making the relevant chapters a valuable manual for all chemists concerned with analytical problems.

The second half of the book deals with the determination of individual elements in a variety of materials, providing much factual information, together with a complete and international bibliography. There are many useful tables, and two appendices which consider wavelengths of brightest spectral lines and peaks of molecular bands of elements excited in flame, and recommended wavelengths of spectral lines and peaks of molecular bands for determination of elements with the aid of a spectrophotometer employing glass optics and using an air-acetylene flame.

Scientists working in the varied fields in which flame photometry is today applicable – in geochemistry and mineralogy for the analysis of waters and minerals, in agrochemistry for the determination of metabolic bases in soils and the analysis of fertilizers and plant materials, in biochemistry and medicine for the investigation of urine, blood serum, and tissues, in industry for production control by analysis of metal alloys, glasses, cements, refractories, reagents, etc. – will find

TECHNIQUES IN FLAME PHOTOMETRIC ANALYSIS
an invaluable handbook.

230 pages **$9.50**

CONSULTANTS BUREAU
ENTERPRISES, INC.
227 W. 17 ST., NEW YORK 11, N. Y.

THE SOVIET JOURNAL OF

ATOMIC ENERGY

A translation of ATOMNAYA ÉNERGIYA,
a publication of the Academy of Sciences of the USSR

(Russian original dated October, 1960)

Vol. 9, No. 4 September, 1961

CONTENTS

Annual subscription $ 75.00
Single issue 20.00
Single article 12.50

CONTENTS (continued)

NOTE

The Table of Contents lists all material that appears in Atomnaya Énergiya. Those items that originated in the English language are not included in the translation and are shown enclosed in brackets. Whenever possible, the English-language source containing the omitted reports will be given.

Consultants Bureau Enterprises, Inc.

NEUTRON-FLUX DISTRIBUTION IN A HOMOGENEOUS BOILING-WATER REACTOR

B. Z. Torlin

Translated from Atomnaya Énergiya, Vol. 9, No. 4, pp. 257-261, October, 1960
Original article submitted January 25, 1960

A method of calculating a homogeneous boiling-water reactor in which the density of the medium varies with the height is calculated in the diffusion and age approximation. For a cylindrical reactor, the solution can be reduced to elliptical integrals. It is shown that, for a reactor whose radius is much greater than its height, the solution is expressed in terms of elementary functions.

In the calculation of reactors in which the heat is removed by the boiling of the moderator we have to deal with the moderator nuclei and the diffusion of neutrons in a medium of variable density. If the vapor bubbles of the moderator are small in comparison with the mean free path of a neutron in the medium, we can regard such a medium as being continuous. If, in addition, the medium is homogeneous, i.e., the atoms of the fissionable material are uniformly distributed among the atoms of the moderator, then at each point $\mathbf{r}$ of density $\gamma(\mathbf{r})$, the neutron scattering length $l_s(\mathbf{r})$, the capture length $l_a(\mathbf{r})$, and the total mean free path $l(\mathbf{r})$ are related to the corresponding quantities l_{s0}, l_{a0}, and l_0 in a medium of density γ_0 by

$$\frac{l_s(r)}{l_{s0}} = \frac{l_a(r)}{l_{a0}} = \frac{l(r)}{l_0} = \frac{\gamma_0}{\gamma(r)} = \beta(r), \tag{1}$$

where $\beta(\mathbf{r})$ is a continuous function. Hereafter, it shall always be assumed that

$$|\operatorname{grad} l(r)| \ll 1.$$

Under these assumptions, it is not difficult to obtain (following the method adopted in [1, 2]) in the diffusion approximation the equations of moderation and diffusion of neutrons in such a medium,*

$$\left.\begin{aligned} \nabla(\beta\nabla N) - \frac{N}{L_0^2\beta} &= -\frac{n(\tau_{0\tau})}{L_0^2\beta}, \\ \nabla(\beta\nabla n) &= \frac{\partial}{\partial\tau_0}\left(\frac{n}{\beta}\right) \end{aligned}\right\} \tag{2}$$

and the initial conditions $n(\mathbf{r}, 0) = kN(\mathbf{r})$. Here N is the thermal neutron density; $\underline{n}$ is the density of the neutron moderator; L_0 is the diffusion length of thermal neutrons in a medium of density γ_0; τ_0 is the age

* It can be assumed here that the moderator is stationary, since during the lifetime of a neutron (approximately 10^{-3} sec) in the active zone there is no appreciable displacement of the medium.

of a moderated neutron in a medium of density γ_0; τ_{0T} is the age of the thermal neutrons in a medium of density γ_0; $\underline{k}$ is the multiplication factor.

We shall consider the case in which the extrapolated boundaries on which N and $\underline{n}$ vanish coincide.

Under the assumptions made above, the solution of the moderation equation can be represented in the form

$$n = kNe^{-\alpha^2\tau_0}.$$

The system of equations (2) then reduces to

$$\beta\nabla(\beta\nabla N) + \alpha^2 N = 0, \tag{3}$$

where α^2 is determined from the condition

$$1 + L_0^2\alpha^2 = ke^{-\alpha^2\tau_{0T}}. \tag{4}$$

If β does not depend on the radius and the angle [$\beta(\mathbf{r}) = \beta(z)$], then for a cylindrical reactor the solution of Eq. (3) can be found in the form

$$N(r) = N_r(r)\,N_z(z).$$

In place of Eq. (3), we then obtain

$$\beta\frac{d}{dz}\left(\beta\frac{dN_z}{dz}\right) + (\alpha^2 - \alpha_r^2\beta^2)N_z = 0 \tag{5}$$

and

$$N_r = J_0(\alpha_r r),$$

where J_0 is the zero-order Bessel function of the first kind; $\alpha_r = 2.4/R_{eff}$ (R_{eff} is the extrapolated radius of the active zone).

For the further investigation of Eq. (5) it is necessary to determine the form of the function or, at least, the relation between β and N_Z. This relation is not difficult to establish if we make the following assumptions:

1) The moderator density is constant over the reactor radius and varies only with the height of the layer;*

2) all the heat released below any cross section is expended on the production of steam, which, in rising to the top, passes through this cross section;

* This assumption is obviously valid for a homogeneous boiling-water reactor, where the intense, turbulent agitation of the medium inevitably tends to equalize the vapor content over the radius. The effect of a small change in the vapor content in the radial direction is probably slight. In fact, if it is assumed that in the upper half of the active zone of the reactor, where the vapor content is the highest, the medium density close to the axis is one-half that at the walls of the vessel, then, according to perturbation theory, one can estimate the change in the Laplacian of the system. For the example cited (see figure) these estimates are $\frac{\Delta\alpha^2}{\alpha^2} \simeq 2\text{-}3\%$. Of course, in a strongly turbulent flow such a large difference in densities cannot actually occur. From the estimates it follows that the difference in densities of the medium at the center and at the periphery does not exceed 10%.

3) the quantity of steam passing through the cross section, as in the case of bubbling, is proportional to F/(1 - F) (F is the fraction of the cross section occupied by steam in the layer) [3];

4) the steam density γ'' is small in comparison with the water density γ', and hence

$$F \simeq \frac{\gamma' - \gamma}{\gamma'}. \tag{6}$$

Under the assumptions above,

$$\int_0^z N_z \frac{dz}{\beta} = a \frac{F}{1-F} \simeq a \left(\frac{\beta}{\beta_0} - 1 \right), \tag{7}$$

where $\beta_0 = \frac{\gamma_0}{\gamma'}$; a is a constant. Introducing the change of variables*

$$\frac{dz}{\beta} = dy \tag{8}$$

and, after differentiating expression (7), we obtain

$$N_z = a \frac{d\beta}{dy}. \tag{9}$$

For a boiling water reactor in which $\alpha_r^2 \beta^2 \ll \alpha^2$ over the entire interval of variation of β, Eq. (5) will have the form

$$\beta \frac{d}{dz} \left(\beta \frac{dN}{dz} \right) + \alpha_0^2 N = 0. \tag{10}$$

Inserting relation (8) into Eq. (10), we obtain

$$\frac{d^2N}{dy^2} + \alpha_0^2 N = 0. \tag{11}$$

The solution of Eq. (11) can be represented in the form

$$N = A \sin \alpha_0 y. \tag{12}$$

Using the condition at the upper boundary of the reactor, we find

$$y_H = \frac{\pi}{H_0}. \tag{13}$$

Integrating expression (9) under the condition $\beta(0) = \beta_0$, we obtain

$$\beta - \beta_0 = C(1 - \cos \alpha_0 y). \tag{14}$$

* The advantage of this change of variables in our problem was kindly pointed out to the author by Ya. V. Shevelev.

For $y = y_H$,

$$C = \frac{\beta_H - \beta_0}{2}.$$

After integration of expression (8),

$$z = \frac{\beta_H + \beta_0}{2} y - \frac{\beta_H - \beta_0}{2\alpha_0} \sin \alpha_0 y. \tag{15}$$

Inserting into expression (15) the value of y_H from formula (13), we obtain the expression for the height H of the active zone:

$$H = \frac{\beta_H + \beta_0}{2} \frac{\pi}{\alpha_0}. \tag{16}$$

From expression (12) it follows that the maximum neutron density occurs for $y_{max} = y_H/2$, or for

$$Z_{max} = \frac{\beta_H + \beta_0}{2} \frac{\pi}{2\alpha_0} - \frac{\beta_H - \beta_0}{2\alpha_0} = \frac{H}{2}\left(1 - \frac{2}{\pi} \frac{\beta_H - \beta_0}{\beta_H + \beta_0}\right), \tag{17}$$

i.e., the maximum of the neutron density is displaced downward with respect to the median plane of the reactor; the greater the difference between the moderator densities in the lower and upper cross sections of the reactor and the greater the over-all height of the reactor, the greater is the displacement.

The mean density of the moderator is determined by the expression

$$\bar{\gamma} = \frac{1}{H} \int_0^H \gamma \, dz = \frac{\gamma_0}{H} y_H. \tag{18}$$

Substituting into expression (18) the value of y_H/H from expression (16), we find

$$\bar{\gamma} = \frac{2\gamma_0}{\beta_H + \beta_0}. \tag{19}$$

Inserting expression (1), and then (6), into (19), we obtain

$$\bar{\nu} = \gamma' \frac{1 - F_H}{1 - F_H/2}, \tag{20}$$

where $F_H = F(H)$.

Since the amount of steam flowing through any cross section of the reactor is proportional to $F/(1 - F)$, the reactor power W is proportional to $F_H/(1 - F_H)$. If we express F_H in terms of $\bar{\gamma}$ and γ_0 by means of expression (20), we obtain

$$W = 2a \frac{\gamma' - \bar{\gamma}}{\bar{\gamma}}. \tag{21}$$

The mean steam content $\bar{F}$ is expressed in terms of the mean density of the moderator $\bar{\gamma}$ by means of the relation

$$\bar{\gamma} = \gamma' (1 - \bar{F}). \tag{22}$$

Inserting (22) into (21), we obtain

$$W = 2a \frac{\bar{F}}{1 - \bar{F}}. \tag{23}$$

Inserting into Eq. (16) the expression $\frac{\beta_H + \beta_0}{2}$, we obtain from Eq. (19)

$$H = \frac{\pi}{\alpha}, \tag{24}$$

where

$$\alpha = \alpha_0 \left(\frac{\bar{\gamma}}{\gamma_0} \right). \tag{25}$$

Expressions (23) - (25) relate the size and power of the reactor to its mean steam content. Here, the height of the boiling-water reactor proves to be exactly the same as the height of a reactor with a constant density equal to the mean density of the moderator in the given solution. For a reactor of finite radius, as we shall show, similar results are obtained. Moreover, it follows from relation (23) that the power of the boiling-water reactor is double that of a reactor whose steam content is constant over its height for the same mean steam content. A check of this circumstance for a cylindrical reactor of finite radius shows that the ratio $2 \frac{\bar{F}/(1-\bar{F})}{F_H/(1-F_H)}$ is somewhat above unity and increases with the mean steam content (Table 1). From this table it also follows that even for $\bar{F} \simeq 0.35$ the error resulting from formula (23) in the determination of the power W of the reactor does not exceed 15%.

TABLE 1

Comparative Characteristics of Boiling-Water Reactors with Constant and Variable Steam Content over the Height for the Same Mean Density of the Medium

$\alpha^2 \cdot 10^4$, cm^{-2}	γ_H, g/cm^3	$\bar{\gamma}$, g/cm^3	H, cm	H_0, cm	$2 \frac{\bar{F}/(1-\bar{F})}{F_H/(1-F_H)}$
19,1	0,846	0,933	131	131	1,04
19,1	0,733	0,850	168	170	1,09
25,8	0,846	0,935	96,8	96,6	1,02
25,8	0,733	0,857	114	112	1,05
25,8	0,550	0,688	208	212	1,14
29,4	0,846	0,935	86,7	86,5	1,02
29,4	0,550	0,703	158	158	1,10
31,4	0,846	0,935	82,3	82,0	1,02
31,4	0,550	0,703	143	140	1,10
31,4	0,525	0,674	160	165	1,14

Note: In the calculations we took $\alpha_a^2 = 8 \cdot 10^{-4}$ cm^{-2}, $\gamma_0 = 1.10$ g/cm^3, and $\gamma' = 1.05$ g/cm^3.

We shall now consider the case of a cylindrical boiling-water reactor of finite radius, which, although more complicated, is of greater practical importance. Inserting expression (8) into (5), we obtain in the new variables

$$\frac{d^3\beta}{dy^3} + (\alpha^2 - \alpha_r^2 \beta^2) \frac{d\beta}{dy} = 0 \tag{26}$$

with the initial conditions $\beta(0) = \beta_0$ and $\frac{d\beta}{dy} = 0$ at the upper and lower extrapolated boundaries of the reactor. After a single integration of Eq. (26), we find

$$p \frac{dp}{d\beta} = \frac{1}{2} C_1 - \alpha^2 \beta + \frac{1}{3} \alpha_r^2 \beta^3, \tag{27}$$

where

$$p = \frac{d\beta}{dy}.$$

Integrating Eq. (27), we obtain

$$p = \sqrt{C_1\beta + C_2 - \alpha^2\beta^2 + \frac{\alpha_r^2}{6}\beta^4}; \tag{28}$$

$$z = \int_{\beta_0}^{\beta} \frac{\beta\, d\beta}{p}. \tag{29}$$

The determination of the constants of integration C_1 and C_2 can be fundamentally simplified if we assume that the boundaries of the boiling-water zone coincide with the extrapolated boundaries of the active zone. This assumption cannot introduce a serious error in the calculations, since the effective additions are small in comparison with the height of the active zone and their contribution to the heat balance of the reactor is negligible.

With this assumption we find that

$$p = \sqrt{(\beta_1 - \beta)(\beta_H - \beta)(\beta - \beta_0)(\beta - \beta_r)}, \tag{30}$$

where $\beta_H = \beta(H)$; H is the effective height of the active zone;

$$\beta_1 = \sqrt{6\frac{\alpha^2}{\alpha_r^2} - \frac{3}{4}(\beta_0^2 + \beta_H^2) - \frac{1}{2}\beta_0\beta_H} - \frac{\beta_0 + \beta_H}{2}; \quad \beta_2 = -\sqrt{6\frac{\alpha^2}{\alpha_r^2} - \frac{3}{4}(\beta_0^2 + \beta_H^2) - \frac{1}{2}\beta_0\beta_H} - \frac{\beta_0 + \beta_H}{2}.$$

In order not to obtain a negative number under the radical sign of expression (30) for a change of β from β_0 to β_H, it is necessary that $\beta_1 \geq \beta_H$. This determines the limiting value of β_H:

$$\beta_{H\,\lim} = \beta_0\left(\sqrt{\frac{2\alpha^2}{\beta_0^2\alpha_r^2} - \frac{2}{9}} - \frac{1}{3}\right). \tag{31}$$

According to expression (9),

$$N_z = ap. \tag{32}$$

The dependence of y on β is expressed by the formula

$$y = \frac{2\sqrt{6}\,u}{\sqrt{(\beta_1 - \beta_0)(\beta_H - \beta_r)}\,\alpha_r}, \tag{33}$$

where $u = F(\varphi, k)$ is the elliptical integral of the first kind [4]. Here

$$\sin\varphi = \sqrt{\frac{(\beta_H - \beta_2)}{(\beta_H - \beta_0)}\frac{(\beta - \beta_0)}{(\beta - \beta_2)}}; \quad k = \sqrt{\frac{(\beta_H - \beta_0)}{(\beta_1 - \beta_0)}\frac{(\beta_1 - \beta_2)}{(\beta_H - \beta_2)}}.$$

For $\beta = \beta_H$

$$y_H = \frac{2\sqrt{6}\,K}{\sqrt{(\beta_1 - \beta_0)(\beta_H - \beta_r)}\,\alpha_r}, \tag{34}$$

where K is the complete elliptical integral of the first kind. The expression for z has the form

$$z = y\left\{\frac{(\beta_0-\beta_2)}{\sqrt{1-k^2}}\frac{\Theta(a)H(a)}{\Theta_1(a)H_1(a)}\left[\frac{\Theta'(a)}{\Theta(a)}-\frac{\sqrt{1-k^2}}{2u}\ln\frac{\Theta(u-a)}{\Theta(u+a)}\right]+\beta_0\right\}, \tag{35}$$

where

$$\sin a = \sqrt{\frac{\beta_1-\beta_0}{\beta_1-\beta_2}},$$

Θ, H, Θ_1, and H_1 are Jacobian theta functions [4]. In this case

$$H = y_H\left[\frac{\beta_0-\beta_2}{\sqrt{1-k^2}}\frac{\Theta'(a)H(a)}{\Theta_1(a)H_1(a)}+\beta_0\right]. \tag{36}$$

If $\beta_H \to \beta_{H\,\lim}$, then y tends to infinity. Hence $\beta_{H\,\lim}$ is the maximum value of β_H at which the reactor remains critical only for an infinite height of the active zone.

TABLE 2

Neutron-Flux Distribution Over the Height of a Boiling-Water Reactor

z, cm	γ, g/cm^3	p, cm^{-1}	N_Z/N_{max}
0	1,05	0,0000	0
25	0,94	0,0007	0,75
34	0,88	0,0116	0,89
43	0,83	0,0126	0,97
51	0,78	0,0129	0,99
60	0,74	0,0127	0,98
70	0,70	0,0121	0,93
81	0,67	0,0112	0,86
93	0,64	0,0099	0,76
109	0,61	0,0082	0,63
129	0,58	0,0061	0,47
162	0,56	0,0033	0,25
208	0,55	0,0000	0

Note: The calculations were performed for values of the parameters given in the caption to the figure.

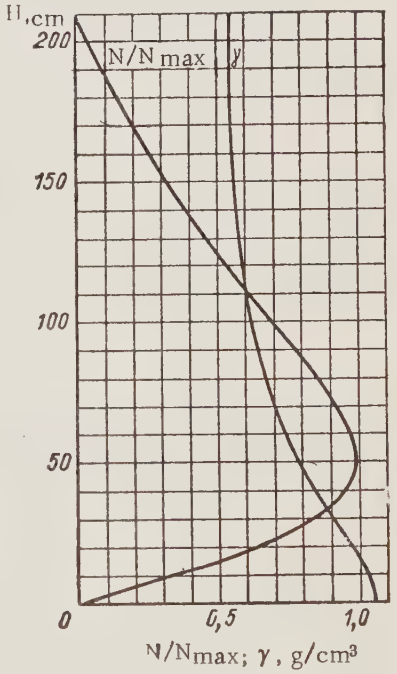

The distribution of the thermal neutron density N and the moderator density γ over the height H for the case $\alpha^2 = 25.8\cdot10^{-4}$ cm^{-2}, $\alpha_r^2 = 8\cdot10^{-4}$ cm^{-2}, $\gamma_0 = 1.10$ g/cm^3, $\gamma' = 1.05$ g/cm^3, $\gamma_H = 0.550$ g/cm^3, $\bar{\gamma} = 0.688$ g/cm^3.

The minimum value of β_H is β_0. The minimum height of the reactor's active zone which corresponds to this value of β_H is

$$H_{\lim} = \lim_{\beta_H\to\beta_0}\int_{\beta_0}^{\beta_H}\frac{\beta\,d\beta}{p}.$$

Using the mean-value theorem, we obtain

$$H_{\lim} = \lim_{\beta_H\to\beta_0}\left[\frac{\sqrt{6}\,\beta^*}{\alpha_r\sqrt{(\beta_1-\beta^*)(\beta^*-\beta_2)}}\int_{\beta_0}^{\beta_H}\frac{d\beta}{\sqrt{(\beta_H-\beta)(\beta-\beta_0)}}\right] = \frac{\pi}{\sqrt{\frac{\alpha^2}{\beta_0^2}-\alpha_r^2}}.$$

Here β^* is some value of β lying inside the segment $[\beta_0; \beta_H]$.

The mean value of the moderator density is determined from the expression

$$\gamma = \frac{1}{H}\int_0^H \gamma\, dz = \frac{\gamma_0}{H} y_H.$$

As $\beta_H \to \beta_0$, we have, according to expression (18), $\bar{\gamma} \to \gamma'$. The minimum mean density of the moderator in the reactor will, of course, occur for $\beta_H \to \beta_{H\,\lim}$. Since $\bar{\gamma}$ can be defined as

$$\bar{\gamma} = \gamma_0 \lim_{z \to H} \frac{y}{z},$$

then, by inserting into the expressions for $\underline{y}$ and $\underline{z}$ the values $\beta_H = \beta_{H\,\lim}$, we obtain, upon integration,

$$\frac{z}{y} = \beta_{H\,\lim} - \frac{\operatorname{Arccosh} \frac{\beta + \beta_{H\,\lim}}{\beta_0 + \beta_{H\,\lim}}}{y},$$

from which it follows that

$$\lim_{z \to H} \frac{y}{z} = \frac{1}{\beta_{H\,\lim}}$$

or

$$\bar{\gamma}_{\lim} = \frac{\gamma_0}{\beta_{H\,\lim}}.$$

Hence, for a given β_0 (moderator density or temperature), β_H (reactor power), α_r (effective radius of the active zone), and α^2, determined by expression (4), one can calculate by means of expressions (18), (31), (35), and (36) the height of the reactor's active zone, the mean density inside it, the critical charge, and also the density distribution of the neutron flux and medium over the height.

The characteristic distribution of the thermal-neutron density over the height and the density of the medium are shown in the figure and in Table 2. Table 1 gives the results of the calculations of the height H from formula (36) and the height H_0 from the formula for the height of a reactor with a medium of constant density in the active zone equal to the density γ of the boiling-water reactor. Comparison of H and H_0 indicates good agreement of both quantities in the case in which the reactor height does not exceed its diameter and the average steam content F does not exceed 35%.

The author expresses his sincere gratitude to Ya. V. Shevelev and B. L. Ioffe for valuable advice and A. D. Galanin for discussion of the results of the work and valuable comments.

LITERATURE CITED

1. A. Akheizer and I. Pomeranchuk, Some Problems on the Theory of the Nucleus [in Russian] (State Technical and Theoretical Press, 1950, 2nd edition).
2. S. Glasstone and M. Edlund, The Elements of Nuclear Reactor Theory [Russian translation] (Moscow, IL, (1954).
3. A. I. Filimonov et al., Teploénergetika 10, 22 (1957).
4. I. M. Ryzhik and I. S. Gradshtein, Tables of Integrals, Sums, Series, and Products [in Russian] (Moscow-Leningrad, State Technical and Theoretical Press, 1951), 2nd edition.

EFFECTIVENESS OF A SYSTEM OF ROD ABSORBERS IN A REACTOR FITTED WITH A REFLECTOR

V. I. Nosov

Translated from Atomnaya Énergiya, Vol. 9, No. 4, pp. 262-269, October, 1960
Original article submitted November 19, 1959

The conditions of criticality and the distributions of the neutron flux for a homogeneous thermal-neutron reactor with a system of absorbing rods are obtained in the two-group approximation. The rods extend through the entire depth of the reactor and are situated around the circumference of the active zone or radial reflector at a uniform distance from one another. The results of the calculation are presented.

Introduction

In a number of articles in the literature [1-3], the effectiveness of a system of rods located in the active zone of thermal reactors is calculated in a simplified way for the case of reactors without reflectors. However, in some cases such an approximation is not sufficient, and it is required to calculate the effectiveness of the system of rods in the active zone of a reactor with a reflector, where the control rods can be located in the reflector itself. This article is devoted to the consideration of the effectiveness of a system of rods in the two-group approximation.

Formulation of the Problem

We shall write the two-group equations for the moderator density $q(\mathbf{r})$ and the thermal-neutron density $n(\mathbf{r})$ [4]:

$$\left.\begin{aligned} \tau\Delta q(\boldsymbol{r}) - q(\boldsymbol{r}) + \frac{k_\infty n(r)}{k_{\text{eff}}\, pl} = 0; \\ L^2\Delta n(\boldsymbol{r}) - n(\boldsymbol{r}) + plq(\boldsymbol{r}) = 0, \end{aligned}\right\} \tag{1}$$

where τ is the neutron age; L^2 is the square of the thermal-neutron diffusion length; l is the lifetime of thermal neutrons in an infinite medium; p is the probability of avoiding resonance capture; k_∞ is the neutron multiplication factor in an infinite medium; k_{eff} is the effective multiplication factor; $q(\mathbf{r})$ and $n(\mathbf{r})$ are functions of the coordinates r, φ, and z.

The solution for q and n in a cylindrical reactor without end reflectors has the form

$$q = S_1\psi_1 + S_2\psi_2; \quad n = \psi_1 + \psi_2. \tag{2}$$

Here S_1 and S_2 are the coupling coefficients;

$$\psi_1 = \sum_{n=0}^{\infty} \left[A_{1n}J_n\left(\sqrt{\varkappa_1^2 - (\pi/H_{\text{ex}})^2}\, r\right) + B_{1n}Y_n\left(\sqrt{\varkappa_1^2 - (\pi/H_{\text{ex}})^2}\, r\right)\right][\cos n\varphi + E_{1n}\sin n\varphi]; \tag{2a}$$

$$\psi_2 = \sum_{n=0}^{\infty} \left[A_{2n} I_n\left(\sqrt{\varkappa_2^2 + (\pi/H_{ex})^2}\, r\right) + B_{2n} K_n\left(\sqrt{\varkappa_2^2 + (\pi/H_{ex})^2}\, r\right)\right] [\cos n\varphi + E_{2n} \sin n\varphi], \qquad (2b)$$

where A_n, B_n, and E_n are constants determined from the boundary conditions; J_n, Y_n, I_n, and K_n are Bessel functions [5]; $\varkappa_1^2$, $\varkappa_2^2$ are the roots of the two-group equation of criticality

$$\frac{k_\infty}{k_{eff}} = (1 + \alpha^2\tau)(1 + \alpha^2 L^2); \qquad (2c)$$

H_{ex} is the reactor height and includes the extrapolation distance and effective additions from the end reflectors. In obtaining relations (2a) and (2b), we assumed that it is possible to separate the variables and that the first root of Eq (2c) is positive, since in the reactors of interest to us one usually has $\frac{k_\infty}{k_{eff}} > 1$.

The solution for the neutron flux with a system of rods in the reactor can be represented as the superposition of two partial solutions, one of which is always regular, while the other (irregular) has singularities at the absorbing rods:

$$q = S_1(\psi_1^{(R)} + \psi_1^{(ir)}) + S_2(\psi_2^{(R)} + \psi_2^{(ir)}); \; n = (\psi_1^{(R)} + \psi_1^{(ir)}) + (\psi_2^{(R)} + \psi_2^{(ir)}), \qquad (3)$$

where the superscript R refers to the regular solution and ir to the irregular solution.

The solutions (3) for q and n should satisfy the following boundary conditions:

1) q and n are bounded at each point of the reactor and vanish at the extrapolated radius of the reactor R_{ex}.

2) At the boundary between the active zone and the reflector the following relations hold:

$$n^{I} = n^{II}; \quad \frac{dn^{I}}{dr} = \gamma_0 \frac{dn^{II}}{dr}; \quad q^{I} = \gamma_1 q^{II}; \quad \frac{dq^{I}}{dr} = \gamma_2 \frac{dq^{II}}{dr}, \qquad (4)$$

where I and II refer to the active zone and reflector, respectively.

3) At the surface of the rod, the conditions for q and n have the form [6, 7]

$$\frac{dq/d\varrho}{q} = \frac{1}{d}\Big|_{\varrho=a}; \quad \frac{dn/d\varrho}{n} = \frac{1}{\gamma}\Big|_{\varrho=a}, \qquad (5)$$

where a is the geometrical radius of the rod.

We shall now proceed directly to the derivation of the equations of criticality.

System of Rods in the Reactor Reflector

In a reactor with a system of rods located at the circumference of the reflector at a uniform distance from one another (Fig. 1), the solution for the thermal neutron density and moderator density has the form*

* If the addition theorem is used, the terms with $I_m(\nu\rho_i)$ and $I_m(\mu\rho_i)$ can be combined with the terms containing $I_{nN}(\nu r)$ and $I_{nN}(\mu r)$, respectively.

$$
\left.
\begin{aligned}
n^{\mathrm{I}} &= \sum_{n=0}^{\infty} [A_{1n}\mathcal{J}_{nN}(\varkappa r) + A_{2n}I_{nN}(\beta r)]\cos nN\varphi;\\
q^{\mathrm{I}} &= \sum_{n=0}^{\infty} [S_1 A_{1n}\mathcal{J}_{nN}(\varkappa r) + S_2 A_{2n}I_{nN}(\beta r)]\cos nN\varphi;\\
n^{\mathrm{II}} &= \sum_{n=0}^{\infty} [C_{1n}I_{nN}(\mu r) + D_{1n}K_{nN}(\mu r)]\cos n\varphi + \sum_{m=0}^{\infty}{}' \sum_{i=1}^{N} B_{1m}K_m(\mu\varrho_i)\cos m\omega_i +\\
&+ \sum_{n=0}^{\infty} [C_{2n}I_{nN}(\nu r) + D_{2n}K_{nN}(\nu r)]\cos nN\varphi + \sum_{m=0}^{\infty}{}' \sum_{i=1}^{N} B_{2m}K_m(\nu\varrho_i)\cos m\omega_i;\\
q^{\mathrm{II}} &= S_3\Big\{\sum_{n=0}^{\infty} [C_{2n}I_{nN}(\nu r) + D_{2n}K_{nN}(\nu r)]\cos nN\varphi + \sum_{m=0}^{\infty}{}' \sum_{i=1}^{N} B_{2m}K_m(\nu\varrho_i)\cos m\omega_i\Big\}.
\end{aligned}
\right\} \quad (6)
$$

Here N is the number of rods; i is the ordering number of a rod;

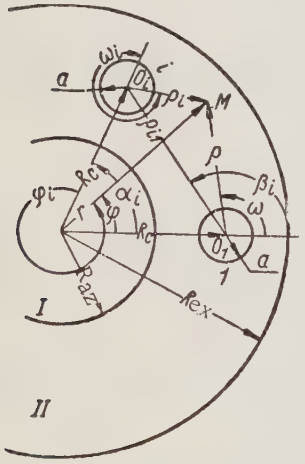

Fig. 1. Position of the rods in the reactor reflector.

$$
\varkappa = \sqrt{\varkappa_1^2 - \left(\frac{\pi}{H_{ex}}\right)^2};\quad \beta = \sqrt{\varkappa_2^2 + \left(\frac{\pi}{H_{ex}}\right)^2};
$$

$$
\mu = \sqrt{\frac{1}{(L^{\mathrm{II}})^2} + \left(\frac{\pi}{H_{ex}}\right)^2};
$$

$$
\nu = \sqrt{\frac{1}{\tau^{\mathrm{II}}} + \left(\frac{\pi}{H_{ex}}\right)^2}.
$$

In obtaining the solution (6), we took into account the fact that in the system chosen for designating the angles, thesolution should be symmetric with respect to φ and ω_i and periodic in φ:

$$
n(r, \varphi) = n(r, \varphi + \alpha_i);\quad q(r, \varphi) = q(r, \varphi + \alpha_i).
$$

From the boundary conditions for the moderator density (4) between the active zone and the reflector, it follows that

$$
A_{2n} = A_{1n}f_n - N\sum_{m=0}^{\infty} B_{2m}\Phi_{nm};\quad C_{2n} = A_{1n}\varphi_n + N\sum_{m=0}^{\infty} B_{2m}\chi_{nm}, \quad (7)
$$

where we have introduced the following notation: *

* Here and in what follows

$$
\mathcal{J}'_{nN}(\alpha R_{az}) = \alpha\frac{\mathcal{J}_{nN-1}(\alpha R_{az}) - \mathcal{J}_{nN+1}(\alpha R_{az})}{2};\quad I'_{nN}(\alpha R_{az}) = \alpha\frac{I_{nN-1}(\alpha R_{az}) + I_{nN+1}(\alpha R_{az})}{2};
$$

$$
K'_{nN}(\alpha R_{az}) = -\alpha\frac{K_{nN-1}(\alpha R_{az}) + K_{nN+1}(\alpha R_{az})}{2};\quad Y_{nN}(\alpha R_{az}) = \alpha\frac{Y_{nN-1}(\alpha R_{az}) - Y_{nN+1}(\alpha R_{az})}{2}.
$$

$$f_n = \frac{S_1\left[\mathcal{J}'_{nN}(\varkappa R_{az}) - \frac{\gamma_2}{\gamma_1}\frac{h_n}{\alpha_n}\mathcal{J}_{nN}(\varkappa R_{az})\right]}{S_2\left[\frac{\gamma_2}{\gamma_1}\frac{h_n}{\alpha_n}I_{nN}(\beta R_{az}) - I'_{nN}(\beta R_{az})\right]}; \quad \varphi_n = [S_1\mathcal{J}_{nN}(\varkappa R_{az}) + S_2 f_n I_{nN}(\beta R_{az})][\gamma_1 S_3 \alpha_n]^{-1};$$

$$\Phi_{nm} = \frac{\delta_n}{2}\frac{S_3\gamma_2\left\{r_{nm}\left[\frac{h_n}{\alpha_n}K_{nN}(\nu R_{az}) - K'_{nN}(\nu R_{az})\right] + (-1)^m v_{nm}[I'_{nN}(\nu R_{az}) - I_{nN}(\nu R_{az})]\right\}}{S_2\left[\frac{\gamma_2}{\gamma_1}\frac{h_n}{\alpha_n}I_{nN}(\beta R_{az}) - I'_{nm}(\beta R_{az})\right]}; \qquad (7a)$$

$$\chi_{nm} = \left\{S_3\gamma_1\frac{\delta_n}{2}[K_{nN}(\nu R_{az})\, r_{nm} - (-1)^m I_{nN}(\nu R_{az})\, v_{nm}] - S_2\Phi_{nm}I_{nN}(\beta R_{az})\right\}[\gamma_1 S_3\alpha_n]^{-1};$$

$$\alpha_n = I_{nN}(\nu R_{az}) - K_{nN}(\nu R_{az})\frac{I_{nN}(\nu R_{ex})}{K_{nN}(\nu R_{ex})}; \quad h_n = I'_{nN}(\nu R_{az}) - K'_{nN}(\nu R_{az})\frac{I_{nN}(\nu R_{ex})}{K_{nN}(\nu R_{ex})};$$

$$r_{nm} = I_{nN+m}(\nu R_c) + I_{nN-m}(\nu R_c); \qquad v_{nm} = K_{nN-m}(\nu R_c) + K_{nN+m}(\nu R_c);$$

$\delta_n = 1$ for $n = 0$; $\delta_n = 2$ for $n > 1$ (R_{az} is the radius of the active zone; R_c is the radius of the circumference along which the rods are situated).

In obtaining formulas (7) and (7a) we used the addition theorem for $K_m(\mu\rho_i)$ and $K_m(\nu\rho_i)$ and the relations for the constants D_{1n} and D_{2n} obtained from the boundary conditions for $\underline{q}$ and $\underline{n}$ at the reactor surface:

$$D_{1n} = -C_{1n}\frac{I_{nN}(\mu R_{ex})}{K_{nN}(\mu R_{ex})}N\sum_{m=0}^{\infty}B_{1m}\frac{\delta_n}{2}[I_{nN+m}(\mu R_c) + I_{nN-m}(\mu R_c)];$$

$$D_{2n} = -C_{2n}\frac{I_{nN}(\nu R_{ex})}{K_{nN}(\nu R_{ex})}N\sum_{m=0}^{\infty}B_{2m}\frac{\delta_n}{2}[I_{nN+m}(\nu R_c) + I_{nN-m}(\nu R_c)]. \qquad (8)$$

From the condition of continuity for the thermal-neutron density at the boundary between the active zone and the reflector, we obtain

$$A_{1n} = N\sum_{m=0}^{\infty}(B_{1m}R_{nm} + B_{2m}T_{nm}); \quad C_{1n} = N\sum_{m=0}^{\infty}(B_{1m}Q_{nm} + B_{2m}\Delta_{nm}), \qquad (9)$$

where

$$R_{nm} = \gamma_0\frac{\delta_n}{2}\frac{l_n[(-1)^m I_{nN}(\mu R_{az})\, a_{nm} - K_{nN}(\mu R_{az})\, b_{nm}] - [(-1)^m I'_{nN}(\mu R_{az})\, a_{nm} - K'_{nN}(\mu R_{az})\, b_{nm}]t_n}{\gamma_0 l_n z_n - u_n t_n};$$

$$Q_{nm} = \frac{\delta_n}{2}\frac{[(-1)^m I_{nN}(\mu R_{az})\, a_{nm} - K_{nN}(\mu R_{az})\, b_{nm}]u_n - [(-1)^m I'_{nN}(\mu R_{az})\, a_{nm} - K'_{nN}(\mu R_{az})\, b_{nm}]\gamma_0 z_n}{\gamma_0 l_n z_n - u_n t_n};$$

$$\Delta_{nm} = \frac{\left[\chi_{nm}\alpha_n + \Phi_{nm}I_{nN}(\beta R_{az}) - \frac{\delta_n}{2}r_{nm}K_{nN}(\nu R_{az}) + (-1)^m\frac{\delta_n}{2}I_{nN}(\nu R_{az})\, v_{nm}\right]u_n}{\gamma_0 l_n z_n - u_n t_n} -$$

$$- \frac{z_n\gamma_0\left[\chi_{nm}h_n + \Phi_{nm}I'_{nN}(\beta R_{az}) - \frac{\delta_n}{2}K'_{nN}(\nu R_{az})\, r_{nm} + (-1)^m\frac{\delta_n}{2}I'_{nN}(\nu R_{az})\, v_{nm}\right]}{\gamma_0 l_n z_n - u_n t_n};$$

$$T_{nm} = z_n^{-1}\left[\Delta_{nm}t_n + \chi_{nm}\alpha_n + \Phi_{nm}I_{nN}(\beta R_{az}) - \frac{\delta_n}{2}r_{nm}K_{nN}(\nu R_{az}) + (-1)^m\frac{\delta_n}{2}I_{nN}(\nu R_{az})\, v_{nm}\right];$$

$$a_{nm} = K_{nN-m}(\mu R_c) + K_{nN+m}(\mu R_c); \quad b_{nm} = I_{nN+m}(\mu R_c) + I_{nN-m}(\mu R_c);$$

$$l_n = I'_{nN}(\mu R_{az}) - K'_{nN}(\mu R_{az})\frac{I_{nN}(\mu R_{ex})}{K_{nN}(\mu R_{ex})}; \quad t_n = I_{nN}(\mu R_{az}) - K_{nN}(\mu R_{az})\frac{I_{nN}(\mu R_{ex})}{K_{nN}(\mu R_{ex})};$$

$$u_n = \mathcal{J}'_{nN}(\varkappa R_{az}) + f_n I'_{Nm}(\beta R_{az}) - \gamma_0\varphi_n h_n; \quad z_n = \mathcal{J}_{nN}(\varkappa R_{az}) + f_n I_{nN}(\beta R_{az}) - \varphi_n\alpha_n.$$

Finally, if we use the boundary conditions (5) for $\underline{q}$ and $\underline{n}$ at the surface of any rod (for example, the first) and the corresponding addition theorem for the Bessel functions for $\rho < R_c$ and $\rho < \rho_{i1}$, then, after some calculations, we arrive at the following equations:*

$$\left.\begin{aligned}
&\sum_{k=0}^{\infty}\sum_{m=0}^{\infty}\sum_{n=0}^{\infty}\{B_{1m}[N(g_{1k}H_{nmk}+g^{\gamma}_{2k}q_{nmk})+\delta_{mk}L_{1k}+g_{1k}\Lambda_{1mk}]+\\
&+B_{2m}[N(g_{1k}\omega_{nmk}+g^{\gamma}_{2k}\pi_{nmk})+\delta_{mk}L^{\gamma}_{2k}+g^{\gamma}_{2k}\Lambda_{2mk}]\}\cos k\omega=0;\\
&\sum_{k=0}^{\infty}\sum_{m=0}^{\infty}\sum_{n=0}^{\infty}\{B_{1m}Ng^{d}_{2k}q_{nmk}+B_{2m}[Ng^{d}_{2k}\pi_{nmk}+\delta_{mk}L^{d}_{2k}+g^{d}_{2k}\Lambda_{2mk}]\}\cos k\omega=0.
\end{aligned}\right\} \quad (10)$$

Here we have introduced the following notations: $\delta_{mk}=1$ for $m=k$, and $\delta_{mk}=0$ for $m\neq k$;

$$\left.\begin{aligned}
g_{1k}&=\frac{I_k(\mu a)}{\gamma}-I'_k(\mu a);\qquad g^{\gamma,\,d}_{2k}=\frac{I_k(\nu a)}{\gamma,\,d}-I'_k(\nu a);\\
L_{1k}&=\frac{K_k(\mu a)}{\gamma}-K'_k(\mu a);\qquad L^{\gamma,\,d}_{2k}=\frac{K_k(\nu a)}{\gamma,\,d}-K'_k(\nu a);\\
\Lambda_{1mk}&=\frac{\delta_k}{2}\sum_{i=2}^{N}[K_{m+k}(\mu\varrho_{i1})\cos(m-k)\beta_i+K_{m-k}(\mu\varrho_{i1})\cos(m+k)\beta_i];\\
\Lambda_{2mk}&=\frac{\delta_k}{2}\sum_{i=2}^{N}[K_{m+k}(\nu\varrho_{i1})\cos(m-k)\beta_i+K_{m-k}(\nu\varrho_{i1})\cos(m+k)\beta_i];\\
H_{nmk}&=\frac{\delta_k}{2}\left[Q_{nm}b_{nk}-(-1)^k a_{nk}\left(Q_{nm}\frac{I_{nN}(\mu R_{ex})}{K_{nN}(\mu R_{ex})}+\frac{\delta_n}{2}b_{nm}\right)\right];\\
q_{nmk}&=\frac{\delta_k}{2}R_{nm}\varphi_n\left[r_{nk}-(-1)^k v_{nk}\frac{I_{nN}(\nu R_{ex})}{K_{nN}(\nu R_{ex})}\right];\\
\omega_{nmk}&=\frac{\delta_k}{2}\Delta_{nm}\left[b_{nk}-\frac{I_{nN}(\mu R_{ex})}{K_{nN}(\mu R_{ex})}(-1)^k a_{nk}\right];\\
\pi_{nmk}&=\frac{\delta_k}{2}\left[(T_{nm}\varphi_n+\chi_{nm})\left(r_{nk}-\frac{I_{nN}(\nu R_{ex})}{K_{nN}(\nu R_{ex})}(-1)^k v_{nk}\right)-(-1)^k v_{nk}r_{nm}\right].
\end{aligned}\right\} \quad (10a)$$

From Eqs. (10) we can obtain the condition of criticality of the problem if we limit ourselves to the approximation of the $\underline{k}$th order; we then obtain a system of $2(k+1)$ of linear homogeneous algebraic equations which should be solved for the $2(k+1)$ unknowns (all terms with $m > k$ should be discarded). The condition that the determinant of this system of equations equal zero will also be a condition of criticality for the problem. The effectiveness of the system of absorbing rods is then characterized by the difference in k_{eff} with and without the system of rods.

System of Rods in the Active Zone of the Reactor

For a reactor with a system of rods placed in the active zone of the reactor with a reflector, the solution for the thermal-neutron density and moderator density will have the following form (the position of the rods and the notation is the same as before):

---

* In obtaining Eq. (10), it was assumed that $\underline{d}$ and γ are independent of the angle.

$$
\left.
\begin{aligned}
n^{\mathrm{I}} &= \sum_{n=0}^{\infty} [A_{1n}\mathcal{J}_{nN}(\varkappa r) + A_{2n}I_{nN}(\beta r)]\cos nN\varphi + \sum_{m=0}^{\infty}\sum_{i=1}^{N} [B_{1m}Y_m(\varkappa\varrho_i) + B_{2m}K_m(\beta\varrho_i)]\cos m\omega_i;\\
q^{\mathrm{I}} &= \sum_{n=0}^{\infty} [S_1A_{1n}\mathcal{J}_{nN}(\varkappa r) + S_2A_{2n}I_{nN}(\beta r)]\cos nN\varphi +\\
&+ \sum_{m=0}^{\infty}\sum_{i=1}^{N} [S_1B_{1m}Y_m(\varkappa\varrho_i) + S_2B_{2m}K_m(\beta\varrho_i)]\cos m\omega_i;\\
n^{\mathrm{II}} &= \sum_{n=0}^{\infty} [C_{1n}I_{nN}(\mu r) + D_{1n}K_{nN}(\mu r)]\cos nN\varphi + \sum_{n=0}^{\infty} [C_{2n}I_{nN}(\nu r) + D_{2n}K_{nN}(\nu r)]\cos nN\varphi;\\
q^{\mathrm{II}} &= S_3\Big\{\sum_{n=0}^{\infty} [C_{2n}I_{nN}(\nu r) + D_{2n}K_{nN}(\nu r)]\cos nN\varphi\Big\}.
\end{aligned}
\right\} \quad (11)
$$

From the boundary conditions (4) for $\underline{q}$ it follows that

$$
A_{2n} = A_{1n}f_n + N\sum_{m=0}^{\infty}(B_{1m}\psi_{nm} - B_{2m}\Phi_{nm}); \quad C_{2n} = A_{1n}\varphi_n + N\sum_{m=0}^{\infty}(B_{1m}F_{nm} - B_{2m}L_{nm}), \quad (12)
$$

where

$$
\left.
\begin{aligned}
\psi_{nm} &= \frac{S_1}{S_2}\frac{\delta_n}{2}\,\frac{r_{nm}\left[Y'_{nN}(\varkappa R_{\mathrm{az}}) - \frac{\gamma_2}{\gamma_1}\frac{h_n}{\alpha_n}Y_{nN}(\varkappa R_{\mathrm{az}})\right]}{\frac{\gamma_2}{\gamma_1}\frac{h_n}{\alpha_n}I_{nN}(\beta R_{\mathrm{az}}) - I'_{nN}(\beta R_{\mathrm{az}})},\\
r_{nm} &= (-1)^m\mathcal{J}_{nN+m}(\varkappa R_{\mathrm{c}}) + \mathcal{J}_{nN-m}(\varkappa R_{\mathrm{c}});\\
\Phi_{nm} &= \frac{\delta_n}{2}\,b_{nm}\,\frac{\frac{\gamma_2}{\gamma_1}\frac{h_n}{\alpha_n}K_{nN}(\beta R_{\mathrm{az}}) - K'_{nN}(\beta R_{\mathrm{az}})}{\frac{\gamma_2}{\gamma_1}\frac{h_n}{\alpha_n}I_{nN}(\beta R_{\mathrm{az}}) - I'_{nN}(\beta R_{\mathrm{az}})}, \quad b_{nm} = I_{nN+m}(\beta R_{\mathrm{c}}) + I_{nN-m}(\beta R_{\mathrm{c}});\\
F_{nm} &= \left[S_1\frac{\delta_n}{2}Y_{nN}(\varkappa R_{\mathrm{az}})\,r_{nm} + S_2\psi_{nm}I_{nN}(\beta R_{\mathrm{az}})\right][\gamma_1 S_3\alpha_n]^{-1};\\
L_{nm} &= S_2\left[-\frac{\delta_n}{2}K_{nN}(\beta R_{\mathrm{az}})\,b_{nm} + I_{nN}(\beta R_{\mathrm{az}})\,\Phi_{nm}\right][\gamma_1 S_3\alpha_n]^{-1}.
\end{aligned}
\right\} \quad (12a)
$$

The functions f_n, φ_n, α_n, h_n have the same form as the functions f_n, φ_n, α_n, h_n in (7a).

From the condition of continuity of the thermal-neutron density at the boundary between the active zone and the reflector, it follows that

$$
A_{1n} = N\sum_{m=0}^{\infty}[B_{1m}R_{nm} + B_{2m}T_{nm}]; \quad C_{1n} = N\sum_{m=0}^{\infty}[B_{1m}Q_{nm} + B_{2m}\Delta_{nm}], \quad (13)
$$

where

$$
R_{nm} = \frac{\begin{aligned}&\gamma_0 l_n\left[\frac{\delta_n}{2}Y_{nN}(\varkappa R_{\mathrm{az}})\,r_{nm} + \psi_{nm}I_{nN}(\beta R_{\mathrm{az}}) - \alpha_n F_{nm}\right] -\\ &-t_n\left[\frac{\delta_n}{2}Y'_{nN}(\varkappa R_{\mathrm{az}})\,r_{nm} + \psi_{nm}I'_{nN}(\beta R_{\mathrm{az}}) - \gamma_0 h_n F_{nm}\right]\end{aligned}}{u_n t_n - \gamma_0 l_n z_n}; \quad (13a)
$$

$$T_{nm}=\frac{\gamma_0 l_n\left[\frac{\delta_n}{2}K_{nN}(\beta R_{az})b_{nm}-\Phi_{nm}I_{nm}(\beta R_{az})+\alpha_n L_{nm}\right]-}{-t_n\left[\frac{\delta_n}{2}K'_{nN}(\beta R_{az})b_{nm}-\Phi_{nm}I'_{nm}(\beta R_{az})+\gamma_0 L_{nm}h_n\right]}{u_n t_n-\gamma_0 l_n z_n};\qquad(13a)$$

$$Q_{nm}=\left[z_n R_{nm}+\frac{\delta_n}{2}Y_{nN}(\varkappa R_{az})r_{nm}+\psi_{nm}I_{nN}(\beta R_{az})-\alpha_n F_{nm}\right]t_n^{-1};$$

$$\Delta_{nm}=\left[z_n T_{nm}+\frac{\delta_n}{2}K_{nN}(\beta R_{az})b_{nm}-\Phi_{nm}I_{nN}(\beta R_{az})+\alpha_n L_{nm}\right]t_n^{-1}.$$

The functions u_n, t_n, l_n, and z_n have the same form as the functions u_n, t_n, l_n, and z_n in (9).

Finally, if we apply the boundary conditions (5) to $\underline{q}$ and $\underline{n}$, we obtain, after some calculations, the following equations:

$$\left.\begin{aligned}&\sum_{k=0}^{\infty}\sum_{m=0}^{\infty}\sum_{n=0}^{\infty}\{B_{1m}[N(g_{1k}^{\gamma}H_{nmk}+g_{2k}^{\gamma}q_{nmk})+\delta_{mk}L_{1k}^{\gamma}+g_{1k}^{\gamma}\Lambda_{1mk}]+\\&\quad+B_{2m}[N(g_{1k}^{\gamma}\omega_{nmk}+g_{2k}^{\gamma}\pi_{nmk})+\delta_{mk}L_{2k}^{\gamma}+g_{2k}^{\gamma}\Lambda_{2mk}]\}\cos k\omega=0;\\&\sum_{k=0}^{\infty}\sum_{m=0}^{\infty}\sum_{n=0}^{\infty}\{B_{1m}[N(S_1 g_{1k}^{\gamma}H_{n\,nk}+S_2 g_{2k}^{\gamma}q_{nmk})+S_1\delta_{mk}L_{1k}^{\gamma}+S_1 g_{1k}^{\gamma}\Lambda_{1mk}]+\\&\quad+B_{2m}[N(S_1 g_{1k}^{\gamma}\omega_{nmk}+S_2 g_{2k}^{\gamma}\pi_{nmk})+S_2\delta_{mk}L_{2k}^{\gamma}+S_2 g_{2k}^{\gamma}\Lambda_{2mk}]\}\cos k\omega=0.\end{aligned}\right\}\qquad(14)$$

Here, we have introduced the notation

$$\left.\begin{aligned}&g_{1k}^{\gamma,d}=\frac{\mathcal{J}_k(\varkappa a)}{\gamma,d}-\mathcal{J}'_k(\varkappa a);\qquad g_{2k}^{\gamma,d}=\frac{I_k(\beta a)}{\gamma,d}-I'_k(\beta a);\\&L_{1k}^{\gamma,d}=\frac{Y_k(\varkappa a)}{\gamma,d}-Y'_k(\varkappa a);\qquad L_{2k}^{\gamma,d}=\frac{K_k(\beta a)}{\gamma,d}-K'_k(\beta a),\\&\Lambda_{1mk}=\frac{\delta_k}{2}\sum_{i=2}^{n}[Y_{m+k}(\varkappa\varrho_{i1})\cos\beta_i(m-k)+(-1)^k Y_{m-k}(\varkappa\varrho_{i1})\cos\beta_i(m+k)];\\&\Lambda_{2mk}=\frac{\delta_k}{2}\sum_{i=2}^{n}[K_{m+k}(\beta\varrho_{i1})\cos\beta_i(m-k)+K_{m-k}(\beta\varrho_{i1})\cos\beta_i(m+k)];\\&H_{nmk}=\frac{\delta_k}{2}R_{nm}r_{nk};\qquad q_{nmk}=\frac{\delta_k}{2}(R_{nm}f_n+\psi_{nm})b_{nk};\\&\omega_{nmk}=\frac{\delta_k}{2}T_{nm}r_{nk};\qquad \pi_{nmk}=\frac{\delta_k}{2}(T_{nm}f_n-\Phi_{nm})b_{nk}.\end{aligned}\right\}\qquad(14a)$$

Hence, as in the case already considered, we obtain for the $\underline{k}$th order approximation a system of $2(k+1)$ linear homogeneous algebraic equations, which should be solved for the $2(k+1)$ unknowns.

Results of the Calculations and Conclusions

In conclusion, we present some results of the calculations and remarks on the solution of the obtained equations of criticality.

Figures 2 and 3 shows the variation of the effectiveness of the system of rods and of a single rod, respectively, as a function of the rod position in the reflector and of the rod radius. Figure 4 shows the change in the interference coefficient as a function of the number of rods. As seen from the curves of Figs. 2 and 3, a rather weak increase in the effectiveness of the system of rods is observed with an increase in their size, and a very sharp drop

is observed with an increase in the radius of the circle on which the rods are situated in the reflector.

The results were obtained under the assumption that the rods are absolutely black to thermal neutrons and do not slow down or absorb fast neutrons. The calculation for the rods was limited to the first-order approximation: k = 0; k = 1.

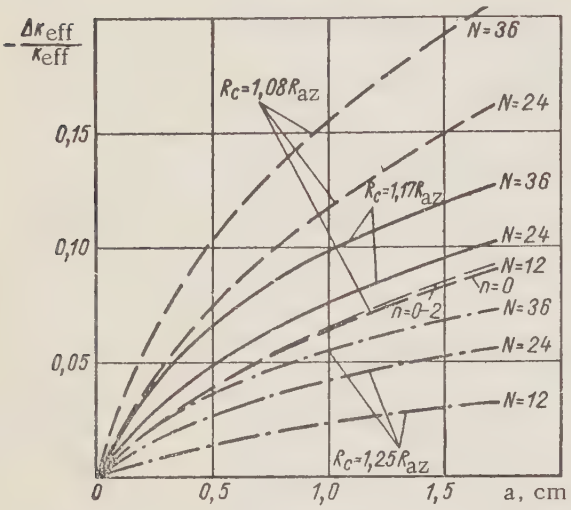

Fig. 2. Change in the effectiveness of a system of rods as a function of their position in the reflector and of the rod radius (n is the number of terms of the series used in the calculations; $R_p = 1.5\ R_{az}$).

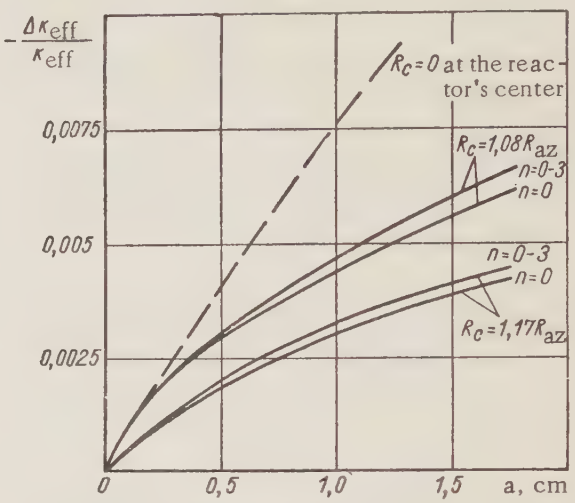

Fig. 3. Change in the effectiveness of a single rod as a function of its position in the reflector and radius (n is the number of terms of the series used in the calculations; $R_p = 1.5\ R_{az}$).

As was to be expected, for small rod sizes it was possible to limit the approximation to the zero order (k = 0) in the equation of criticality with a good degree of accuracy (in Figs. 2 and 3), the curves for k = 0 and k = 1 merge), i.e., to neglect the angular dependence of the neutron flux on the rod surfaces. Moreover, from the calculations it follows that, for a s fficiently large number of rods situated at some distance from the edge of the reactor, one can also neglect in the equation of criticality the angular dependence of the neutron flux by setting n = 0. For example, for N = 12, the magnitude of the reactivity, when the next two higher terms of the series are taken into account, increases by only approximately 2% (see Fig. 2). At the same time (see Fig. 3) for a single rod, the neglecting of the higher terms of the expansion leads to a considerably smaller value of the effectiveness (approximately 5% less than the value obtained when the next three higher terms of the series in n are kept).

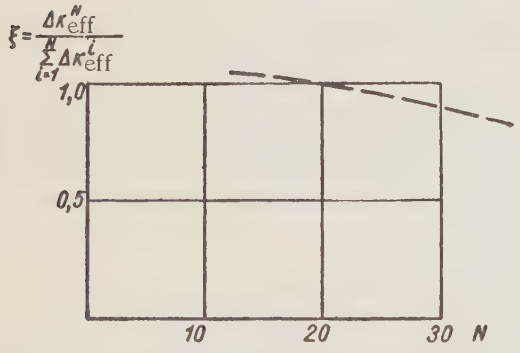

Fig. 4. Change in the interference coefficient ξ as a function of the number of rods N (Δk^N_{eff} is the effectiveness of the entire system of rods; Δk^i_{eff} is the effectiveness of a single rod; $R_p = 1.5\ R_{az}$; $R_c = 1.08\ R_{az}$; a = 1.25 cm).

The interference coefficient (see Fig. 4) can be greater or less than unity [8]. This results from the fact that in the neighborhood of each rod, the relative magnitude of the neutron density is reduced, and at large distances, the neutron density is enhanced (as compared to a reactor without rods). Therefore, when the number of rods is small, the effectiveness of the rod in the system exceeds the effectiveness of a single rod located in the same place.

The author expresses his gratitude to Ya. V. Shevelev for discussing basic questions connected with this work, and also to N. N. Ponomarev-Stepnii and E. S. Glushkov for aid and critical remarks. Numerous and difficult calculations were performed by R. V. Kulev, to whom the author is very grateful.

LITERATURE CITED

1. R. Avery, Nuclear Sci. and Eng. 3, 5, 504 (1958).
2. I. Carlvik and H. McCririck, Report No. 152 presented by Sweden at the Second International Conference on the Peaceful Uses of Atomic Energy [Russian translation] (Geneva, 1958).
3. G. V. Sinyutin and V. G. Semenov, Proceedings of the Second International Conference on the Peaceful Uses of Atomic Energy, Geneva, 1958 [in Russian], Report of Soviet Scientists, Vol. 2 - Nuclear Reactors and Nuclear Power (Moscow, Atomic Energy Press, 1959) p. 613.
4. A. D. Galanin, Theory of Thermal-Neutron Nuclear Reactors [in Russian] (Moscow, Atomic Energy Press, 1957).
5. G. N. Watson, Theory of Bessel Functions [Russian translation] (Moscow, IL, 1949).
6. D. F. Zaretskii, Proceedings of the International Conference on the Peaceful Uses of Atomic Energy, Geneva, 1955 [in Russian] (Moscow, Acad. Sci. USSR Press, 1958) Vol. 5, p. 624.
7. R. Murray and J. Niestlie, Nucleonics 13, 2, 18 (1955).
8. United States Atomic Energy Commission Reports, Nuclear Reactors, Vol. 1, Physics of Nuclear Reactors [Russian translation] (Moscow, IL, 1956) p. 271.

THE METALLURGY OF URANIUM

N. P. Galkin

Translated from Atomnaya Énergiya, Vol. 9, No. 4, pp. 270-281, October, 1960
Original article submitted April 18, 1960

This review gives general information on the history of the development and the modern state of uranium metallurgy outside the Soviet Union. There is a brief description based on practice in the USA) of methods for producing metallic uranium. The article deals with the production of the starting materials (UO_2, UF_4), the theory and practice of magnesium-thermic reduction and the process for refining the heat. There is a discussion of the problem of obtaining metal from uranium hexafluoride, enriched and poor in U^{235} isotope. In conclusion, there is a discussion of the possibilities for development in uranium metallurgy.

Metallic uranium has been produced on a commercial scale for not more than 15-20 years, although the industrial treatment of uranium ores started more than half a century ago. The demand for uranium increased very rapidly after the demonstration of uranium nuclear fission under the action of neutrons and the use of the energy of this fission on an industrial scale. The fragmentary data existing at that time on uranium metallurgy could not be used directly for the production of large amounts of metallic uranium with physical and chemical properties satisfying the requirements of nuclear physics. Metal for nuclear reactors should be nuclear-pure, i.e., free from harmful impurities which are able to capture neutrons to a large extent and which have high density. Metallurgists were faced with the problem of developing techniques for producing uranium which would remove the harmful impurities.

TABLE 1

Thermodynamic Characteristics of Uranium, Magnesium, and Calcium Compounds Used in Metallothermic Processes [3]

Compound	Melting point, °C	Heat of formation at 25 °C, kcal/g·atom metalloid	Free energy of formation at 1500°C		Compound	Melting point, °C	Heat of formation at 25°C, kcal/g·atom metalloid	Free energy of Formation at 1500 ° C, kcal/g·atom metalloid
			v	kcal/g atom metalloid				
U_3O_8	Decomposes above 900 °C	107	—	—	MgO	2800	143,8	90
UO_2	2800	129,6	2,18	94	CaO	2550	151,7	110
UF_4	1036	111	3,6	83	MgF_2	1263	131,7	92
UF_3	1430	113	3,5	81	CaF_2	1418	145,3	111
UCl_4	590	63	1,9	44	$MgCl_2$	714	76,6	45
UCl_3	935	71	1,9	44	$CaCl_2$	782	95,2	68

In a comparatively short time in various countries (USSR, USA, Britain), uranium salts and metallic uranium were produced which were nuclear-pure, as well as essential chemical reagents and construction materials. The production of nuclear fuel was then rapidly organized. The world production of uranium [1] has now reached considerable proportions, comparable with the production of other rare and nonferrous metals (Fig. 1); and as regards costs of annual production, it considerably exceeds many of them.

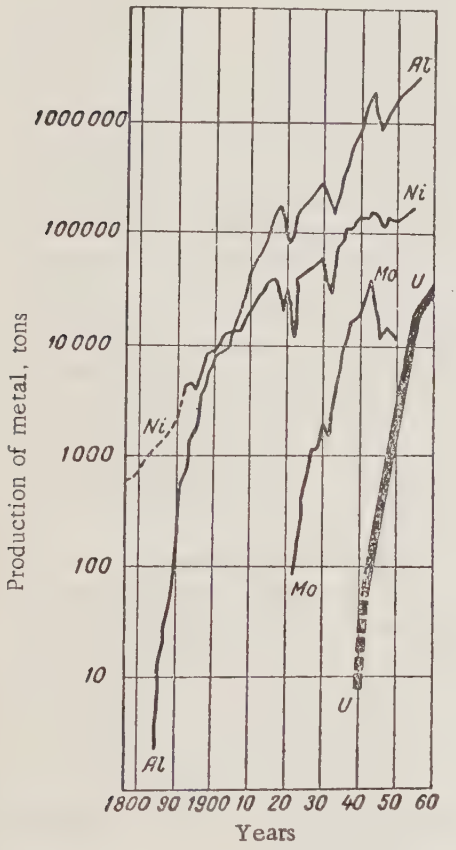

Fig. 1. Comparative graph showing the increase in world production of uranium, molybdenum, nickel, and aluminum.

Uranium has a density of 19.05 g/cm^3, a melting point of 1130° C, and high chemical activity. It reacts readily with all metalloids, forming stable compounds. This property determines the special features of uranium metallurgy.

Nuclear-pure compounds of uranium must be reduced with powerful and noncontaminating metal reduction agents. The apparatus and medium in which the metallurgical operations are carried out should be inert to uranium or protected from reaction with it.

The history of uranium metallurgy [2] shows that the more or less successful attempts to obtain the pure metal have amounted to the development and testing of the following methods: 1) reduction of the oxides; 2) reduction of the halides; 3) electrolysis of the melts; 4) thermal decomposition of the compounds.

The types of neutral medium used were: vacuum, helium, argon, and sometimes fused salts of alkali and alkali-earth metals. Experience has shown that MgF_2, CaF_2, BeO, MgO, CaO, ThO_2 are stable to heated and fused uranium and (at temperatures which are not too high) graphite, used as refractories and cladding materials. The usual reduction agents (hydrogen, carbon, silicon, aluminum) were unsuitable either due to their inefficiency or to the fact that they contaminated the metal. Good results were obtained by the metallothermic method for reducing oxides and halides of uranium by lithium and the alkali earth metals and also the reduction of chlorides by sodium and potassium. For economic reasons, only magnesium and calcium were suitable for production purposes. Table 1 gives the characteristics of the main compounds of uranium, magnesium, and calcium needed for the thermodynamic evaluation of metallothermic reduction and electrolysis.

In uranium metallurgy, the first three methods are used for various purposes. The method of thermal decomposition [4], checked under laboratory conditions (the decomposition of uranium tetraiodide), was not developed further due to the complexity of the process and apparatus.

The reduction of uranium oxides (UO_2, U_3O_8, UO_3) by calcium in the presence of a flux ($CaCl_2$, excess of calcium) or by magnesium gives a powder of round particles of metal [5]. This method is used in the powder metallurgy of uranium.

The metallothermic reduction of halide salts was the simplest, quickest, and cheapest method for preparing uranium. The reduction of UCl_4 by calcium, giving good results [6], did not find widespread application due to operating difficulties with the strongly hygroscopic chloride. Most metallic uranium is now produced in the form of ingots by reducing the tetrafluoride with calcium or magnesium.

The electrolysis of melts cannot compete economically with the metallothermic reduction of uranium tetrafluoride and is only used for preparative purposes (for producing very pure metal from UCl_3 [7]). However, further investigations are being carried out to improve this method and make it cheaper for use both in the production of the pure metal [8] and also for refining [9].

Before the First International Conference on the Peaceful Uses of Atomic Energy, it seemed that the main raw material for producing metallic uranium was the tetrafluoride, reduced by calcium or magnesium. The

Second International Conference on the Peaceful Uses of Atomic Energy showed that in foreign practice greater emphasis is placed on the magnesium-thermic method, which is now used not only in the USA, but also in Canada and Britain [10, 11]. In Italy the double fluorides are reduced by magnesium [12]. In France [13] and Sweden [14] uranium tetrafluoride is reduced by metallic calcium.

The advantages and disadvantages of using these metal reduction agents are as follows:

1. The specific consumption of magnesium per unit of reduced uranium tetrafluoride is 1.6 times less than calcium.

2. The cost of magnesium is 5-10 times less than calcium.

3. Methods for producing magnesium have been developed to a high level and can ensure a minimum content of impurities in the pure metal.

4. Reduction by magnesium must be carried out in a closed bomb and the charge must be heated before the start of reaction. This is due to the fact that, in the first place, magnesium boils at 1130° C, i.e., below the melting point of the slag (the melting point of MgF_2 is 1263° C), and in an open apparatus it would vaporize, without reacting with the uranium tetrafluoride; in the second place, because the heat of reduction of uranium tetrafluoride by magnesium is insufficient (− 83.5 kcal) to melt the reaction products.

5. The calcium-thermic reduction of uranium tetrafluoride can be carried out in an open apparatus without preliminary heating of the charge. The extraction of uranium from slags based on calcium fluoride is also much easier than from magnesium fluoride.

The Calcium-Thermic Reduction of Uranium Tetrafluoride. As yet, there is no literature on detailed investigations of this process not requiring complex apparatus.

In most countries where the calcium-thermic method of reduction is used, the main efforts have been directed at improving the reaction apparatus and the ignition device [13, 14]. There are descriptions [13] of reduction heats in which crude ingots of metallic uranium are obtained weighing not more than 100 kg. These ingots have a perfectly satisfactory surface state and sufficient purity, which means that the metal can be used to make rods and fuel elements for reactors without further treatment.

In Sweden [14], where the heats are much smaller (the ingots only weigh 30 kg), the crude uranium is subjected to vacuum, refining-remelting with simultaneous casting of the uranium rods.

The Magnesium-Thermic Reduction of the Double Fluoride of Uranium. The double fluoride is obtained by precipitation according to the reaction [12, 15]

$$UO_2(NO_3)_2 + HCOOH + 2SO_2 + 5NaF = NaUF_5 + 2NaSO_3 + 2NaHCO_3 + CO_2.$$

It is readily precipitated from solutions and is easily dehydrated at about 120° C.

The possible advantages of this method are:

1) the elimination from the production cycle of intermediate precipitation of the higher oxide and reduction to uranium dioxide;

2) complex apparatus is no longer needed in the furnaces for reduction and fluorination;

3) the elimination of reactions with expensive pure hydrogen fluoride, which is replaced by the cheaper solid fluoride of an alkali metal;

4) lower consumption of reagents;

5) a complex composition slag is obtained, melting at about 1000° C. The magnesium-thermic reduction of the double fluoride uses the same method as the reduction of uranium tetrafluoride. The charge is heated to 750° C. Up to 60 kg of uranium is obtained in the heat.

The double fluoride can serve as the starting product for the preparation of uranium hexafluoride.

The Magnesium-Thermic Reduction of Uranium Tetrafluoride. This process is used in its most highly developed form in the USA [16, 17]. The reduction (see the flow diagram, Fig. 2) is carried out in two variants. The crude metal of the usual reduction heat (140-180 kg) is subjected to refining by remelting in vacuum, or large scale reduction smelting is carried out (approximately 1500 kg) providing the pure metal directly, i.e., direct reduction is carried out.

The starting material is uranium trioxide, obtained by the continuous roasting of pure uranyl nitrate hexahydrate at temperature of 510-538° C. Table 2 gives the specifications for this material. The impurities to be checked are divided into groups characterizing the role of the impurities in the process. Metallurgical impurities affect the physical properties of uranium, its workability and behavior in subsequent heat-treatment and radiation in the neutron field of the reactor. Technological impurities appear due to contamination of the semifinished uranium products by the material of the apparatus (stainless steel, monel, etc.) and reagents (for example, magnesium) and partially affect the quality of the metal, in the same way as the metallurgical impurities. The forbidden impurities reduce the possible degree of burn-up of U^{235} in the nuclear reactor.

TABLE 2

Specifications for Semifinished Product and Metallic Uranium [17]

Material	Impurity, 10^{-4} %													Additional requirements
	Metallurgical				Technological				Forbidden					
	H	C	N	Si	Fe	Cr	Ni	Mg	B	Gd	Dy	Cd	Ag	
UO_3	—	100	—	20	30	10	15	—	0,2	0,05	0,1	0,2	1	Weight of shakedown equal to 4.2-4.3 g/cm³
UF_4	—	—	—	—	35	5	15	—	—	—	—	—	—	$UF_4 > 96,5$ weight %; moisture $\geq 0,07$ weight %; $UO_2F_2 > 2,3$ weight %; uranium oxide $> 1,2$ weight %**
U	1	400	50	50	50	20	40	5	0,2	—	—	0,2	1	Density 18.96 g/cm³
Direct reduction U	4,5	30	10	20	45	6	20	10	0,15	—	—	—	—	Density 19.01 g/cm³

* Determined by dissolving in water.
** Determined by dissolving in ammonium oxalate.

Uranium trioxide is reduced by hydrogen or by cracked ammonia to uranium dioxide at a maximum temperature of 625-650° C in various types of continuous reduction reactors.

Uranium dioxide is subjected to hydrofluorination in continuous reactors. In an advanced type of such a reactor with a moving layer, the sintered UO_2 is hydrofluorinated [18], moving through a vertical tapered monel tube countercurrent to the hydrogen fluoride flowing upward. The temperature in the upper part of the reactor is 300-400° C and in the lower part, 500-600° C. The consumption of HF is 110% of the theoretical. The product contains up to 98% UF_4 (see Table 2).

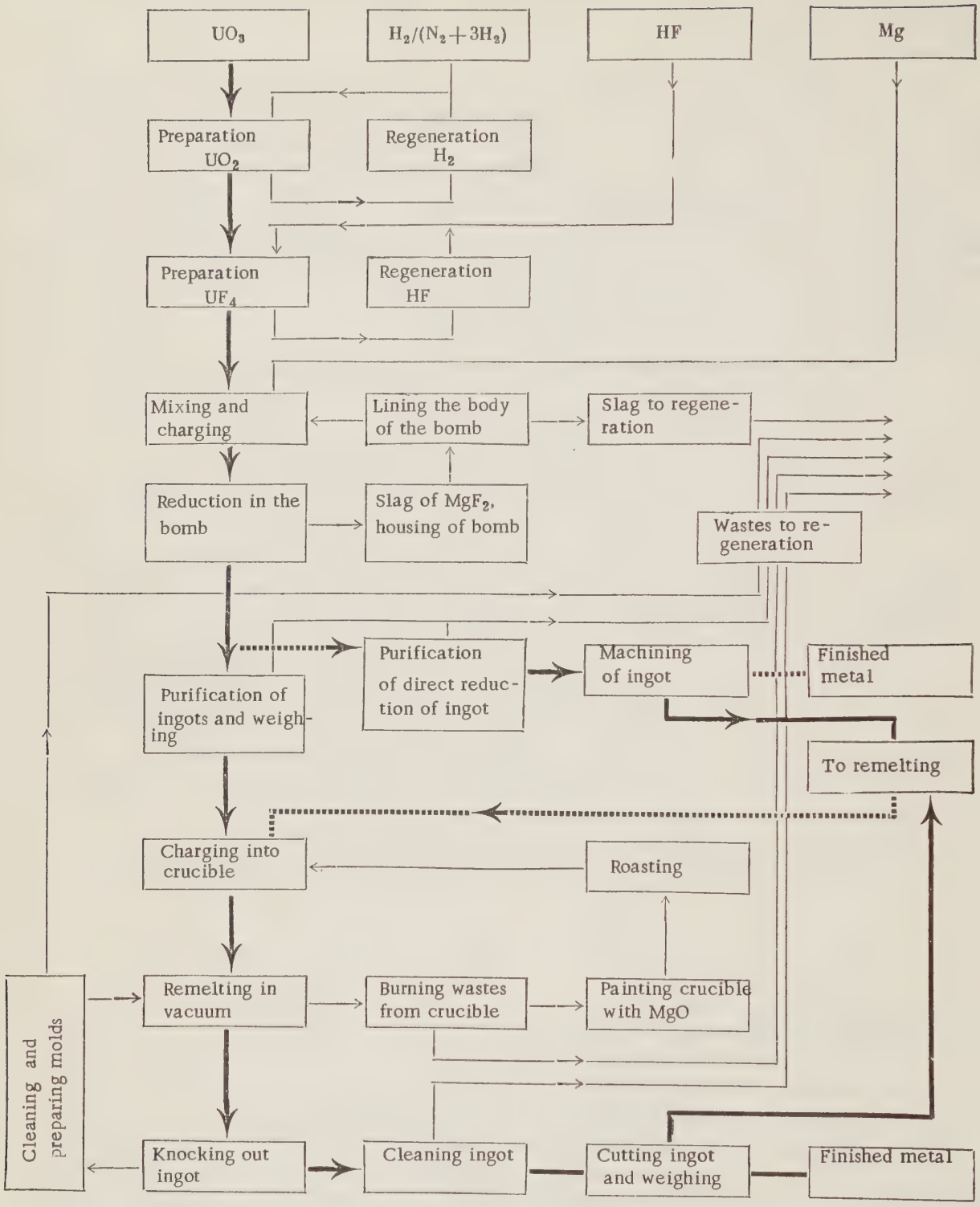

Fig. 2. Flow diagram for the preparation of metallic uranium [17]. The thick line shows the direct reduction operations.

The reduction of uranium tetrafluoride by magnesium is carried out in a closed, but not hermetically sealed, bomb, carefully lined with dry magnesium fluoride obtained from the ground slag of previous heats. To obtain the crude metal, a 4% excess of magnesium is taken. The charge is mixed in a double cone mixer and carefully packed in the body of the bomb with a special charging machine [17]. The density obtained is almost 15% higher than with ordinary charging. A layer of magnesium fluoride of not less than 30 mm thickness is poured and tightly tamped on the layer of tamped charge. The bomb is then closed with a steel lid fastened by bolts placed in a furnace and heated to 700° C for about $4^1/_2$ hours. Depending on the changes in the composition of the charge, the apparatus, etc., the heating of the furnace can vary between 677 and 760° C.

The reduction begins in the range 600-650° C by reaction of magnesium vapor with tetrafluoride and occurs in steps:

$$UF_4 + 0{,}5Mg \rightarrow UF_3 + 0{,}5MgF_2, \quad (1)$$

$$UF_3 + 1{,}5Mg \rightarrow U + 1{,}5MgF_2. \quad (2)$$

In order to melt the reaction product the charge must be heated to not less than 200° C. The heating is carried out so that the reaction is excited from the bottom. The reaction front travels at a rate of about 5 mm/sec. The heating system is determined by the thermal conductivity of the charge and its volume. The larger the volume of the charge and the lower its thermal conductivity, depending on the density of the charge, the slower the charge should be heated. If the heating is carried out very rapidly (high temperature), the reaction begins before the inner layers are heated to the required temperature and insufficient heat is introduced. At a temperature below the optimum in the charge, secondary reactions will take place over a long period (see below); the partial reduction [reaction (1)] and the melting will be unsatisfactory.

In Britain [19-21], instead of a powdery charge they use brickettes made at a pressure of 1.1-1.4 tons/cm^2, with diameter 60-100 mm, height 50 100 mm, and density of 3 g/cm^3.

Investigations [11, 17] have shown that the yield of metal as ingots depends not only on the type of heating of the charge, but also on the content of impurities in the uranium tetrafluoride (moisture, oxide, and uranyl fluoride) and magnesium (see Table 2).

The role of these impurities can be clearly seen from the example of secondary reactions of uranyl fluoride

$$UO_2F_2 + H_2O \rightleftarrows UO_3 + 2HF, \quad (3)$$

$$Mg + 2HF \rightleftarrows MgF_2 + H_2, \quad (4)$$

$$UO_2F_2 + H_2 \rightleftarrows UO_2 + 2HF, \quad (5)$$

$$UO_2 + 2Mg \rightleftarrows U + 2MgO. \quad (6)$$

The reaction cycle (4) + (5) and others in the presence of the smallest traces of moisture (3) lead to the formation of a film on the particles of MgF_2 and to an increase in the time of heating of the charge (increase in temperature at the start of the reaction) due to difficulty in vaporizing the magnesium. The quantity of heat transmitted to the charge then increases. Reduction of the uranyl fluoride [reactions (4) + (5) + (6)] gives twice as much heat as the main reaction (1) + (2), which has a favorable effect on the thermal balance of the process.

The magnesium oxide (6) which forms in the reduction of the uranyl fluoride dissolves in the slag. Small amounts of it reduce the melting point of the slag (by 40° C at 5.5 weight % MgO); large amounts increase the temperature and seriously hinder the separation of the metal.

Experience shows that the best yields (> 97%) are obtained with 1 weight % UO_2F_2 and 1 weight % of uranium oxides. A content of UO_2F_2 greater than 2.3-2.5 weight % is undesirable, since the yield of metal in this case falls below 95 weight %.

Impurities of oxides give a small amount of heat. The thermal effect of reaction (6) is almost a third of that of the main reaction. The presence of more than 2 weight % of oxides in the tetrafluoride is therefore not permissible, since it spoils the thermal balance and the magnesium oxide which forms interferes with the separation of the slag and metal.

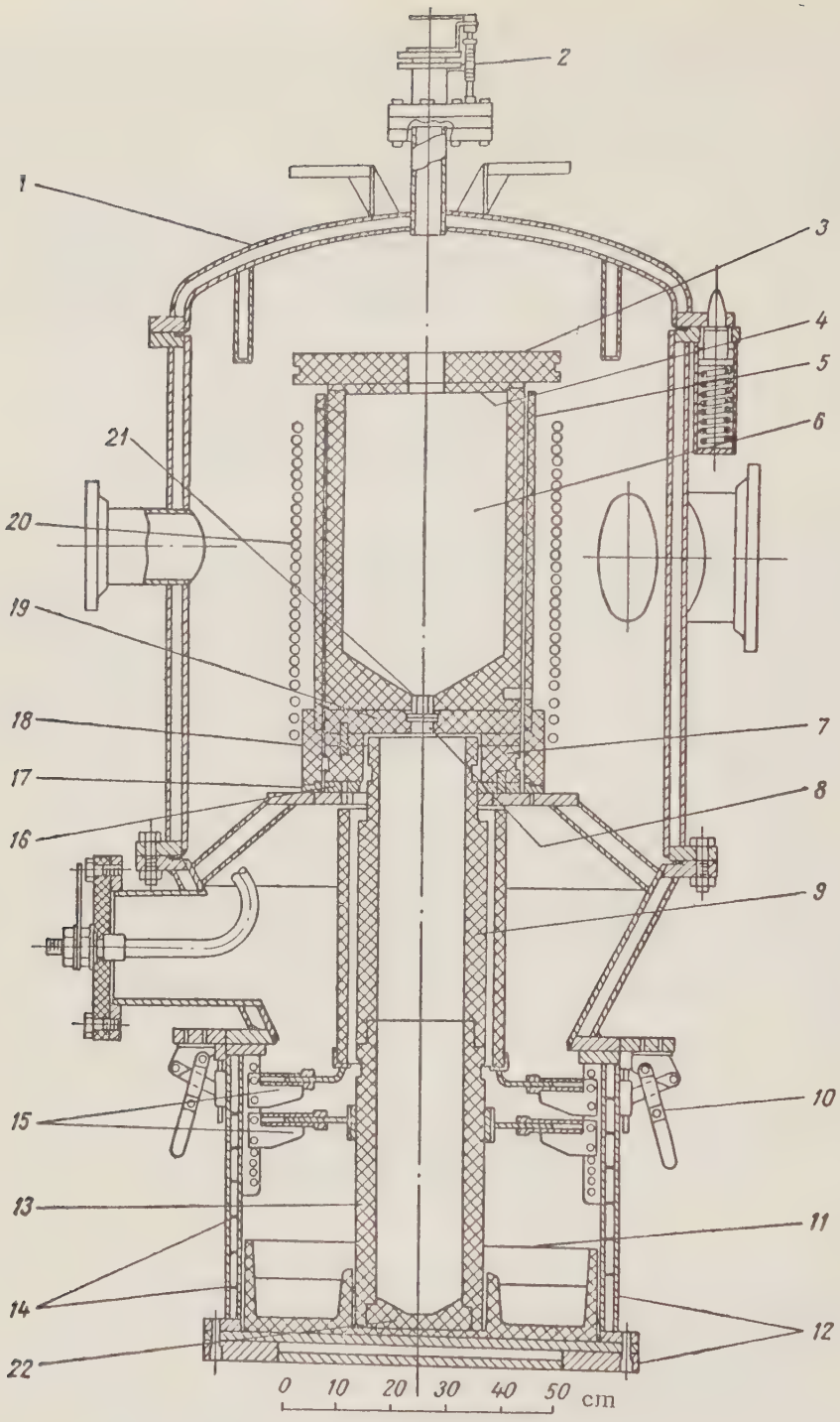

Fig. 3. Diagram of induction furnace for the vacuum remelting of crude uranium [17]: 1) top cover; 2) valve for inspection window; 3) insulator cover; 4) cover; 5) screen; 6) crucible; 7) base insulator; 8) slides; 9) top of mold; 10) lever clamp; 11) bottom insert; 12) cooling jacket for mold; 13) bottom of mold; 14) baffle; 15) support for thermal insulation; 16) ring for crucible base; 17) support ring for zirconium screen; 18) external insulator ring; 19) disc with slot; 20) spiral; 21) plug; 22) cupped support for mold.

When there is moisture in the charge, the following secondary reactions take place:

$$UF_4 + 2H_2O \rightleftarrows UO_2 + 4HF, \quad (7)$$

$$Mg + H_2O \rightleftarrows MgO + H_2, \quad (8)$$

$$H_2 + U \rightleftarrows U, \text{ saturated } H_2. \quad (9)$$

With a dolomite lining, the following reaction takes place

$$CaO + 2HF \rightleftarrows CaF_2 + H_2O. \quad (10)$$

The reaction of hydrolysis (7) and the cycle of reactions (7) and (10), commencing at a temperature of 400° C, oxidize the uranium tetrafluoride. If the charge is kept for a long time while heating above this temperature, the yield of the metal is considerably reduced [11]. For this reason magnesium fluoride is now used instead of a dolomite lining, and the water content in the initial products of the heats is kept to a minimum. The hydrogen, contaminating the uranium is removed during the vacuum remelting.

To improve the thermal balance, some investigators [22] suggest carrying out the magnesium-thermic reduction of uranium tetrafluoride in an atmosphere of oxygen. The success of the magnesium-thermic method is due to the fact [10] that it uses a method for producing uranium tetrafluoride which does not involve moisture and oxygen.

The ingots of the crude uranium are subjected to vacuum remelting to refine the metal. At the same time, billets are cast for further rolling or extrusion [17].

The refined remelted uranium is mainly bottom poured (Fig. 3). The basic material for crucibles and molds is graphite. In order to improve the refining process and to break up oxide films on the metal, before the start of the vacuum melting operation or during it, metallic calcium or magnesium should be added [23].

Vacuum remelting is the main method for alloying uranium, preparing its alloys and casting components from it [24-28].

A characteristic tendency of modern vacuum melting is the increase sizes (the furnace capacity is as high as 4 tons of metallic uranium) and greater accuracy is casting (deviations of ± 15 μ with an external diameter of components 41 mm) [29, 30].

The direct reduction of 2000 kg UF_4 is carried out with an excess of magnesium (0.5 weight %) giving a satisfactory yield of metal and, which is more important, reducing the vapor pressure of magnesium in the bomb. The mixing and loading of the charge in this process is the same as in the smelting of the crude metal. The bomb is placed in a 400 kw electric resistance furnace (Fig. 4) with three heating zones. During the first five hours all three zones are at 621° C. The upper and middle zones are then switched off, and after nine hours the reaction occurs. The temperature in the furnace can increase, depending on the physical and chemical properties of the charge, the quality of the lining, etc. to 673° C. There can also be fluctuations in the time the charge is heated before the start of reaction. The hot, low thermal conductivity slag of magnesium fluoride which collects over the molten metal forms a "hot cap" in the receiver, which retards the cooling of the ingot and c causes directional crystallization in the metal from the bottom to the top. This results in very good separation of the slag and very pure metal is obtained (Fig. 5) with a yield of 97% and more. However, the side surfaces and especially the top of the ingot are contaminated with slag inclusions. The surface of the ingot is therefore machined on a lathe and a slug of pure metal is obtained with a direct yield of 82-85%. The direct reduced metal is purer than the ordinary crude metal as regards most of the impurities (see Table 2), but contains more hydrogen [see reaction (9)], which is undesirable since hydrogen interferes with the sealing of the uranium blocks and spoils their performance in the reactor. More work must therefore be done on the direct reduction process. Examples of measures for reducing the amount of hydrogen in the metal are [17] the thorough removal of moisture from the lining and the components of the charge, the removal of moisture by selecting a system for heating the charge (experience shows that if the whole charge is heated to above 370° C before the reactions, the amount of hydrogen is reduced to the normal value), sweeping the heated charge with a neutral gas before the start of reaction, etc.

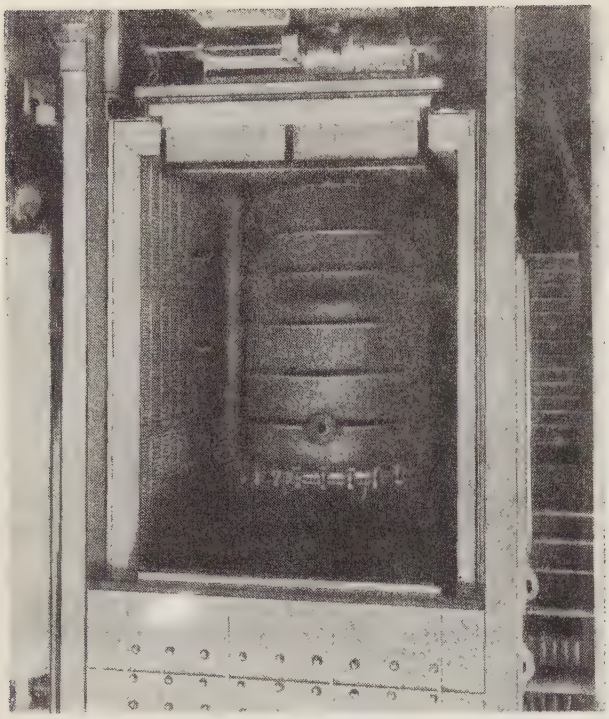

Fig. 4. Magnesium-thermic direct reduction bomb on a trolley in an electric furnace.

Fig. 5. Structure of direct reduced uranium; metal not etched. Bright field (x 125).

Preparing Uranium Enriched and Poor in U^{235} Isotope. The starting product for the preparation of enriched uranium is uranium hexafluoride supplied by the gas diffusion plants. When working with uranium compounds and metallic enriched uranium, it is essential to carefully observe a new condition – nuclear safety [17]. If the nuclear safety limit is exceeded, the critical mass of U^{235} is reached and a uranium fission chain reaction starts with the liberation of a large quantity of heat and nuclear radiation, extremely dangerous for the operating personnel and contaminating the expensive material and surrounding apparatus. The detailed rules for nuclear safety are established in each actual case by specialist physicists and will not be discussed here. The general rules limit the masses, volumes, and concentrations of enriched uranium which can be reprocessed, its arrangement, and the composition of the surrounding medium (water, light materials, etc.) in the operating buildings and during transport. They also recommend the best shapes for the apparatus and containers for enriched materials.

Uranium hexachloride is reduced to the tetrafluoride and is converted to metal according to the above described arrangement for producing the crude metal and refining it in vacuum. The method for reducing uranium hexafluoride to the tetrafluoride has not yet been finalized.

Attempts to use as reducing agents sulfur dioxide, ethylene, trichlorethylene, ammonia, etc. have had very little success, since they have not been used on an industrial scale [31, 32]. An indication of the lack of success in this field is the fact that in Britain and the USA for a number of years they have been using a multistage hydrolysis method, the serious drawbacks of which are well known.

The search for methods for reducing uranium hexafluoride is very important not only to increase the output of the gaseous diffusion plants, but also to reprocess uranium oxides and uranium concentrates to uranium hexafluoride by direct fluorination [33-35]. Furthermore, these methods are essential for reprocessing uranium hexafluoride which is poor in the light isotope. Serious attention is therefore paid to the reduction of uranium hexafluoride by carbon tetrachloride [31], both in batches and continuous.

This simple and effective method, giving high-purity uranium tetrafluoride, has all the advantages of a single-stage process. When it is used for highly enriched uranium, the requirements of nuclear safety can readily be fulfilled. Furthermore, the comparatively small apparatus can have a very high output. At the same time

in the unfinished production there is a small amount of the expensive product. Also of interest is the method for reducing uranium hexafluoride with hydrogen [32, 36].

Uranium tetrafluoride obtained by the reduction of uranium hexafluoride with carbon tetrachloride or hydrogen contains hardly any water and has the theoretical composition with regard to fluorine and uranium. Good yields are therefore obtained in the metallothermic reduction. The by-products of the reduction of uranium hexafluoride (hydrogen fluoride, fluorine and chlorine derivatives of carbon) can be regenerated and used in the nuclear engineering industry, and the fluorine and chlorine derivatives can be used separately as freons.

Possibilities for the Development of Uranium Metallurgy. It is rather difficult to predict the trends in this new and rapidly growing branch of metallurgy. However, some idea can be obtained of the development trends in the metallurgical processes by considering the leading investigations and the changes in requirements for purity of the metal.

At the first stage of reactor construction, exceptionally rigid requirements were made on the content of impurities in the metal. This made it necessary to accurately carry out all preparatory and main operations in the reduction of uranium. The apparatus for these processes was very complex. The reduction was carried out in an atmosphere of inert gas – argon, and the sizes of the reduction heats did not reach 100 kg metal.

With development in reactor construction and the development of various types of fuel elements, large quantities of uranium were required. This made the problem of reducing the cost of metallic uranium particularly acute; that of simplifying the technological processes for producing the metal and the possibilities of using these processes directly at ore plants or in fuel cycles (when reprocessing nuclear materials) also became acute.

It is possible that the production of metallic uranium will develop in parallel with the development of new methods for producing uranium tetrafluoride, the technology of which is complex and expensive. It is also possible that in the near future the use of successive reactions of hydrofluorination and fluorination in the processing of concentrates [33, 34] to obtain very pure hexafluoride will make it possible to avoid the multistage processes of so-called fine chemical purification, i.e., dissolving the concentrates in nitric acid, extraction with organic solvents, reextraction and precipitation of the uranium in the form of an insoluble salt with subsequent roasting of this precipitate to the trioxide. When these operations are eliminated there will no longer be huge quantities of harmful waste solutions requiring additional treatment.

On reaction with reduction agents (H_2, CCl_4, NH_3, C_2H_2) the obtained uranium hexafluoride is easily converted to uranium tetrafluoride, and the latter is reduced to the metal.

Another very promising trend in the technology of uranium is a method based on the conversion of uranium oxides to chlorides [37]. The charge, consisting of uranium oxides, barium sulfide, and the eutectic mixture NaCl + KCl or KCl + $BaCl_2$, is heated to 750–800° C. Gaseous chlorine is delivered to the heated charge through a quartz tube. The process of conversion of uranium oxides to uranium tetrachloride can be represented by the following reactions:

$$2BaS + 2UO_2 + 6Cl_2 \longrightarrow \tag{11}$$

$$\longrightarrow 2BaCl_2 + 2UCl_4 + 2SO_2, \quad 2UCl_4 + BaS \longrightarrow BaCl_2 + 2UCl_3 + S, \tag{12}$$

$$3BaS + 2UO_2 + 6Cl_2 \longrightarrow 2UCl_3 + 3BaCl_2 + 2SO_2 + S. \tag{13}$$

After all of the sulfide has changed to chloride, with subsequent chlorination uranium tetrachloride will again be formed:

$$2UCl_3 + Cl_2 \longrightarrow 2UCl_4. \tag{14}$$

The obtained alloy is treated with magnesium, and metallic uranium separates out. This method is very interesting and it is possible that it will be introduced on an industrial scale after further development.

At the present time up to 2000 kg of uranium tetrafluoride is reduced in one calcium-thermic heat [17]. However, in principle it is quite possible to have a continuous process of reduction of fluorine or chlorine compounds

of uranium, which will considerably reduce the volume of the apparatus and completely automate the process. Development work has been done on this continuous process for reducing uranium since 1953 [17], but it is not yet used on an industrial scale, and it is not likely to be used in the near future. In the continuous process it is difficult to separate the slag from the metal, which reduces the yield of uranium. Difficulties also arise in selecting constructional materials for the reduction apparatus. Furthermore, at the present time the scale of uranium production is not so great as to make it imperative to introduce a continuous process on an industrial scale. In the near future the attention of scientists and technologists will most likely be concentrated on developing large-dimension apparatuses which will increase the scale of simultaneous reduction of uranium tetrafluoride to the metal.

From the economic point of view it is perhaps better to produce uranium in the form of an ingot weighing several tons than to produce it in the course of several days by a continuous process in small apparatuses. The continuous process would require 24-hour operation at high temperatures, which needs close attention.

A further detailed study of the reduction smelting and refining of the metal in one apparatus should considerably reduce the cost of this metallurgical method.

In connection with the development of vacuum metallurgy and improvements in vacuum apparatus, it may be possible to reduce the cost and introduce into production the carbothermic process for producing uranium from oxide, the flow sheet of which was recently published [17].

Also very interesting are investigations connected with the use during reduction of a combined charge consisting, for example, of a mixture of compounds of two or three metals and a reducing agent [17]. As fuel elements in modern reactor construction, more use is being made of alloys of uranium with other metals (diluents). Many alloys can be produced by metallothermic reduction. There is reason to suppose that work on the preparation of alloys by the metallothermic method will be successfully developed.

Of considerable interest is the development of a process for the direct reduction of uranium hexafluoride to the metal. In the Oak Ridge National Laboratory the possibility has been shown on a small scale of reducing uranium hexafluoride by calcium and iodine, the result being compact metallic uranium [17]. Studies have also been made of the reduction of uranium hexafluoride by magnesium vapors at temperatures of 1000-1500°C. In this case the product was finely powdered uranium [17]. The promising features of these processes have led to extensive investigations in this direction. Studies are being made of processes for reducing uranium hexafluoride by sodium vapors according to the reaction

$$UF_6 + 6Na \rightleftarrows U + 6NaF, \qquad (15)$$

and also by a mixture of sodium and magnesium vapors; in the latter case compact metal and a very easily fusible slag can be obtained. However, this process involves increased consumption of the metal reduction agent; it is therefore necessary to carry out research work to provide cheaper reduction agents.

There is no doubt that the direct reduction of uranium hexafluoride to the metal combined with the above-mentioned processes of hydrofluorination and fluorination has tremendous technological and economic advantages.

LITERATURE CITED

1. V. Ripar Jaderná Energia 4 (5) 128 (1958).
2. J. Van Impe, Chem. Engng Progr. 50, 230 (1954).
3. A. Glassner, ANL 5750 (1957).
4. C. Prescott, et al., AEC Report MDDC-437 (1946).
5. J. Buddery, Metallurgy and Fuels 1, Pergamon Press (1956) p. 24.
6. J. Goggins, et al., Ind. Eng. Chem. 18, 114 (1926).
7. B. Blumenthal and R. Noland, Metallurgy and Fuels 1, Pergamon Press (1956) p. 62.
8. L. Niedroch. Nucleonics 16, 64 (1958).
9. J. Antill et al., Metallurgy and Fuels 2, Pergamon Press (1959) p. 38.

10. Melvanin, Proceedings of the Second International Conference on the Peaceful Use of Atomic Energy (Geneva, 1958). Selected reports of non-Soviet scientists, Vol. 7. The Technology of Nuclear Raw Materials [in Russian] (Moscow, Atomic Energy Press, 1959) p. 436
11. J. Harper and A. E. Williams, The Extraction and Purification of Rare Metals [Russian translation] (Moscow Atomic Energy Press, 1960).
12. A. Cacciari et al., Report No. 1399 presented by Italy to the Second International Conference on the Peaceful Use of Atomic Energy (Geneva, 1958).
13. Decrop et al., Proceedings of the Second International Conference on the Peaceful Use of Atomic Energy (Geneva, 1958). Selected reports of non-Soviet scientists, Vol. 7. The Technology of Nuclear Raw Materials [in Russian] (Moscow, Atomic Energy Press, 1959) p. 485.
14. Gelin et al., Proceedings of the Second International Conference on the Peaceful Use of Atomic Energy (Geneva, 1958). Selected reports of non-Soviet scientists. Vol. 7. The Technology of Nuclear Raw Materials [in Russian] (Moscow, Atomic Energy Press, 1959) p. 417.
15. Brodsky and Pagny, Proceedings of the Second International Conference on the Peaceful Use of Atomic Energy (Geneva, 1958). Selected reports of non-Soviet Scientists, Vol. 7. The Technology of Nuclear Raw Materials [in Russian] (Moscow, Atomic Energy Press, 1959) p. 494.
16. H. E. Thayer, Proceedings of the Second International Conference on the Peaceful Use of Atomic Energy (Geneva, 1958). Selected reports of non-Soviet scientists. Vol. 6. Nuclear Fuel and Reactor Material [in Russian] (Moscow Atomic Energy Press, 1959) p. 5.
17. C. Harrington and A. Ruehle, Uranium Production Technology, Van Nostrand Company (1959).
18. Yu. V. Gagarinskii, Atomnaya Énergiya 6, 2, 124 (1959).*
19. Metal Ind. 94, 7, 127 (1959).
20. Williams, Improvements in the Production of Uranium, British Patent No. 780,974 (1957).
21. Atomic World 10, 3, 99 (1959).
22. Wotek, Improvements in the Production of Uranium, British Patent No. 806,031, (1958).
23. Colbeck, British Patent No. 806,001 (1958).
24. W. Hayward and P. Corzine, Proceedings of the Second International Conference on the Peaceful Use of Atomic Energy (Geneva, 1958). Selected reports of non-Soviet scientists. Vol. 6. Nuclear Fuel and Reactor Material [in Russian] (Moscow, Atomic Energy Press, 1959) p. 561.
25. K. J. Turner and L. R. Williams, Proceedings of the Second International Conference on the Peaceful Use of Atomic Energy (Geneva, 1958). Selected reports of non-Soviet scientists. Vol. 6. Nuclear Fuel and Reactor Material [in Russian] (Moscow, Atomic Energy Press, 1959) p. 570.
26. J. Storr, M. Englander, and M. Gotron, Proceedings of the Second International Conference on the Peaceful Use of Atomic Energy (Geneva, 1958). Selected reports of non-Soviet scientists. Vol. 6. Nuclear Fuel and Reactor Material [in Russian] (Moscow, Atomic Energy Press, 1959) p. 515.
27. M. D. Jepson et al., Proceedings of the Second International Conference on the Peaceful Use of Atomic Energy (Geneva, 1958). Selected reports of non-Soviet scientists. Vol. 6. Nuclear Fuel and Reactor Material [in Russian] (Moscow, Atomic Energy Press, 1959) p. 96.
28. Stivenson, J. Inst. Metals 87, 6, 174 (1959).
29. H. Hardung, Vakuum-Technik 7, 6, 135 (1958).
30. Flancke, Vacuum, April, p. 59 (1959).
31. Nairn et al., Proceedings of the Second International Conference on the Peaceful Use of Atomic Energy (Geneva, 1958). Selected reports of non-Soviet scientists. Vol. 7. The Technology of Nuclear Raw Materials [in Russian] (Moscow, Atomic Energy Press, 1959) p. 553.
32. Smiley and Brater, Proceedings of the Second International Conference on the Peaceful Use of Atomic Energy (Geneva, 1958). Selected reports of non-Soviet scientists. Vol. 7. The Technology of Nuclear Raw Materials [in Russian] (Moscow, Atomic Energy Press, 1959) p. 561.
33. Smiley and Brater, Proceedings of the Second International Conference on the Peaceful Use of Atomic Energy (Geneva, 1958). Selected reports of non-Soviet scientists. Vol. 7. The Technology of Nuclear Raw Materials [in Russian] (Moscow, Atomic Energy Press, 1959) p. 587.
34. Lawroski et al., Proceedings of the Second International Conference on the Peaceful Use of Atomic Energy (Geneva, 1958). Selected reports of non-Soviet scientists. Vol. 7. The Technology of Nuclear Raw Materials [in Russian] (Moscow, Atomic Energy Press, 1959) p. 615.

*Original Russian pagination. See C.B. translation.

35. Powell, Proceedings of the Second International Conference on the Peaceful Use of Atomic Energy (Geneva, 1958). Selected reports of non-Soviet scientists. Vol. 7. The Technology of Nuclear Raw Materials [in Russian] (Moscow, Atomic Energy Press, 1959) p. 641.
36. Cuthbert et al., Proceedings of the Second International Conference on the Peaceful Use of Atomic Energy (Geneva, 1958). Selected reports of non-Soviet scientists. Vol. 6. Nuclear Fuel and Reactor Material [in Russian] (Moscow, Atomic Energy Press, 1959) p. 551.
37. Gibson and Buddery, The Extraction and Purification of Rare Metals [Russian translation] (Moscow, Atomic Energy Press, 1960).

THE SOLUBILITY PRODUCT OF THE HYDROXIDE OF TETRAVALENT URANIUM

M. A. Stepanov and N. P. Galkin

Translated from Atomnaya Énergiya, Vol. 9, No. 4, pp. 282-285, October, 1960
Original article submitted March 18, 1960.

This article gives a calculation of the solubility product of the hydroxide of tetravalent uranium, a knowledge of which is essential for the efficient operation of many processes in the treatment of uranium and methods for determining it. The calculation is based on experimental data obtained in the potentiometric titration of a chloride solution of tetravalent uranium by alkali. The activity of the hydrogen ions was determined by a tube potentiometer LP-5; the active concentration of the quadruple charged ion of tetravalent uranium was calculated from the analytically found concentration of tetravalent uranium with an allowance for hydrolysis and the value of the ionic strength. It is shown that the required solubility product is equal to $(1.10 \pm 0.72) \cdot 10^{-52}$.

The hydroxide of tetravalent uranium is a slightly soluble compound. Knowing the value of the solubility product of this type of material, it is possible to determine its thermodynamic parameters.

The information in the literature on the solubility product of tetravalent uranium hydroxide is very contradictory. The value of the equilibrium constant given in [1]

$$U(OH)_4 \rightleftarrows U^{4+} + 4OH^- \qquad (1)$$

is equal to 10^{-45}. This value was found by a calculation method (by comparing the ionic radii and the solubility products of thorium and tetravalent plutonium) and therefore requires experimental confirmation. There are also data [2] on the solubility product of tetravalent uranium hydroxide, calculated on the basis of the reaction

$$UO(OH)_2 \rightleftarrows UO^{2+} + 2OH^-.$$

The constant of the given equilibrium is equal to $1.3 \cdot 10^{-28}$, and the change in free energy is equal to 41 kcal/mole. However, the existence of the UO^{2+} ion is open to doubt [3]. The low solubility of tetravalent uranium hydroxide is the basis for the analytical methods for separating tetravalent and hexavalent uranium [4] and also a number of technological processes [5-8]. It is therefore important to determine the solubility product of tetravalent uranium hydroxide.

The basis for determining the solubility product was the potentiometric method, one of the most reliable in this type of experiment [9]. The point of inflection of the potentiometric (more accurately the pH-metric) curve corresponds to the start of formation of the hydroxide precipitate. All the pH-metric measurements were made on a LP-5 tube potentiometer, which gives an accuracy in this range of ± 0.05 units. All hydrolysis of tetravalent uranium occurred in the pH range between 1 and 6, i.e., in the region where a linear relationship is observed between the potential and pH. The potentiometer was adjusted and checked with a series of acetate-chloride buffer solutions prepared by the method described in [9].

Chloride solutions of tetravalent uranium were used, prepared by dissolving uranium metal of 99.76% purity [10]. The insoluble residue was filtered off after being allowed to stand. The tetravalent uranium solution was kept in an opaque flask, which reduced the rate of oxidation [11]. The air was removed from the flask by oxygen-free argon [12]. The oxidation of the tetravalent uranium was checked by reaction with potassium ferrocyanide [13, 14]. During 15 days no oxidation of uranium was detected.

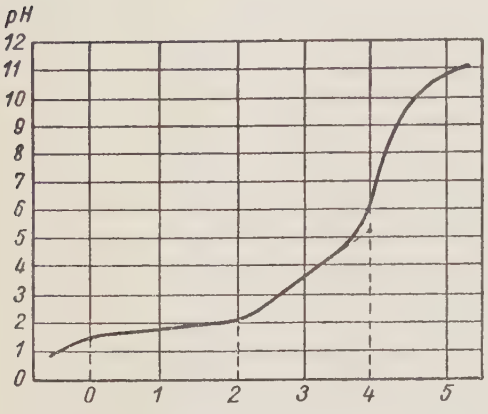

A typical curve of a pH titration of a chloride solution of tetravalent uranium with alkali. Concentration of tetravalent uranium about $1 \cdot 10^{-2}$ - $1 \cdot 10^{-3}$ g·ion/liter.

The concentration of tetravalent uranium was determined by titration with potassium bichromate. All solutions of reagents were made from analyzed chemicals and boiled distilled water. The content of excess acid was found by titration with alkali using phenolphthalein as the indicator. Allowance was made for the amount of alkali used in forming the hydroxide of tetravalent uranium. The concentration of the initial solution was 0.590 M with respect to uranium and 1.02 M with respect to hydrochloric acid. To obtain smaller concentrations of uranium, the solution mentioned was diluted with distilled water.

The precipitating agents were solutions of ammonium hydroxide, caustic soda, and caustic potash (graded "pure for analysis") of concentrations 0.464, 1.992, 2.184 N, respectively.

When carrying out the experiment, a fixed amount of initial solution was placed in a reaction vessel, into which portions of the precipitation agent were added from a microburette with continuous mixing. The pH values of the reaction medium were determined with a glass electrode in the system, 3 and 8 minutes after introducing the portion of precipitation agent. There was practically no difference between the first and second measurements of pH. When pH = 7-9 was reached, the experiment was stopped since further additions of precipitation agent led to an increase in alkali content which was not connected with hydrolysis of uranium. The dependence of pH on the amount of precipitation agent added to the system was shown graphically (see figure). The inflection points of the curve near the molar ratio of alkali to uranium equal to two corresponding to the start of formation of the hydroxide of tetravalent uranium.

It was found by the pH titration that in a solution containing $5.75 \cdot 10^{-3}$ g·ion/liter of tetravalent uranium and $3.28 \cdot 10^{-2}$ g·ion/liter of chlorine, the formation of uranium hydroxide begins at pH = 2.38 (the average from several experiments using the above precipitation agent). On the basis of these data a calculation was made of the solubility product SP of the hydroxide of tetravalent uranium: $SP = [U^{4+}][OH^-]^4$, where $[U^{4+}]$ and $[OH^-]$ are the equilibrium concentrations of the quadruple-charged ion of tetravalent uranium and hydroxyl. The calculation of the solubility product from the pH where the hydroxide begins to form is described in the literature [9, 15-17]; in particular this method was used to determine the solubility product of the hydroxide of tetravalent plutonium [1].

After substituting the ionic product of water and the concentration of hydrogen ions and converting to logarithms, we obtain a trinomial

$$pSP = npJ + pM - npH, \qquad (2)$$

in which pSP is the negative logarithm of SP; pJ is the negative logarithm of the ionic product of water; pH is the pH value for the start of formation of the hydroxide; pM is the negative logarithm of the cation concentration at the instant of formation of the hydroxide; $\underline{n}$ is the charge on the cation.

In calculating the equilibrium concentrations, allowance was made for the processes of hydrolysis and complex formation of tetravalent uranium in the solution. The following equations were used:

$$U^{4+} + Cl^- = UCl^{3+},\ K_1 = \frac{[UCl^{3+}]}{[U^{4+}][Cl^-]} = 1{,}91;$$

$$U^{4+} + 2Cl = UCl_2^{2+},\quad K_2 = \frac{[UCl_2^{2+}]}{[U^{4+}][Cl^-]^2} = 1{,}27; \qquad [18]$$

$$U^{4+} + H_2O = UOH^{3+} + H^+,\ K_3 = \frac{[UOH^{3+}][H^+]}{[U^{4+}]} = 7{,}25\cdot 10^{-2}*;$$

$$U^{4+} + 2H_2O = U(OH)_2^{2+} + 2H^+,\ K_4 = \frac{[U(OH)_2^{2+}][H^+]^2}{[U^{4+}]} = 5{,}25\cdot 10^{-3}*.$$

Using the laws of acting masses and conservation of mass together with the above equations, we obtain the polynomials

$$C_U = [U^{4+}](1 + K_1[Cl^-] + K_2[Cl^-]^2 + K_3/[H^+] + K_4/[H^+]^2), \qquad (3)$$

$$C_{Cl} = [Cl^-] + K_1[U^{4+}][Cl^-] + 2K_2[U^{4+}][Cl^-]^2, \qquad (4)$$

where C_U and C_{Cl} are the total, analytically determined concentrations, respectively, of the tetravalent uranium and chlorine.

We assume that $q = 1 + \frac{K_3}{[H^+]} + \frac{K_4}{[H^+]^2}$. Solving Eqs. (3) and (4) relative to $[Cl^-]$, we obtain the identity

$$K_2[Cl^-]^3 + (K_1 + 2K_2C_U - K_2C_{Cl})[Cl^-]^2 + (q + K_1C_U - K_1C_{Cl})[Cl^-] - qC_{Cl} = 0. \qquad (5)$$

After substituting the constants of the reactions and the values of the corresponding concentrations in identity (5), we confirm that $[Cl^-] = C_{Cl}$. Solving the system of polynomials (3) and (4) relative to the $[U^{4+}]$, we obtain

$[U^{4+}] = 1{,}79\cdot 10^{-5}$ g·ion/liter $[UOH^{3+}] = 3{,}16\cdot 10^{-4}$ g·ion/liter $[U(OH)_2^{2+}] = 5{,}42\cdot 10^{-3}$ g·ion/liter

The equilibrium active concentrations must be used in calculating the solubility product [20].

We determine the activity of the U^{4+} ion from formulas based on the Debye-Hückel theory [21],

$$a = \gamma[U^{4+}];\quad \lg\gamma = -A\sqrt{\mu};\ A = \frac{1{,}823\cdot 10^6 n_1\cdot n_2}{(\varepsilon T)^{3/2}};\quad \mu = \frac{1}{2}\sum C_i z_i^2,$$

where n_1 and n_2 are the charges on the ions forming the salt; T is the absolute temperature; ϵ is the dielectric constant of the solvent (for water this is 80 [22]); μ is the ionic strength of the solution; C_i is the total concentration of the ion i with charge z_i.

In calculating the activity of tetravalent uranium the following values were assumed: pJ = 14.07 [23]; pH = 2.38; $[U^{4+}] = 1.79\cdot 10^{-5}$ g·ion/liter; T = 293° C; A = 2.075; $\mu = 4.73\cdot 10^{-2}$ (concentrations of chlorine and ammonium ions equal to $3.28\cdot 10^{-2}$ g·ion/liter); $\gamma = 0.353$. Consequently, the activity of the quadruple-charged ion of tetravalent uranium is equal to $6.32\cdot 10^{-6}$ g·ion/liter ($pM_{active} = -\log a = 5.20$). After

* The value of the data for the equilibrium constants were obtained by extrapolation of values given in [19], to zero ionic strength and subsequent potentiometric measurement.

substituting pM_{active} in Eq. (2) we obtain pSP = 51.96.*

To calculate the absolute error in the solubility product for tetravalent uranium hydroxide we use the formula given in [24]:

$$\Delta y = \left(\frac{\delta f}{\delta \alpha_1}\right)\Delta\alpha_1 + \left(\frac{\delta f}{\delta \alpha_2}\right)\Delta\alpha_2 + \ldots,$$

where Δy is the error in the value of y, being a function of the variable α_1, α_2, ...; $\frac{\delta f}{\delta \alpha_1}$ — the partial derivative of the function f.

In the case under consideration, when the solubility product of the hydroxide is determined by Eq. (1), we have

$$\Delta SP = (J \cdot 10^{pH})^4 \{\Delta [U^{4+}] + 9{,}2 [U^{4+}] \Delta pH\}. \quad (6)$$

As mentioned above, the accuracy in measuring the pH is 0.05 units of pH. The relative error in determining the content of tetravalent uranium is due to the value of the least accurate calculated constant of hydrolysis (error 20%); consequently, $\Delta [U^{4+}] = 1{,}26 \cdot 10^{-6}$ g·ion/liter. In this case $\Delta SP = \pm 0.72 \cdot 10^{-52}$. When calculating ΔSP it is found that the error is mainly due to the error in measuring the pH of the medium.

The solubility product of tetravalent uranium hydroxide has therefore been determined by pH titration and the calculation of the equilibrium-active concentration of the quadruple charged ion of tetravalent uranium during hydrolysis. Its value is $(1.10 \pm 0.72) \cdot 10^{-52}$.

LITERATURE CITED

1. W. Latimer, The Oxidation States of Elements and Their Potentials in Aqueous Solutions [Russian translation] (Moscow, Foreign Literature Press, 1954).
2. K. Gayer and H. Leider, Nucl. Sci. Abstrs., No. 3321, 398 (1954).
3. K. Kraus and F. Nelson, J. Am. Chem. Soc. 72, 3901 (1950).
4. Tsubaki and Hara, Japan Analyst 4, 357 (1955).
5. I. Ya. Bashilov, An Introduction to the Technology of the Rare Elements [in Russian] (Moscow, State Chemical and Theoretical Press, 1932).
6. N. P. Galkin, A. A. Maiorov, and U. D. Veryatin, The Technology of Uranium Concentrate Processing [in Russian] (Moscow, Atomic Energy Press, 1960).
7. R. Gelin, G. Mogard, and B. Nelson, Proceedings of the Second International Conference on the Peaceful Use of Atomic Energy (Geneva, 1958). Selected reports of non-Soviet scientists. Vol. 7. The Technology of Nuclear Raw Material [in Russian] (Moscow, Atomic Energy Press, 1959) p. 417.
8. D. Kaufman and S. E. Bailey, The Extraction of Uranium from Ores. U. S. Patent No. 2,780,519 (1957).
9. H. Britton, Hydrogen Ions [in Russian] (Moscow, United Scientific and Technical Press, 1936).
10. The Analytical Chemistry of Uranium and Thorium. Edited by Rodden [Russian translation] (Moscow, Foreign Literature Press, 1956).
11. V. N. Ushatskii and Yu. M. Tolmachev, Trudy Radievogo Inst. 7, Khimiya i Tekhnologiya, 98 (1956).
12. K. V. Chmutov, Techniques of Physicochemical Investigations [in Russian] (Moscow-Leningrad, State Chemistry Press, 1948).
13. N. A. Tananaev and P. A. Panchenko, The Drop Method for Detecting Titanium and Uranium [in Russian] (Kiev, 1926).

* The value for the solubility product of tetravalent uranium hydroxide which we calculated previously [6] differs from this value since in the previous work no allowance was made for the hydrolysis processes.

14. N. A. Tananaev, The Drop Method [in Russian] (Moscow, State Chemistry Press, 1954).
15. I. M. Korenman, Zhur. Obshchei Khim. 25, 1859 (1955).
16. I. M. Korenman, F. S. Frum, and A. S. Kudinova, Collection of Papers on General Chemistry, Vol. 1 [in Russian] (Moscow, Acad. Sci. USSR Press, 1953) p. 83.
17. V. L. Zolotavin and V. V. Sergovskaya, Trudy Ural'skogo Politekh, In-ta, 57, 66 (1956).
18. R. Day, R. Wilhite, and F. Hamilton, J. Am. Chem. Soc. 77, 3180 (1955).
19. S. Hietanen, Acta Chem. Scand. 10, 1531 (1956).
20. A. F. Kapustinskii, Zhur. Priklad. Khim. 16, 51 (1943).
21. V. A. Kireev, A Course of Physical Chemistry [in Russian] (Moscow, State Chemistry Press, 1955).
22. D. Kay and T. Labey, A Handbook of Practical Physics [Russian translation] (Moscow, Foreign Literature Press, 1949).
23. Yu. Yu. Lur'e, Calculation Tables for Chemists [in Russian] (Moscow, State Chemistry Press, 1947).
24. N. K. Vorob'ev, V. A. Gol'shmidt, and M. Kh. Karapet'yants, Practical Physical Chemistry [in Russian] (Moscow-Leningrad, State Chemistry Press, 1950).

THE SORPTION EXTRACTION OF URANIUM FROM PULPS AND SOLUTIONS

B. N. Laskorin

Translated from Atomnaya Énergiya, Vol. 9, No. 4, pp. 286-296,
October, 1960
Original article submitted April 14, 1960

Extensive use is made of ion-exchange techniques in the uranium industry. Sorption from acid and carbonate solutions and pulps is used in the treatment of uranium ores and the production of pure compounds of uranium. This article deals with the basic regularities of these processes. It gives the characteristics of various types of ion-exchange materials, which can be used for the selective absorption of uranium, and it also deals with a number of accompanying elements. The article also describes the various types of apparatus used in the sorption of uranium from pulp, making it possible to process all pulps containing up to 40% solid material. Further improvement in sorption techniques is connected with the use of ion-exchange materials having high kinetic characteristics and high selectivity with regard to uranium.

Experience in the industrial treatment of uranium ores has shown that the extraction systems, as well as the sorption systems, are very efficient economically.

In the leaching of uranium, a large quantity of accompanying impurity goes into solution, such as iron, aluminum, magnesium, alkali metals, etc. Methods have recently been developed which considerably reduce the quantity of impurities which are dissolved when uranium ores are leached. However, in a number of cases the content of the salts in solution for various types of ores can vary over wide limits from 2 to 30%.

When most of the ore mass is separated by filtration methods, large floor areas are taken up with the filtering apparatus. In order to reduce the losses of uranium when separating the hydrate cakes of iron and aluminum, many repulping operations are needed. The most important problem in the hydrometallurgy of uranium ores is, therefore, to develop methods allowing the selective absorption of uranium from solutions and ore pulps having complex salt composition, and also the intensification of the filtration process or the development of filtrationless methods, eliminating the most laborious and power-consuming operations. These problems are best solved on the basis of sorption techniques.

Ion-Exchange Resins for Uranium Extraction

Cation-exchange materials and various types of ion-exchange materials are used in the Soviet Union for the absorption of uranium [1]. As first shown in [2], in sulfate solutions, particularly important for the hydrometallurgy of uranium ore, the uranium is present in cationic and anionic forms, the relationship between which depends on the concentrations of the sulfate ions and uranium. It can therefore be assumed that the uranium will be sorbed from sulfate solutions by cation-exchange and anion-exchange materials. This was confirmed in the study of sorption of uranium from pure solutions containing no impurities. One of the production problems which arises is sorbing uranium from solutions with a complex salt composition. For the selection and correct evaluation of sorbents which selectively absorb uranium, it is essential to have data on the effect of the salt composition on the sorption of uranium.

Only sorbents which retain an absorption capacity for uranium at high salt composition of the solutions can be of any practical interest. Figure 1 shows the relationship between the sorption capacity for uranium of a sulfo-cation-exchange material KU-2 and a carboxyl cation-exchange material type SG-1 on the concentration of sodium sulfate at pH = 3.5. As can be seen from the diagram, with a sodium sulfate concentration in the solution of more than 10 g/liter, the sorption capacity for uranium of the sulfo-cation-exchange material KU-2 (sulfonated copolymer of styrene with divinylbenzene) approaches zero, which indicates the sharp drop in sorption capacity for uranium of strongly acid cation-exchange materials with increase in the salt composition of the solution. On the basis of similar facts, workers in various countries [3] have decided on the unsuitability of cation-exchange materials for the sorption extraction of uranium. Carboxyl resins, and also other ion-exchange materials with weakly acid ion-exchange groups, have been dismissed due to the low degree of dissociation of the corresponding weakly acid ion-exchange groups in acid medium and, consequently, their low value of exchange capacity.

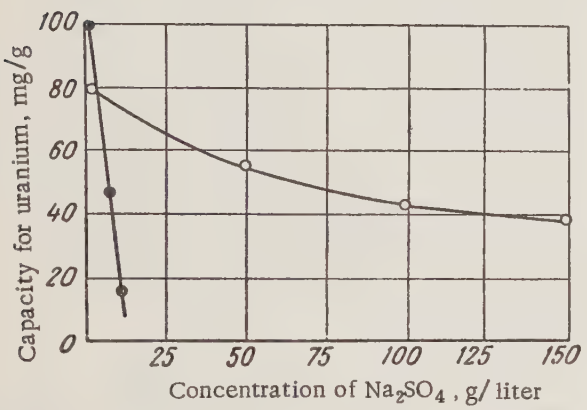

Fig. 1. The dependence of the sorption capacity for uranium of a sulfo-cation-exchange material KU-2 (●) and a carboxyl cation-exchange mat material type SG-1 (○) on the concentration of sodium sulfate .

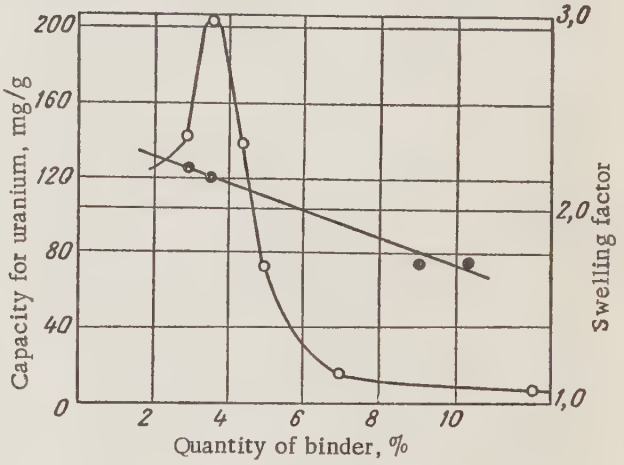

Fig. 2. The dependence of the swelling factor (●) and sorption capacity (○) for uranium of copolymers of methacrylic acid on the quantity of binder.

In 1948, the author found that carboxyl resins based on acrylic and methacrylic acids selectively absorbed uranium from weakly acid solutions containing high concentrations of salts (150 g/liter of chlorides, nitrates and sulfates). Due to the low degree of dissociation, the ion-exchange properties under these conditions are considerably depressed, and therefore the ballast impurities sorb in small quantities and the uranium, together with the ordinary ion-exchange, can be absorbed due to the formation of complexes as in the case of reaction with carboxylic acids such as oxalic or acetic acids. The industrially produced ion-exchange materials based on acrylic and methacrylic acids (KB-4, amberlite IRC-50, etc.) are intended for use in a medium close to neutral or even weakly alkaline. They contain a large amount of binder*, and due to the low capacity they are not suitable for the extraction of uranium from acid industrial solutions. The sorption capacity for uranium of copolymers of acrylic and methacrylic acids depends on the chemical nature of the binder and its quantity. This dependence was studied by the author with co-workers for various specimens of carboxyl resins synthesized on the basis of acrylic and methacrylic acids using various binders.

Figure 2 shows the dependence of the swelling factor and the sorption capacity for uranium of methacrylic acid copolymers on the quantity of binder (dimethacryl ester of ethylene glycol). It can be seen from the figure that the swelling factor increases linearly with increase in the content of binder between 1 and 12 %, whereas the maximum sorption capacity for uranium is achieved with a content of 3.5-5% binder in the copolymer – an ester of methacrylic acid and ethylene glycol or di- and triethylene glycol.

The SG-1 resin is made by the method of pearl polymerization and has high mechanical strength. It has been shown that SG-1 type copolymers in large amounts begin to sorb uranium at pH = 1.7-1.9; with further increase in pH to 3-4, the sorption capacity for uranium increases several times.

* The amount of binder means the content of transverse-binding reagent such as divinylbenzene, the dimethacryl ester of ethylene glycol, etc. (as percentages of the monomer).

Figure 3 shows the dependence on pH of the sorption capacity of SG-1 resin for uranium and some frequently encountered accompanying impurities. As follows from Fig. 3, pH = 2.8-3.5 is the optimum value in the absorption of uranium by SG-1 type carboxyl resins; in this case there is high sorption capacity for uranium and the selective properties of the sorbent are retained. With increase in the pH of the solution (up to 3.8-4.0) due to increase in the dissociation constant of the ion-exchange groups, there is an increase in the exchange capacity of the SG-1 resin. There is an increase in the absorption of accompanying impurities, which leads to a reduction of the selectivity of the copolymer for uranium.

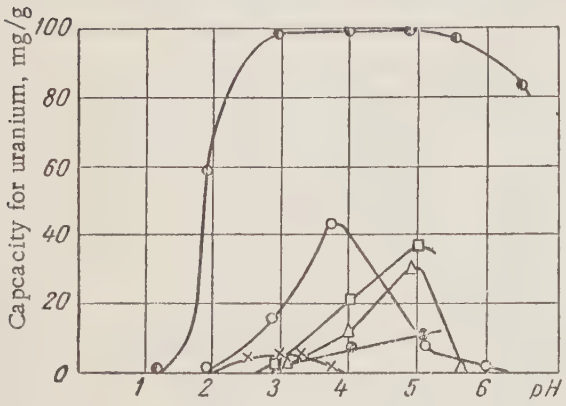

Fig. 3. The dependence of the sorption capacity of SG-1 resin for uranium and accompanying impurities on the pH of the medium. Content of impurity (g/liter): ◐) UO_2^{2+} – 1.0 (uranium); x) 0.05 Fe^{3+}; △) 2.5 Fe^{2+}; ○) 1.0 Al^{3+}; ●) 0.02 Cu^{2+}; □) 5.0 Mn^{2+}.

The trivalent iron forms rather stable complexes with copolymers such as the SG-1 resin, which are poorly desorbed under ordinary conditions of regeneration. However, at values of pH = 2.8 - 3.5 in solutions and pulps, the content of the ferric ion does not exceed 10-15 mg/liter, which is due to the low sorption capacity for it in the working range of pH values.

The divalent iron, copper, and manganese are sorbed in small quantities and this is not reflected in the value of the sorption capacity for uranium. Aluminum is sorbed by the SG-1 carboxyl resin in the range pH = = 2-5.0. With comparable concentrations of uranium and aluminum in the solution, the latter is sorbed by SG-1 resin in much smaller amounts than uranium. The uranium is able to extract from the resin the previously sorbed aluminum.

All elements which are present in solution only in the anionic form, are hardly sorbed at all by the SG-1 type carboxyl resins. The presence in these solutions of noticeable amounts of phosphate, arsenate, fluorides, and oxalates can lead to a considerable reduction in the sorption capacity for uranium of the SG-1 type resin. It should be noted that during lime neutralization of production solutions of pulps, these interfering impurities are precipitated and hence do not affect the sorption capacity of the SG-1 resin for uranium. As regards the effect of the anionic composition of the solution on the sorbability of uranium by the SG-1 resin, it should be mentioned that the presence in the solution of even 100-150 g/liter of the nitrate ion does not affect the sorbability of uranium. From solutions containing 50-100 g/liter acetate, uranium is also well sorbed by the SG-1 resin; with the equilibrium concentration of uranium at 0.08-0.2 g/liter and the sorption capacity for uranium being 100-110 mg/g.

Figure 4 gives the isotherms for the sorption of uranium by SG-1 resin from various solutions. The copolymers of SG-1 are chemically stable and are not decomposed during prolonged action of solutions with high β and γ activity. The desorption of uranium from SG-1 resin is accomplished by dilute solutions (2-3% sulfuric, nitric or hydrochloric acids).

Figure 5 gives a typical curve for the regeneration of SG-1 resin by a solution of sulfuric acid. In the process of regeneration, 90-95% of the sorbed uranium is extracted in volumes comprising 0.8-1.0 of the volume of the regenerated sorbent (the whole of the regeneration process finishes after the passage of four to five volumes), which ensures minimum consumption of chemicals for the regeneration and a high degree of concentration.

The low cost of the SG-1 type resin, its high mechanical and chemical stability, and also its large sorption capacity for uranium in its extraction from sulfate, nitrate, and chloride solutions and pulps (at pH = 2.8-3.8) have ensured the widespread use of this type of cation-exchange material.

For the sorption of uranium from sulfate, phosphate, and carbonate solutions and pulps, various types of anion-exchange materials are also used.

A statement has been made [3] on the suitability of only strongly basic anion-exchange materials such as quaternary ammonium bases for the extraction of uranium from sulfate and carbonate media. We have shown that in a number of cases, weakly basic anion-exchange materials can be successfully used to extract uranium

from solutions of complex salt composition with a large excess acidity, and also with a high content of phosphates and other interfering impurities, firmly linked to the strongly basic anion-exchange materials.

Depending on the salt composition of the solution and its excess acidity, it is possible to use weakly basic anion-exchange materials such as AN-2F, medium basic types ÉDÉ-10P, or strongly basic quaternary ammonium bases such as AM and AMP.

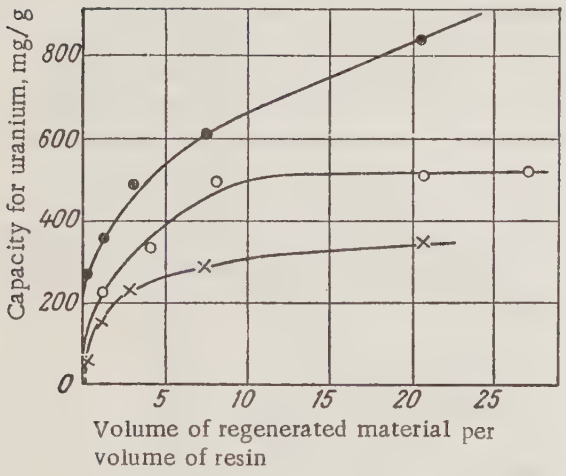

Fig. 4. Isotherms for the sorption of uranium by SG-1 resin from solutions: ●) sulfate; ○) sodium acetate ($UO_2 : CH_3COO^- = 1 : 10.8$); ×) sulfate with 50 g/liter sodium sulfate.

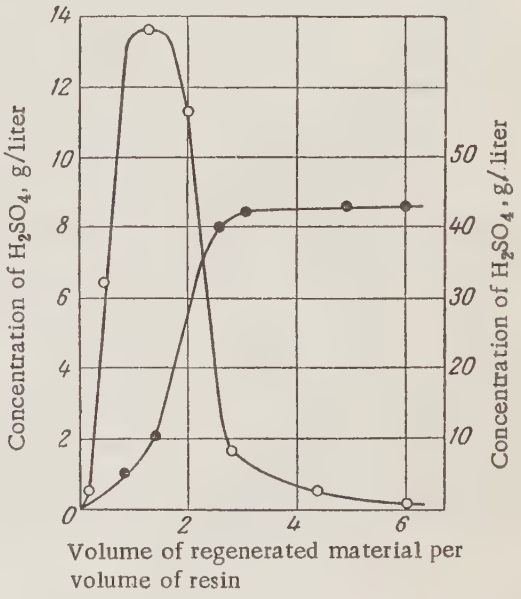

Fig. 5. Curve for regeneration of the SG-1 resin by a sulfuric acid solution: ●) sulfuric acid; ○) uranium.

The anion-exchange materials AM-2F, a product of the polycondensation of methylol derivatives of phenol and polyethylenepolyamines, can be obtained in the form of beads by the method of pearl polycondensation. It has high selectivity and sorption capacity for uranium in the absorption of uranium from solutions with a high excess acidity. The anion-exchange material ÉDÉ-10P is the product of the polycondensation of epichlorhydrin and polyethylenepolyamine. It has high sorption capacity for uranium in the extraction of uranium from phosphate solutions. The anion-exchange materials which we prepared are polymerization resins of the quaternary ammonium base type, containing a trialkylamine, pyridine or its derivative. The anion-exchange material AM is a product similar to amberlite IRA-400 or Dowex-1. The AM and AMP materials can be used in a number of cases for sorption from acid solutions with a small excess acidity (pH = 1.0-2.0) and in all cases for sorption from carbonate solutions and ore pulps.

Figure 6 shows the dependence of the sorption capacity for uranium of some anion-exchange materials on the excess acidity. With a sodium sulfate concentration of 50 g/liter, sulfuric acid 30-40 g/liter, and an equilibrium concentration of uranium of 1 g/liter the sorption capacity for uranium of AN-2F is twice that of the strongly basic AM.

The AN-2F type materials can be successfully used to extract uranium from colored solutions containing 20-50 g/liter of free sulfuric acid. With increase in the free acidity, there is a sharp drop in the absorption of trivalent iron; hence the selectivity for uranium increases. Since the sorption complex of uranium is held much more strongly than the complex of trivalent iron, then to obtain uranium concentrates of high quality before the desorption of uranium, the AN-2F material should be washed with a 1-2% solution of sulfuric acid; the uranium is hardly desorbed and the iron is almost completely removed.

Figure 7 shows the dependence of the sorption capacity for uranium and iron of AN-2F on the excess acidity. With increase in the excess acidity from 10-30 g/liter, the sorption capacity for uranium changes very little, whereas the capacity for iron falls from 60 to 10 mg/g.

Another example of the efficient use of weakly basic (AN-2F) and medium basic (ÉDÉ-10P) anion-exchange materials for the extraction of uranium is its sorption from solutions containing large amounts of phosphate ions. These solutions where the concentration of phosphoric acid reaches 150-350 g/liter are usually obtained in the treatment of uranium-containing phosphorites.

Figure 8 shows the relationship between the sorption capacity for uranium of various anion-exchange materials and the concentration of phosphoric acid in the solution.

In all cases the sorption capacity for uranium of ÉDÉ-10P is more than twice the capacity of strongly basic materials such as AM (amberlite IRA-400). Molybdates and vanadates have a very noticeable depressing action. This difference is especially noticeable when comparing the capacity of AN-2F and AM. The vanadate ion has hardly any effect on the sorption capacity of uranium on weakly basic AN-2F type materials, whereas the capacity of the strongly basic material AM under these conditions is reduced by more than a half. For example, in the sorption of uranium (concentration 0.74 g/liter) from solutions containing vanadium (concentration 0.42 g/liter), the sorption capacity for uranium of AN-2F is reduced by 7%, and AM or amberlite IRA-400 by 50 and 56%, respectively. The selection of the ion-exchange material to treat a given type of uranium ore should be made after determining the optimum conditions for leaching and after ascertaining the salt composition of the solution.

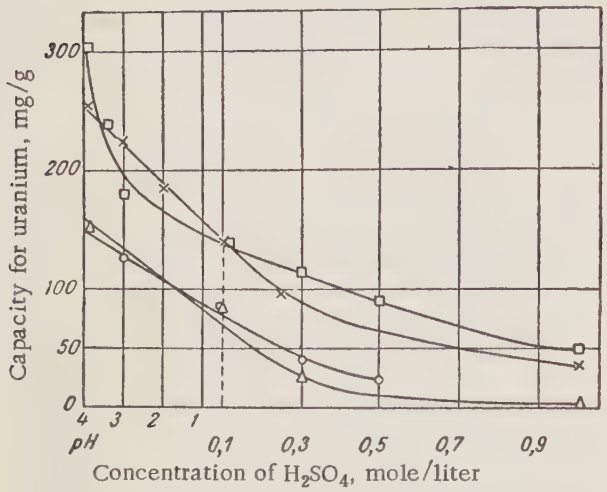

Fig. 6. The effect of excess acidity on the sorption capacity for uranium of the anion-exchange materials AN-2F (x); EDE-10P (□); AM (△) and amberlite IRA-410 (○) (concentration of uranium 0.5 g/liter).

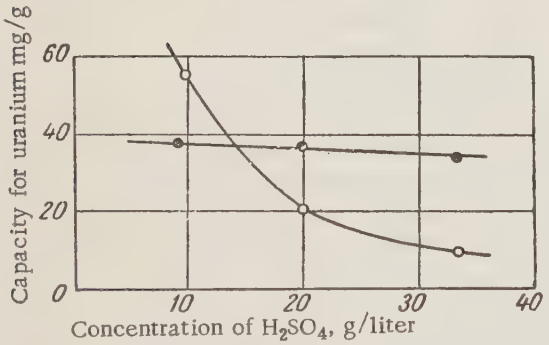

Fig. 7. The effect of excess acidity on the sorption capacity for uranium (●) and iron (○) of the anion-exchange material AN-2F.

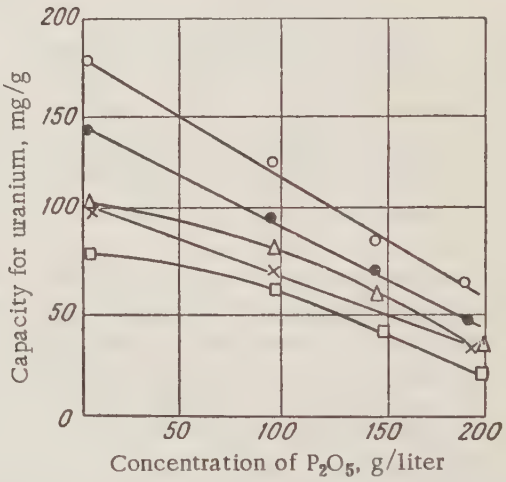

Fig. 8. The effect of concentration of phosphoric acid on the sorption capacity for uranium for various anion-exchange materials: ○) ÉDÉ-10P; ●) Wofatit L-150; △) AMP; ×) AN-2F; □) AM (concentration of uranium 1 g/liter, H_2SO_4 10 g/liter).

The various types of absorbents for uranium differ considerably from one another in their kinetic characteristics. For the SG-1 cation-exchange material, acceptable equilibrium is reached after 60-80 minutes, whereas for the AN-2F anion-exchange materials 40-50 minutes are needed and for AMP, 20-30 minutes. During desorption the equilibrium of all absorbents for uranium is established after 15-20 minutes.

The types of ion-exchange materials differ considerably in their behavior during regeneration. As can be seen from the data given in Fig. 9, 90-95% of uranium absorbed by the carboxyl resin SG-1 is desorbed by 0.8-1.0 volume of regenerating agent per volume of sorbent; and in the regeneration of AN-2F type anion-exchange materials and AMP, two to three volumes per volume of resin, respectively. The regenerating mixtures

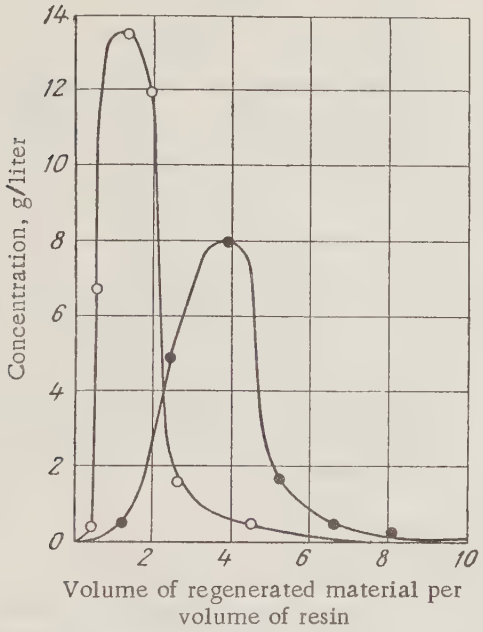

Fig. 9. Regeneration curves: ○) carboxyl resin SG-1 (by a 3% solution of sulfuric acid); ●) AN-2F (by a nitric mixture).

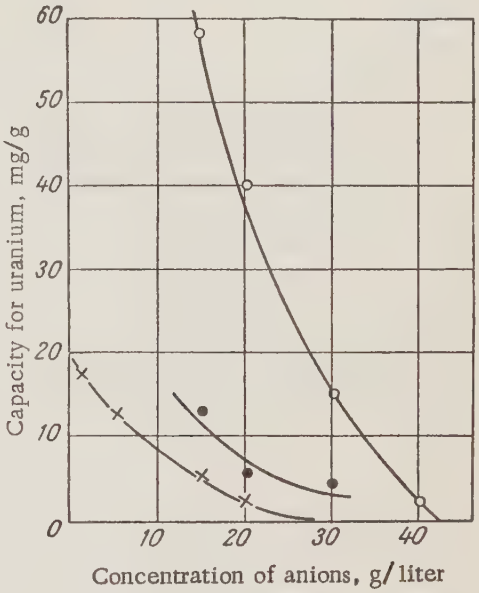

Fig. 10. The relationship between the sorption capacity for uranium of ÉDÉ-10P and the concentration of carbonates (×), bicarbonates of sodium (●) and ammonium (○).

used for the anion-exchange materials are nitrates or chlorides of sodium with the addition of the corresponding acids. The addition of small amounts of complex-forming materials somewhat improves the regeneration process and reduces the consumption of regenerating solution.

For the sorption of uranium from carbonate and bicarbonate solutions and pulps, as already mentioned, AM, AMP, and ÉDÉ-10P type resins are used. The sorption capacity of these anion-exchange materials, other conditions being equal, depends on the concentration of carbonate and bicarbonate.

Figure 10 shows the dependence of the sorption capacity for uranium of ÉDÉ-10P on the concentration of carbonates and bicarbonates of sodium and ammonium. If the carbonate solution obtained during the leaching of uranium ore is carbonated to change the carbonates to bicarbonates, the sorption capacity for uranium of the ÉDÉ-10P type anion-exchange material increases.

Figures 11 and 12 show the dependence of the sorption capacity for uranium of ÉDÉ-10P and AM materials during absorption from a carbonate solution on the concentration of depressing ions (initial concentration 1 g/liter, excess carbonate 5 g/liter, grain size + 0.3 to − 0.5 mm). It can be seen from the figures that the sorption of uranium is most reduced by chloride ions. In a 0.5 N solution of nitric ions, the sorption capacity for uranium of AM anion-exchange material is reduced by a quarter, and with the same concentration of chloride ions it is reduced to less than a fifth. The regeneration of anion-exchange materials after sorption of uranium from soda solutions and pulps should therefore be carried out by dilute solutions of soda with sodium chloride, which considerably improves this process.

The table gives a comparative evaluation of anion-exchange materials made in various countries.

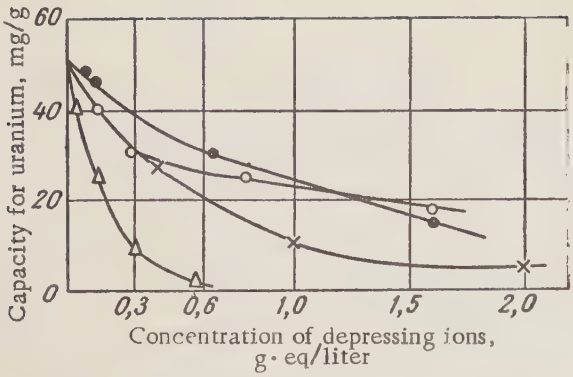

Fig. 11. Dependence of the sorption capacity for uranium of ÉDÉ-10P on the concentration of depressing ions: ●–PO_4^{3-}; ○–NO_3^-; ×–SO_4^{2-}; △–Cl^-.

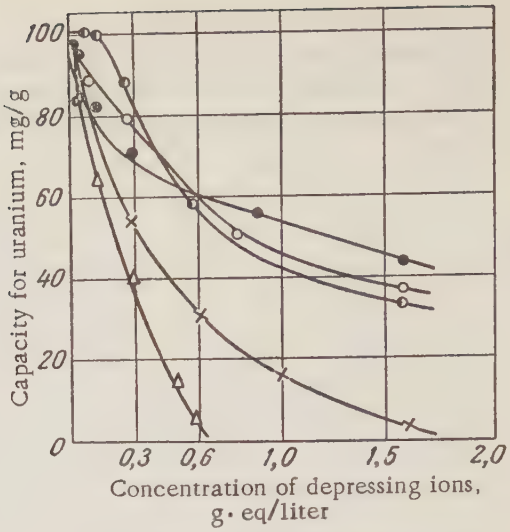

Fig. 12. Dependence of the sorption capacity for uranium of the anion-exchange material AM on the concentration of depressing ions: ◐–F^-; ○–NO_3^-; ●–PO_4^{3-}; ×–SO_4^{2-}; △–Cl^-.

The Sorption of Uranium from Clarified Solutions

In the treatments of uranium ores, clarified solutions can be obtained by percolation, filtration or counter-current decantation. The presence of small amounts of suspended particles does not hinder the process of sorption in a stationary layer. In some cases, to remove the suspended particles control filtration is used. The dynamics of sorption of uranium by various types of cation-exchange and anion-exchange materials can be described with sufficient accuracy for practical purposes by the equation of [4], used in 1929 [5] to describe the dynamics of sorption from solutions of activated carbon:

$$W = K(L - h). \tag{1}$$

In the sorption of uranium by a stationary layer of ion-exchange material after a certain volume of solution passes through the layer of sorbent, stationary transfer of the front of depletion of the ion-exchange material is established. The length of the ion-exchange layer L_0, at which the concentration of the absorbed ion changes from the initial value to c = 0 during the steady process, is called the length of the working layer. The stationary transfer of the front of depletion of the ion-exchange material will only occur on the condition that the length of the ion-exchange layer in the sorption column L is much greater than the length of the working layer L_0. In accordance with Eq. (1) the relationship of the volume W of the filtered solution of uranium on L (with the condition $L \gg L_0$) is expressed by a linear equation. The angular coefficient characterizing the slope of the straight line is equal to the coefficient of filtration action k, determining the rate of movement of the depletion front per unit of length of the ion-exchange layer. The section h cutting the straight line at one of the axes, is equal to the loss in filtration action and is directly connected with the kinetic characteristics of the ion-exchange material. In a general form the volume of the filtered solution of uranium depends on L, the static sorption capacity a, the concentration of uranium in the initial solution c_0, the rate of filtration v, the salt composition of the solution, and the pH. The theory of sorption dynamics was further developed in [6-8]. The equation of the "output curve" can be obtained from the equation of balance of the sorbed material and has the form

$$c = c_0 e^{-\frac{\beta L_0}{v}}, \tag{2}$$

where c is the concentration of the material behind the layer of ion-exchange material after passing through the filter; β is a kinetic coefficient $\left(\beta = \varrho \frac{D}{d^n}\right)$, directly proportional to the diffusion coefficient (D) of the sorbed material inside the grain of the ion-exchange material and inversely proportional to the grain diameter (d^n). The length of the working layer can be determined from (2)

$$L_0 = \frac{v}{\beta} \ln \frac{c_0}{c} = \frac{vd^n}{\varrho D} \ln \frac{c_0}{c} . \qquad (3)$$

Sorption Capacity of Various Anion-Exchange Materials for Uranium

Anion-exchange material	Country	Active ionogenic groups	Compositions of solutions				
			1 g/liter uranium (pH = 1.0)	1 g/liter uranium 50 g/liter Na_2SO_4 (pH = 1.0)	1 g/liter uranium 30 g/liter H_2SO_4	1 g/liter uranium 30 g/liter H_2SO_4, 50 g/liter Na_2SO_4	1 g/liter uranium 30 g/liter H_2SO_4, 136 g/liter H_3PO_4
AN-2F	USSR	$-NH_2$; $=NH$; $\equiv N$	84	64	32	24	20
ÉDÉ-10P	USSR	$=NH$; $\equiv N$; $\equiv \overset{+}{N}$	80	70	70	60	60
AMP	USSR	$-\overset{+}{N}\left(\begin{smallmatrix}\diagup\\ \diagdown\end{smallmatrix}\right)$	86	82	20	10	10
AM	USSR	$-\overset{+}{N}(CH_3)_3$	73	64	13	8	8
Wofatit	E. Germany	$\equiv \overset{+}{N}$; $\equiv N$; $=NH$	96	70	67	60	55
Wofatit	E. Germany	$-\overset{+}{N}(C_2H_5)_3$	68	40	8	4	5
Amberlite	USA	$-\overset{+}{N}(CH_3)_3$	82	72	20	16	18
Dowex 1-X8	USA	$-\overset{+}{N}(CH_3)_3$	88	80	20	15	15
Dowex 2-X8	USA	$-\overset{+}{N}\begin{smallmatrix}C_2H_4OH\\(CH_3)_2\end{smallmatrix}$	82	76	20	14	15
Deacidite FF	Britain	$-\overset{+}{N}(CH_3)_3$	88	80	20	7	20

From the shape of the output curve (sloping steeply or gently), it is therefore possible to obtain an idea of the kinetic characteristics of the ion-exchange material or, by determining the value of β, to determine L_0 from Eq. (3). Equations (1) to (3) can be used in the analysis of data on the dynamics of sorption of uranium from acid and carbonate solutions on carboxyl resin and anion-exchange materials and in calculations of sorption apparatuses.

In accordance with Eqs. (2) and (3) in the sorption of uranium from clarified solutions by a stationary layer of ion-exchange material, it is essential to use the smallest possible grain size of the ion-exchange material. It has been found that during the sorption of uranium from solutions in large industrial columns, the ion-exchange material grain size should be between + 0.2 and − 0.8 mm. The optimum rate of flow of the solution during passage through a layer of ion-exchange material changes somewhat depending on the salt composition of the solution, the concentration of uranium, and the type of ion-exchange material and is between 6 and 12 m /hr.

For the maximum use of the sorption capacity for uranium of the ion-exchange material, the concentration of uranium behind the layer of ion-exchange material before the column is disconnected for regeneration should be equal to the initial concentration in the solution, i.e., $c/c_0 = 1$. To ensure a closed sorption-desorption cycle (providing continuous treatment of the solutions) with a minimum number of sorption columns, L should be not less than 1.5-2.5 m. The number of columns used in the sorption-desorption cycle can also vary, depending on the salt composition and the excess acidity of the solution. Depending on the output of the unit, sorption columns of 30-35 m^2 cross section can be used. The use of small cross section sorption columns (3-5 m^2) in installations with high productivity is economically undesirable, since apart from the increase in capital expenses, there is an increase in the operating costs and the automation of the whole production process. The desorption of uranium for various types of ion-exchange materials is carried out at a flow rate of 3-8 m/hr. With increase in L there is a decrease in the volume of the desorbed solution. The latter is divided into three or four fractions; the main fraction, containing 90-95% sorbed uranium, is taken out for further treatment, the remaining two or three fractions are returned and used for the desorption of uranium from the next column. The main impurity in the concentrates when using SG-1 resin is aluminum, the content of which can reach 10-12%, and when using the anion-exchange materials AN-2F, AM, and AMP it is iron, the content of which reaches 5-12%. To obtain high-purity uranium compounds it is possible to use sorption or extraction purification of commercial fractions of regeneration materials using tributyl phosphate (TBP) or trioptyl amine (TOA).

The Sorption Extraction of Uranium from Ore Pulps

In 1953, the author proposed a filtrationless method for treating uranium ores, consisting of the suspension of precipitate or finely ground material in which the uranium was distributed between solid and liquid phases. A granular sorbent was added which selectively absorbed the product to be extracted. After absorption of uranium by the sorbent from the solid and liquid phases of the pulp, it was separated by means of a mesh or in a rising stream. Almost at the same time and independently, the method of sorption of uranium from pulps by strongly basic anion-exchange materials was developed by American scientists [9].

We have now tested several variants of sorption filtration-less systems for processing uranium ores, differing in the arrangement of the apparatus. The main regularities of sorption of uranium by ion-exchange materials from solutions are fully preserved for processes of sorption from pulps containing up to 40-50% of solid material. Sometimes a difference is observed in the kinetic characteristics due to the fact that the attainment of equilibrium in the system depends not only on the concentration of uranium in the solution, but also on the kinetics of its desorption from the solid phase of the pulp. Uranium which has been put into solution during leaching is quantitatively extracted from all types of ore pulps; in a number of cases additional extraction is observed during the sorption treatment of pulp. The treatment of pulp by a resin which selectively absorbs uranium is similar to very efficient repulping.

To achieve maximum efficiency in the sorption process during the preparation of the ore pulp, it is essential to ensure the maximum possible concentration of uranium in it, minimum excess acidity or carbonate content, and minimum amount of salts which are also dissolved during leaching.

The process of sorption from pulps can be carried out in reactors with an impeller stirrer, Pachuca tanks, or in special sorption apparatuses.

The variants of the method for sorption of uranium from ore pulps can be put into two main types: the static method and the dynamic method of sorption of uranium from pulps in fluidized bed of sorbent.

The sorption of uranium from ore pulps by the static method is carried out in ordinary reactors, Pachuca tanks, or in special sorption apparatuses. The resin and pulp are separated on screens of various designs. At each part of the sorption a stage is reached which is close to equilibrium (by analogy with the static sorption experiment of this type the arrangements are called static). The larger the stages of sorption, the larger the value of

the sorption capacity, since the equilibrium concentration approaches the initial value. However, the maximum permissible number of sorption stages is limited by economic considerations. Continuous and batch sorption processes for treating uranium ores have been established.

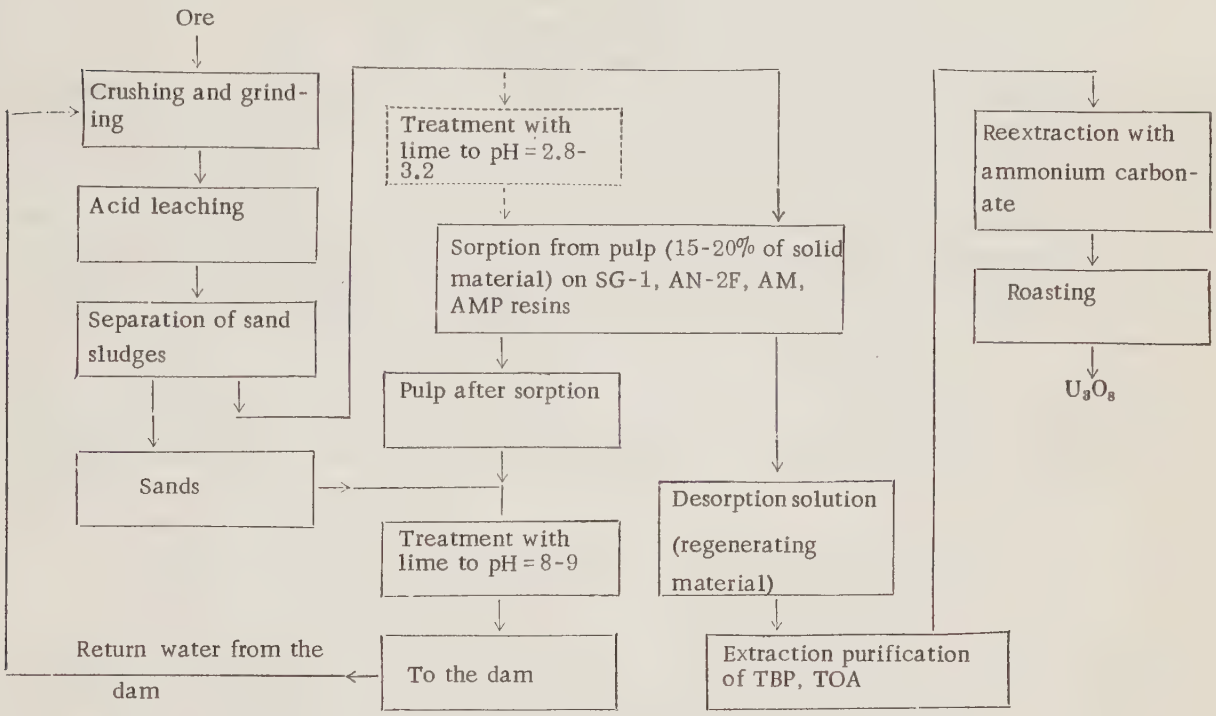

Fig. 13. Flow sheet for the treatment of ore pulps in a fluidized bed of sorbent.

The sorption of uranium from a pulp is carried out according to a continuous countercurrent 3- or 4- stage system. With the dynamic method of sorption of uranium from pulps in a fluidized bed of sorbent (Fig. 13), the preparation of the ore pulp (grinding, leaching, and classification) is carried out as in the case of other sorption systems. The pulp, after careful separation of sands and control screening, is fed to the sorption columns from the bottom to the top at a rate which ensures the formation of a fluidized bed of sorbent. The uranium is sorbed during passage of the pulp through a fluidized bed of sorbent. The coefficient of expansion depends on the density and viscosity of the ore pulp and also on the speed of the "rising" stream. When using the process of sorption from pulp in a rising stream, it is very important to have an ion-exchange material with a high specific gravity. In production specimens of ion-exchange materials the main fraction held is that with a specific gravity of 1.20-1.25 g/cm^3. Ion-exchange materials of higher specific gravity are more difficult to obtain. With the method of sorption in a fluidized bed of sorbent it is possible to process ore pulps containing 10-20% of solid material.

Further improvement in the sorption methods for extracting uranium can be achieved by introducing the following measures:

1) reducing the consumption of resin in the continuous arrangements for sorption of uranium from ore pumps;

2) intensifying processes of sorption and desorption due to the use of ion-exchange materials with high kinetic properties;

3) developing sorbents with high selectivity and sorption capacity for uranium;

4) reducing the consumption of chemicals when using new methods of desorption and separating pure compounds of uranium;

5) combining processes of leaching and sorption of uranium from pulps.

LITERATURE CITED

1. D. I. Ryabchikov and M. M. Senyavin, Material of the International Conference on the Peaceful Use of Atomic Energy (Geneva, 1955), Vol. 8 [in Russian] (Moscow, Metallurgy Press, 1958) p. 328.
2. C. Diffrich, Phys. Chem. 29, 499 (1899).
3. Preuss and Kunin, Material of the International Conference on the Peaceful Use of Atomic Energy (Geneva, 1955), Vol. 8 [in Russian] (Moscow, Metallurgy Press, 1958) p. 60.
4. N A. Shilov, L. K Lepin', and S. A. Voznesenskii, Zhur. Russ Khim. Obshchestva 51, 1107 (1929).
5. S. A. Voznesenskii, Physicochemical Processes in the Purification of Water [in Russian] (Moscow, State Construction Press, 1934).
6. M. M. Dubinin, Physicochemical Fundamentals of Sorption Technology [in Russian] (Moscow, State Chemical and Technical Press, 1932).
7. A. A. Zhukhovitskii, A. N. Tikhonov, and Ya L. Zabezhinskii, Zhur. Fiz. Khim. 19, 253 (1945).
8. N. N. Tunitskii and E. P. Cherneva, Zhur. Fiz. Khim. 24, 11, 1350 (1950).
9. Hollis and McArthur, Material of the International Conference on the Peaceful Use of Atomic Energy (Geneva, 1955), Vol. 8 [in Russian] (Moscow, Metallurgy Press, 1958) p. 71.

LETTERS TO THE EDITOR

ENERGY DEPENDENCE OF THE DIFFERENTIAL CROSS SECTIONS AND MECHANISM OF THE (d, p) REACTION

V. B. Belyaev, B. N. Zakhar'ev, and V. G. Neubachin

Translated from Atomnaya Énergiya, Vol. 9, No. 4, pp. 298-299, October, 1960
Original article submitted February 10, 1960

In a number of articles [1], the ratios of the reduced widths of the γ^2 levels obtained from the (d, p) reaction data are used as spectroscopic characteristics in discussions of nuclear models. The calculation of γ^2 from the differential cross sections of the (d, p) reaction is carried out by means of the Born approximation formula for the stripping mechanism [2, 3]

$$\frac{d\sigma}{d\Omega}=\frac{2J+1}{2j+1}\frac{k_p}{k_d}\frac{M_f}{M_f+M_n}\frac{M_i}{M_i+M_d}4\pi N_d^2\quad\sum\left|\frac{1}{Z}\left(\frac{1}{\alpha^2+K^2}-\frac{1}{\beta^2+K^2}\right)\quad(j'_e-g_e i_e)\right|^2\frac{2Mc}{\hbar^2}\gamma^2.$$

If the stripping mechanism were unique, the Born approximation with distorted waves [3] would be a good one, since the deformation of the internal wave function of the deuteron is evidently not very great [4]. Meanwhile, the experimental results connected with the investigation of forbidden stripping [5] indicate that in the (d, p) reaction with a deuteron energy of the order of several million electron-volts, and knock-on of a proton by a deuteron with the capture of the deuteron is an important process [the (d, p) reaction is of this type]. In those cases in which ordinary stripping is allowed, the angular distribution of the reaction products can differ little from the Butler distribution, since for a knock-on process it is characterized, as in the case of stripping, by a maximum at small angles. The cross section of the knock-on effect, however, is described by a formula of a type different from that in the case of stripping and with a different energy dependence [6, 7]. In the analysis of the energy distribution of the (d, p) reaction cross section, it is convenient to use the Born approximation formula for stripping [2] and to investigate the dependence of the quantity γ^2 appearing in this formula in the form of a multiplier of the energy. If the stripping mechanism were basic, then the dependence of γ^2 on E_d obtained by means of the Butler formula would have the form of a monotonic, smoothly increasing curve tending to a limit for E_d greater than the barrier height for deuterons. The height of the barrier depends, of course, on the charge of the nucleus and the orbital angular momentum of the captured neutron.* In the presence of the competitive processes indicated above, the energy dependence will be different and will not be connected so simply with the reduced widths.

For the analysis of the experimental data, we have chosen cases with a sufficiently large deuteron energy ($E_d > 4$ Mev) in order to decrease the role of the various corrections to the Butler formula, for example, Coulomb corrections.

The results of experiments for various reactions are presented in the table.

* The effect of the distortion of the proton and deuteron waves due to the nuclear interaction between the proton and the deuteron can be neglected if Bowcock's method is used.

The dependence of the relative reduced widths γ^2 on E_d are of the order 50%, and the errors for the relative values are much less (about 10%).

As can be seen, both the relative and absolute values of the reduced widths, in a number of cases, vary with E_d. The change in γ^2 with E_d was noted previously [18], but it was not analyzed, owing to insufficient data.

Experimental Results for Different Reactions

Reaction	Level of final nucleus Mev	Level spin and parity	Transition characteristic	Reduced widths * E_d, Mev				
				8 [2]	8,9 [9]	9 [10]	14,8 [11]	19 [12]
$C^{12}(d, p)C^{13}$	ground state	$1/2^-$	$p^8 \rightarrow p^9$	2,2	1,3	1,2	1,9	0,9
	3,09	$1/2^+$	$p^8 \rightarrow p^8 s_{1/2}$	3,0	3,8	6,5	8,3	1,6
	3,684	$3/2^-$	$p^8 \rightarrow p^9$	0,16	0,48	0,38	0,28	—
	3,855	$5/2^+$	$p^8 \rightarrow p^8 d_{5/2}$	3,5	2,6	1,4	5,7	1,1
				3,6 [2]	9 [10]	14 [13]		
$Be^9(d, p)Be^{10}$	ground state	0^+	$p^5 \rightarrow p^6$	1,2	22 (relative)	0,093 **	—	—
	3,37	2^+	$p^5 \rightarrow p^6$	0,19	8 (relative)	0,012 **		
				4,11 [14]	7,7 [2]	7,73 [15]	9 [10]	19,1 [15]
$O^{16}(d, p)O^{17}$	ground state	$5/2^+$	$p^{12} \rightarrow p^{12} d_{5/2}$	0,66	1,0	2,5	3 (relative)	1,8
	0,875	$1/2^+$	$p^{12} \rightarrow p^{12} s_{1/2}$	1,1	2,6	7,0	9 (relative)	3,7
				8 [2]	9 [10]	14,8 [17]		
$N^{14}(d, p)N^{15}$	ground state	$1/2^-$	$p^{10} \rightarrow p^{11}$	2,1	—	1,0	—	—
	6,33	$3/2^-$	$p^{10} \rightarrow p^{11}$	—	0,23	0,18		
	8,32	$1/2^+$	$p^{10} \rightarrow p^{10}_{1/2}$	11,5	4,5	5,4		

* All results except those denoted by (**) are in units of 10^{-19} erg/cm

** The results are in units of $3\hbar^2/(2ma)$

It is interesting that, in the examples considered, there are cases in which 1) the captured neutron is outside a filled shell (capture of s and d neutrons by C^{12} and O^{16}), and 2) the captured nucleon is simply added to the unfilled shell (in all cases of neutron capture considered above, $l = 1$). These cases have the following differences: 1) in the first case, the remaining direct processes (proton knock-on by a deuteron and stripping of a heavy particle) are difficult (in comparison with ordinary stripping); the cause for this lies not only in the binding energy of the core nucleons, but also in the fact that when a deuteron is captured, one of its nucleons should lie in the 1p orbit and the other in the 1d or 2s orbit; 2) the ratio of the two reduced widths in the Born approximation for processes in the second case will be practically constant, and for processes in the first case (where the widths are compared for the capture of a neutron with different l) it will change slightly with the energy. We see that the data in the table apparently reflect both these circumstances. In fact, for the case of the capture of p nucleons, the change in the reduced widths is sharper, which, perhaps, indicates the role of other direct processes. It should, however, be noted that the data used in our work was obtained at different times and by different authors; this reduces their accuracy. But in any case, analysis shows that, first, the use of the reduced widths in Butler's formulas for quantitative spectroscopic purposes is not entirely reliable, and second, it is of great interest to carry out a series of experiments in which the dependence of the absolute differential cross sections on the energy is studied. It will be very important to increase the accuracy of the experimental data, which will make it possible to obtain information on the mechanism of the (d, p) reaction, supplementing the results of the investigations of forbidden stripping and stripping of heavy particles.

LITERATURE CITED

1. T. Averbach and J. Freuch, Phys. Rev. 98, 1276 (1955); K. Standing, Phys. Rev. 101, 152 (1956); B. Flauers, Proceedings of the All-Union Conference on Nuclear Reactions at Low and Medium Energies [in Russian] (Moscow, Acad. Sci. USSR Press, 1958) p. 536.
2. S. Yoshida, M. Fujimoto, and H. Kikuchi, Progr. Theor. Phys. 11, 264 (1954).
3. W. Tobocman, Phys. Rev. 94, 1655 (1954); W. Tobocman and M. Kalos, Phys. Rev. 97, 132 (1955).
4. W. Tobocman, Phys. Rev. 108, 74 (1957); K. A Ter-Martirosyan, Zhur. Éksp. Teor. Fiz. 29, 713 (1955).
5. N. Evans and W. Parkinson, Proc. Phys. Soc. 67A, 684 (1954).
6. A. French, Phys. Rev. 107, 1655 (1957); N. Evans and A. French, Phys. Rev. 109, 1272 (1958).
7. V. G. Neudachin, Zhur. Éksp. Teor. Fiz. 35, 1166 (1958).
8. J. Bowcock, Proc. Phys. Soc. 68, 512 (1955).
9. F. El Bedew, Proc. Phys. Soc. 69A, 3, 221 (1956).
10. T. Green and R. Middleton, Proc. Phys. Soc. 69A, 1, 28 (1956).
11. R. Freemantle, W. Gibson, and J Rotblat, Phil. Mag. 45, 370, 1200 (1954).
12. J. McGruer, E. Warburton, and R. Bender, Phys. Rev. 100, 1, 235 (1955).
13. J. French and A. Fujii, Phys. Rev. 105, 2, 652 (1957).
14. E. Baumgartner and H. Fulbreit, Phys. Rev. 107, 1, 219 (1957).
15. W. Fairbairn, Proc. Phys. Soc. 67, 564 (1954).
16. E. Warburton and J. McGruer, Phys. Rev. 105, 2, 639 (1957).
17. G. Owen and L Madansky, Phys. Rev. 105, 1766 (1957).
18. T. Fulton and G. Owen, Phys. Rev. 108, 789 (1957).

HIGH ENERGY γ-RAY BEAMS

V. S. Barashenkov and Hsien Ting-ch'ang

Translated from Atomnaya Énergiya, Vol. 9, No. 4, pp. 300-301, October, 1960
Original article submitted April 4, 1960

It is known that experiments with high-energy γ quanta are of great interest for the investigation of the structure of elementary particles and for verifying electrodynamics at small distances [1].

In order to obtain hard γ quanta, one ordinarily uses electron accelerators. The maximum energy of the γ quanta obtained in this way is 1.06 Bev (the Stanford linear accelerator). Intense beams of still harder γ quanta can be obtained from the large proton accelerators: the Joint Institute of Nuclear Studies' proton synchrotron at Dubna and the recently finished accelerator in Geneva. The main source of γ quanta in these accelerators is the decay of π° mesons generated in collisions between the accelerated protons and nucleons of a target.

Statistical calculations show that the number of γ quanta produced in a single nucleon-nucleon collision is, on the average, equal to the number of charged π mesons produced in the collision. From Fig. 1, in which the results of these calculations are shown, it is seen that the intensity of γ-quanta beams can be very great.

If the π°-meson distribution is described by the function W_π (p; θ), where p is the momentum and θ is the angle of emission of the π° mesons produced in nucleon– nucleon collisions, then the corresponding distribution of the γ quanta is expressed by the function

$$W_\gamma(k;\,\theta) = 2\int_K^{P_{max}} W_\pi(p;\,\theta)\,\frac{dp}{\sqrt{p^2+\mu^2}} \simeq 2\int_k^{P_{max}} W_\pi(p;\,\theta)\,\frac{dp}{p},$$

where $K = \sqrt{k^2(1+k_0^2/k^2)-\mu^2}$; $\underline{k}$ and θ are the energy and angle of emission, respectively, of the γ quanta in the laboratory system; k_0 is the energy of the γ quanta in the π° meson rest system; μ is the π° meson mass.

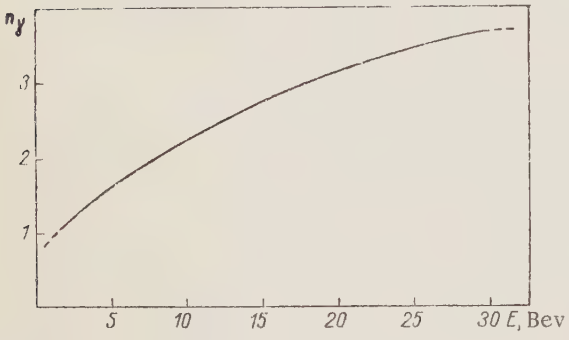

Fig. 1. Mean number of γ quanta produced in the decay of π° mesons generated in a single nucleon-nucleon collision (n_γ). (E is the kinetic energy of the accelerated protons in the laboratory system.)

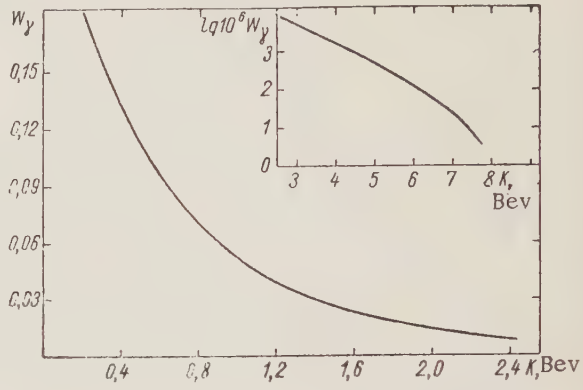

Fig. 2. Energy spectrum of γ quanta integrated over all angles [$W_\gamma \equiv W_\gamma$ (k)]. At high energies the values of log [10^6 W_γ (k)] are given ($\underline{k}$ is the γ-quanta energy in the laboratory system.)

This formula is applicable for $k \gtrsim 0.5$ Bev, but it can also be used for estimations at energies $k \simeq$ $\simeq 0.2$ Bev [2].

Since the experimental values of the function W_π (p; θ) for the Joint Institute of Nuclear Studies' proton synchrotron are not known at the present time, we calculated this function by means of the statistical theory of multiple production of particles (accelerated-proton kinetic energy E = 10 Bev).

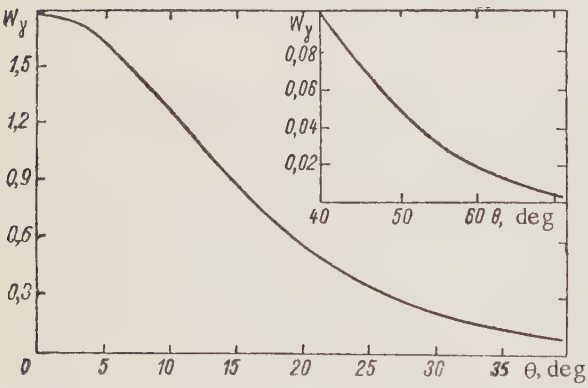

Fig. 3. Angular distribution of γ quanta integrated over all energies [$W_\gamma \equiv W_\gamma$ (θ)]. (θ is the scattering angle in the laboratory system.)

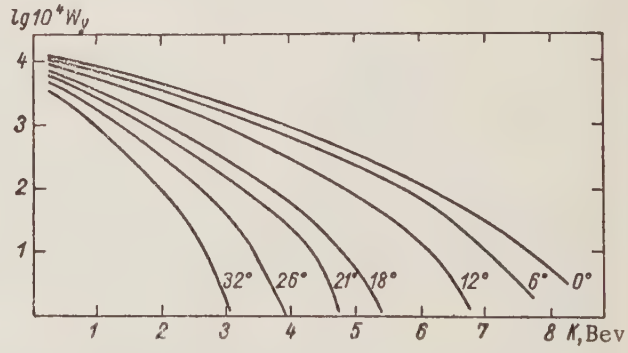

Fig. 4. Energy spectrum of γ quanta for different angles [$W_\gamma \equiv W_\gamma$ (k; θ)]. ($\underline{k}$ is the γ-quanta energy in the laboratory system.)

Figures 2 and 3, respectively, show the calculated spectrum and angular distribution of the γ quanta:

$$W_\gamma(k) = 2\pi \int_0^\pi W_\gamma(k;\ \theta) \sin\theta\, d\theta,$$

$$W_\gamma(\theta) = \int_{0,2}^{k_{max}} W_\gamma(k;\ \theta)\, dk.$$

Figure 4 shows the calculated spectrum of γ quanta W_γ (k; θ) for various angles θ. (In all cases the angle θ is the angle of emission of the γ quanta with respect to the direction of the accelerated proton beam.)

For the function W_γ (k; θ), we carry out the normalization

$$2\pi \int_0^\pi \sin\theta\, d\theta \int_0^{k_{max}} W_\gamma(k;\ \theta)\, dk = 1.$$

As can be seen, the basic part of the γ radiation is concentrated in the small-angle region. With an increase in the γ-quanta energy, the intensity of the radiation drops rapidly. *

In conclusion, we consider it our duty to thank M. A. Markov, on whose initiative we carried out the calculations, for discussion and advice, and V. I. Veksler for valuable comments in the discussion of the results.

LITERATURE CITED

1. I. M. Zlatev and P. S. Isaev, Nuovo cimento 13, 1 (1959); Zhur. Éksp. Teoret. Fiz. 37, 1161 (1959); V. A Petukhov, A. A. Komar, and M. I. Yakimenko, Joint Institute of Nuclear Studies, Preprint R-283 (1959); D. I. Blokhintsev, V. S. Barashenkov, and B. M. Barbashov, Uspekhi Fiz. Nauk 68, 417 (1959).
2. R. Sternheimer, Phys. Rev. 99, 277 (1955).

* The intensity of the γ radiation also drops rapidly as $k \to 0$. This part of the spectra is not shown in the figures.

EFFECTS OF THE LEAKAGE FIELDS OF A SECTIONAL MAGNET ON THE DOUBLE FOCUSING OF A BEAM

Yu. A. Kholmovskii

Translated from Atomnaya Énergiya, Vol. 9, No. 4, pp. 301-303, October, 1960
Original article submitted May 4, 1960

In a number of articles [1-3] devoted to the double focusing of a beam of charged particles by a sectional magnetic field, it is assumed in the derivation of the horizontal focusing conditions that there is no leakage field (the magnetic field at the edge of the magnet suddenly drops to zero from the homogeneous field intensity). In derivation of the vertical focusing conditions, the leakage field region is considered to be so narrow that the vertical coordinate and approach angle of the particle trajectory in it do not have time to change.

In the present work, the influence of the leakage field on the vertical focusing of charged particles is investigated, and a method of calculating a sectional magnet with double focusing with allowance for the leakage field is presented.

The influence of the leakage field on the horizontal focusing of sectional magnets is considered in [4]. It is readily shown that the variation of the angle of approach of the particle trajectory, as the particle travels through the leakage field, can be determined from the expression

$$\sin\varepsilon_e-\sin\varepsilon_e=\frac{\delta}{\varrho_0}\int_{y_b}^{y_e}\frac{H}{H_0}\,d\left(\frac{y}{\delta}\right), \tag{1}$$

where ϵ_b is the angle between the normal to the edge of the magnet and the tangent to the trajectory at the point of entry into the leakage field (the angle of approach at the beginning of a leakage field); ϵ_e is the angle of approach at the end of the leakage field; ρ_0 is the radius of curvature of the particle trajectory in a homogeneous field; y_b and y_e are the coordinates of the trajectory at the beginning and end of the leakage field, respectively; H_0 is the homogeneous field intensity; H is the field intensity at an arbitrary point of the leakage field; δ is the air gap between the poles; y is the coordinate of the particle.

If the law according to which the field intensity drops at the edge of the magnet is known, then the integral $\int_{y_b}^{y_e}\frac{H}{H_0}\,d\left(\frac{y}{\delta}\right)$ can be calculated. It is simpler, however, to replace the decreasing field by a homogeneous one with intensity H_0. The width of the homogeneous field b/δ is chosen so that $\int_{y_b}^{y_e}\frac{H}{H_0}\,d\left[\frac{y}{\delta}\right]=\frac{b}{\delta}$. The boundary of the resulting field is then at a distance κ/δ from the edges of the pole-faces (Fig. 1). The axis of ordinates on this figure coincides with the boundary of the pole. In practice, κ/δ is determined as the difference between the areas F_1 and F_2, and, for the usual magnet designs, it is equal to 0.6-0.7.

In the region of the leakage field, the particles move along a complicated curve. As a result, the real trajectory is displaced with respect to the calculated one by a distance a. In general form

$$a=y_e\operatorname{tg}\varepsilon_e+\varrho_0(\cos\varepsilon_b-\cos\varepsilon_e)-\int_{y_b}^{y_e}\frac{\sin\varepsilon_0+\int_0^y\frac{dy}{\varrho}}{\sqrt{1-\left(\sin\varepsilon_0+\int_0^y\frac{dy}{\varrho}\right)^2}}\,dy.$$

The quantity a was calculated by a graphical-analytical method for a given range of values of δ/ρ and approach angles of the trajectories ϵ_e (or ϵ_b). The results of the calculations are shown in Fig. 2. From this figure it is seen that for large δ/ρ_0 and ϵ_e, the displacement essentially depends on ϵ_e, which leads to the increasing of the focal distance, and to additional spreading of the focus. For small δ/ρ_0 and ϵ_e, this effect only increases the focal distance. The calculations show that for $\rho/\delta_0 \leq 0.1$ and $\epsilon_e \leq 10°$, the increase in the focal distance does not exceed 1%.

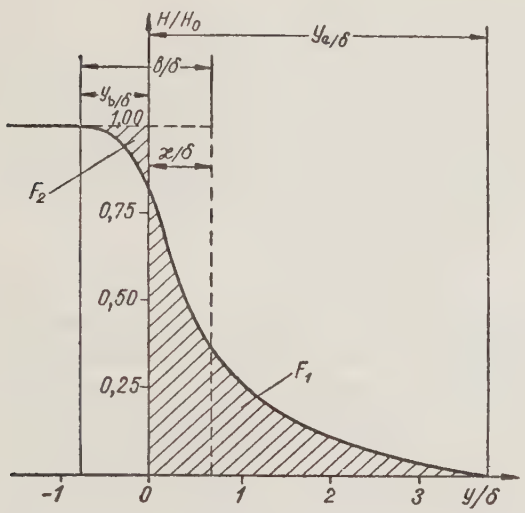

Fig. 1. Variation of the magnetic-field intensity at the edge of the magnet.

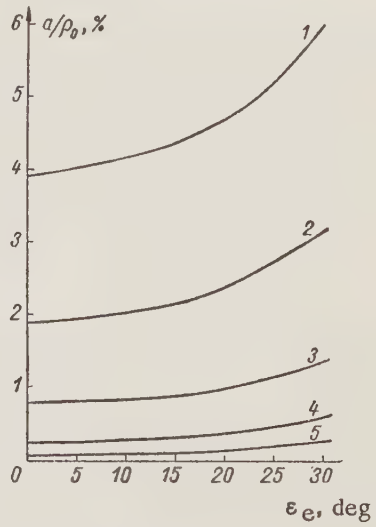

Fig. 2. Dependence of the size of the "drift" on the approach angle for different values of the parameter δ/ρ_0: 1) 0.32; 2) 0.22; 3) 0.14; 4) 0.08; 5) 0.04.

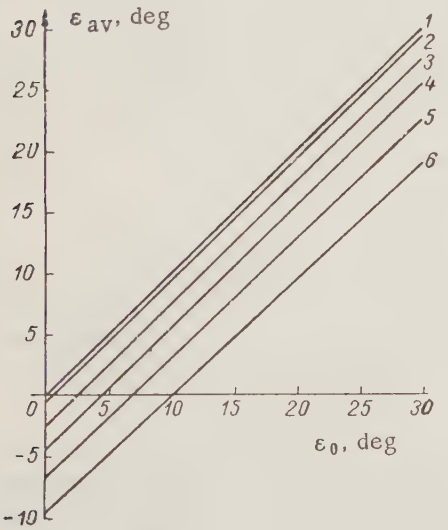

Fig. 3. Dependence of the average approach angle on the initial approach angle for various values of the parameter δ/ρ_0: 1) 0; 2) 0.02; 3) 0.08; 4) 0.14; 5) 0.22; 6) 0.32.

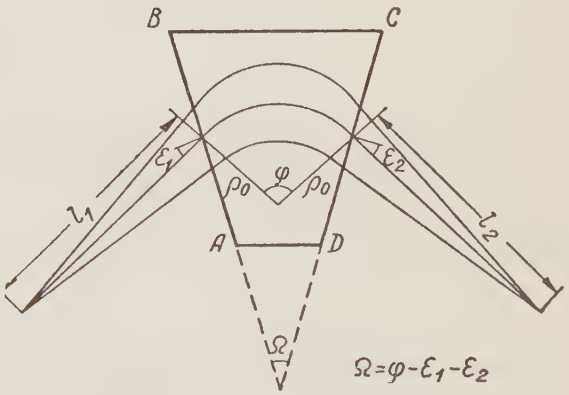

Fig. 4. Horizontal focusing by a sectional magnetic field.

Influence of the leakage field on the vertical focusing. As shown by the calculations, the conditions of vertical focusing given in [1] and [2] are valid only in the case of a long-focus system ($\delta/l \leq 0.05$) for $\delta/\rho_0 \leq 0.02$). For $\delta/\rho_0 \geq 0.02$, the basic error in the calculations of such systems is contributed by the change in the approach angle ϵ, while the

change in the vertical coordinate plays a secondary role. The change in the angle is taken into account by the fact that in the vertical focusing conditions, the initial approach angle ϵ is replaced by some average angle ϵ_{av} determined by a graphical analytical method from the expression

$$\operatorname{tg}\varepsilon_{av}\left(\frac{\delta}{\varrho_0},\ \varepsilon\right)=\int_0^1 \operatorname{tg}\varepsilon d\left(\frac{H}{H_0}\right). \tag{3}$$

In the calculations, we used the curve for the drop in the field intensity shown in Fig. 1; the results of the calculations are shown in Fig. 3.

As an example, we shall use data and results of the calculations of a magnetic system with the following parameters: $\delta = 20$ cm; $\rho_0 = 100$ cm; $\epsilon = 18.43°$. The focal distance l, calculated on the basis of [1], is equal to 300 cm; exact calculation showed that the real focal distance is then equal to 859 cm. If we replace ϵ by ϵ_{av} (see Fig. 3), then $l = 311$ cm; i.e., for the case of long-focus systems it is sufficient to take into account only the change in the approach angle. For short-focus systems, it is necessary also to take into account the change in the vertical coordinate.

Calculation of sectional magnet with a double focus and allowance for the influence of the leakage field. In order to take into account accurately the leakage field, one should know the shape of the decrease in field of a given magnet. One may, however, carry out the calculations with sufficient accuracy for some "typical" shapes of the curve (see Fig. 1). The basic contribution to the leakage field will be taken into account if the calculation of the horizontal focusing is carried out for a uniform field whose dimensions are increased in comparison with the dimensions of the pole-faces by the value κ / δ (equivalent homogeneous field) — quadrangle ABCD (Fig. 4). The influence of the leakage field on the vertical focusing is taken into account by the fact that the initial approach and exit angles are replaced by the average angles obtained from Fig. 3. The conditions of double focusing given in [2] can then be represented in the form

$$\operatorname{tg}\varphi=\frac{\left(\operatorname{tg}\varepsilon_1+\frac{\varrho_0}{l_1}\right)+\left(\operatorname{tg}\varepsilon_2+\frac{\varrho_0}{l_2}\right)}{1-\left(\operatorname{tg}\varepsilon_1+\frac{\varrho_0}{l_1}\right)\left(\operatorname{tg}\varepsilon_2+\frac{\varrho_0}{l_2}\right)}, \tag{4}$$

$$\varphi=\frac{1}{\operatorname{tg}\varepsilon_{1\,av}-\frac{\varrho_0}{l_1}}+\frac{1}{\operatorname{tg}\varepsilon_{2\,av}-\frac{\varrho_0}{l_2}}. \tag{5}$$

The notation in these expressions is clear from Fig. 4.

By means of the method of successive approximations for given parameters of the magnet and particle energy (κ, δ, and ρ_0), one may find the values $\epsilon_{av}=f\left(\varepsilon,\frac{\delta}{\varrho_0}\right)$, l, and φ, which satisfy the simultaneous Eqs. (4) and (5).

If a magnetic system with the parameter $\delta/\rho_0 \geq 0.15$ and a large angle of beam divergence is calculated, then one should introduce corrections for the displacement of the trajectories and the increase in the focal distance due to this displacement. The calculation of the system of parameters should then be carried out, according to expressions (4) and (5), with this new value of the focal distance.

In conclusion, the author expresses his gratitude to E. S. Mironov for suggesting the topic of this work, for his constant interest, and valuable advice.

LITERATURE CITED

1. M. Camac, Rev. Sci. Instr. 22, 197 (1951).
2. W. Cross, Rev. Sci. Instr. 22, 717 (1951).

3. H. Hintenberger, Rev. Sci. Instr. 20, 743 (1949).
4. Experimental Nuclear Physics, edited by E. Segrè [Russian translation] (Moscow, IL, 1955) Vol. I, p. 513.

BEAM LOSS AT THE LIMITING RADIUS IN A PHASOTRON

V. P. Dmitrievskii, B. I. Zamolodchikov, and V. V. Kol'ga

Translated from Atomnaya Énergiya, Vol. 9, No. 4, pp. 303-305, October, 1960
Original article submitted March 28, 1960

The resonance interaction of the radial and vertical oscillations close to n = 0.25 is considered. It has been shown that this resonance is considerably more harmful than the parametric excitation of the vertical oscillation, which is caused by the first harmonic in the magnetic field structure.

In actual high-energy phasotrons (400-700 Mev), the limiting energy to which the particles are accelerated corresponds to the radius at which the exponent of the magnetic-field fall-off lies in the limits $0.25 > 0{,}25 > n > 0{,}2$ $\left(n = -\frac{r}{H}\frac{dH}{dr} \right)$. The coupled oscillations in the zone n = 0.2 cannot lead to the complete loss of the beam [1]. The region of parametric excitation of vertical oscillations at a frequency $Q_z = 0.5$ (n = 0.25) penetrates directly into this zone. In actual phasotrons, parametric excitation cannot cause an essential increase in the amplitude, since the width of the resonance zone for a first harmonic of $\epsilon_1 \simeq 0.001$ is usually less than 100 revolutions [2].

We shall consider the effects which may be evoked by an increase in the vertical oscillation amplitude in the presence of an azimuthal inhomogeneity of the magnetic field.

In this case, the betatron oscillations (r, z, φ) are described by the equations *

$$z'' + [n + \varepsilon_1 n \cos(\varphi + \varphi_0)]\, z - \frac{2}{r}(d - n)\, z\varrho - \frac{z'\varrho'}{R} = 0,$$

$$\varrho'' + (1 - n)\,\varrho + \frac{1 - 2n + d}{R}\varrho^2 - \frac{\varrho'^2}{2R} - \frac{1}{2R}(2d - n)\, z^2 + \frac{1}{2R} z'^2 = -\varepsilon_1 R \cos(\varphi + \varphi_0), \qquad (1)$$

where $n = -\frac{R}{H(R)}\frac{dH}{dr}\Big|_{r=R}$; $d = \frac{1}{2}\frac{R^2}{H(R)}\frac{d^2H}{dr^2}\Big|_{r=R}$; $\varrho = r - R$; $H_z = H(r)[1 + \varepsilon_1 \cos(\varphi + \varphi_0)]$ (the prime denotes differentiation with respect to the azimuthal angle).

We shall consider the coupled oscillations which result from the distortion of the closed orbit of the azimuthal magnetic field with an inhomogeneity in the structure. The equation for the vertical oscillations in this case can be represented in the form

$$z'' + \left\{ n + \frac{\varepsilon_1^2 d^2}{n^2(1 - n)} + \varepsilon_1 n \left[1 + \frac{2(d - n)}{n^2} \right] \cos(\varphi + \varphi_0) \right\} z = 0. \qquad (2)$$

* In the system (1), only the resonance terms containing ϵ_1 are retained.

For all actual phasotrons, the quantity $\frac{2|d-n|}{n^2} \gg 1$ for n = 0.25, i.e., the beam loss at the limiting radii due to the coupling of the oscillations and not from the parametric excitation of the vertical oscillations of the first magnetic field harmonic. From Eq. (2), it follows that the oscillation amplitude is 2.7 times as great for ν revolutions, where

$$\nu = \frac{n}{2\pi\varepsilon_1 |d-n|}. \tag{3}$$

Taking into account the fact that $d \simeq -\frac{r}{2}\frac{dn}{dr}$, we readily obtain the radial width of the resonance zone:

$$\Delta r = \frac{\varepsilon_1}{n} R. \tag{4}$$

If the average increase in energy in the accelerator is equal to eV, then the number of revolutions for the width of the resonance zone is

$$\nu = \varepsilon_1 \frac{1-n}{n} \frac{E_k}{eV} \frac{2E_0 + E_k}{E_0 + E_k}, \tag{5}$$

where E_k is the kinetic energy of the field. Thus, under conditions of quasi-static operation, one can estimate from (3) and (5) the increase in the amplitude of an ion in the resonance zone:

$$\ln \frac{a_{max}}{a_0} = 2\pi\varepsilon_1^2 d \frac{1-n}{n^2} \frac{E_k}{eV} \frac{2E_0 + E_k}{E_0 + E_k}. \tag{6}$$

Using the method of averaging [3], we can estimate the increase in the amplitude for dynamical operation:

$$\ln \frac{a_{max}}{a_0} = 4\sqrt{\pi}\frac{\varepsilon_1 d}{\sqrt{\chi}}, \tag{7}$$

where χ is the rate of change of the characteristic frequency in the resonance zone n = 0.25. This rate is determined from the expression

$$\chi = \frac{4d}{3\pi}\frac{eV}{E_k}\frac{E_0 + E_k}{2E_0 + E_k}. \tag{8}$$

The results were checked on an ÉMU-8 electronic simulator. The simulator made it possible to solve the problem of the dynamic passage of particles through the resonance of the coupling with forced radial oscillations for n = 0.25. Equation (2), which could be represented in the system of two equations

$$\begin{aligned} z'' + n(\varphi) z + \frac{2\varepsilon_1 d}{n} U z = 0, \\ U'' + U = 0, \end{aligned} \tag{9}$$

where $n(\varphi) = n_0 + \chi\varphi$; $U(\varphi_0) = 1$; $U'(\varphi_0) = 0$; $z(\varphi_0) = a_0$; $z'(\varphi_0) = 0$. was integrated on the ÉMU-8.

Since the time was used as the variable in the solution of the system (9) on the electronic simulator, it was possible to make an arbitrary choice of the initial phase φ_0.

In the integration, φ_0 was chosen in such a way so as to obtain the maximum increase in amplitude of the vertical oscillations in the process of the particle passing through the resonance of the coupling for $n_0 = 0.25$.

The maximum oscillation amplitude was observed directly on the screen of the indicator and was determined from the voltage at the output of the integrator. The accuracy of the solution is 1%.

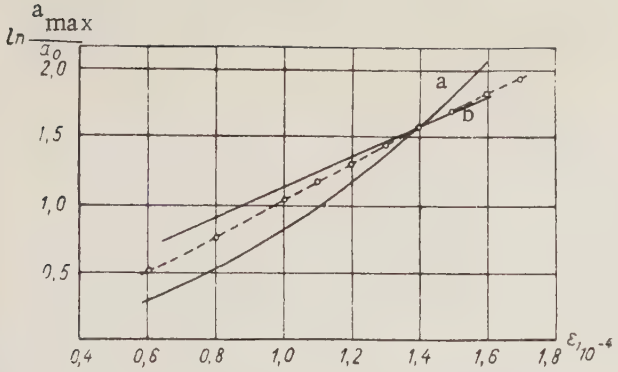

Fig. 1. Variation of the maximum amplitude with the size of the first harmonic of the magnetic field for a phasotron with $E_k = 680$ Mev.

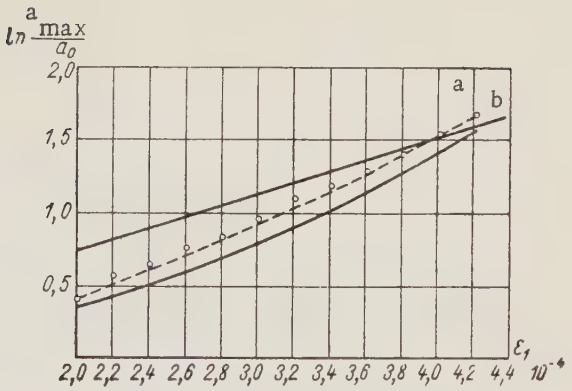

Fig. 2. Variation of the maximum amplitude with the size of the first harmonic of the magnetic field for a phasotron with $E_k = 57$ Mev.

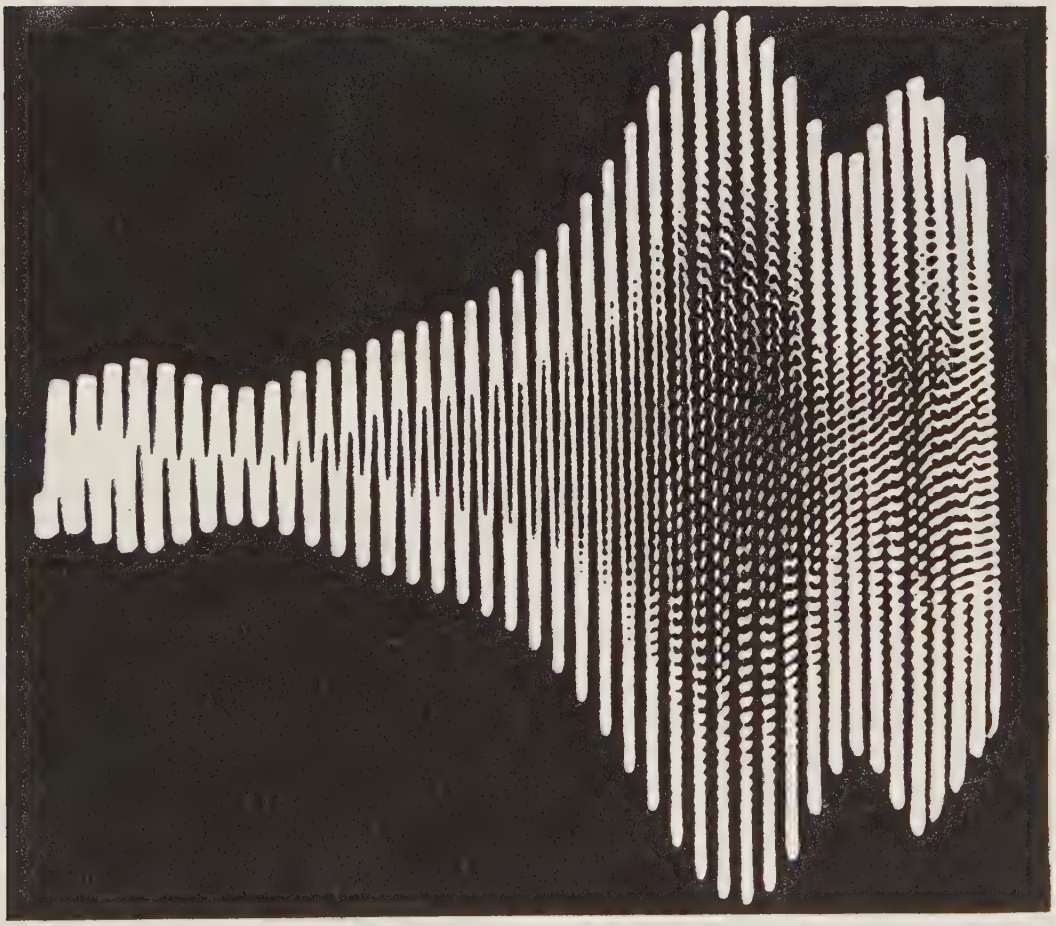

Fig. 3. Process of passing through the resonance zone for a phasotron with $E_k = 57$ Mev for $\epsilon_1 = 4 \cdot 10^{-4}$.

The system of equations (9) was solved for the following values of the parameters corresponding to two real phasotrons (the phasotron of the Joint Institute of Nuclear Studies at Dubna and the phasotron of the Institute of Nuclear Research in Tokyo):

$$E_k = 680 \text{ Mev}; \quad V = 10 \text{ kv} \quad d = -10;$$
$$E_k = 57 \text{ Mev}; \quad V = 7 \text{ kv} \quad d = -7{,}5.$$

The obtained variations of $\ln \frac{a_{max}}{a_0} = f(\epsilon_1)$, after passage through the resonance of the coupling for n = 0.25 are shown in Figs. 1 and 2 (dotted curves). Shown in the same figures are curves calculated from formula (6) by means of the quasi-static method (curve a) and from formula (7) by the method of averaging (curve b).

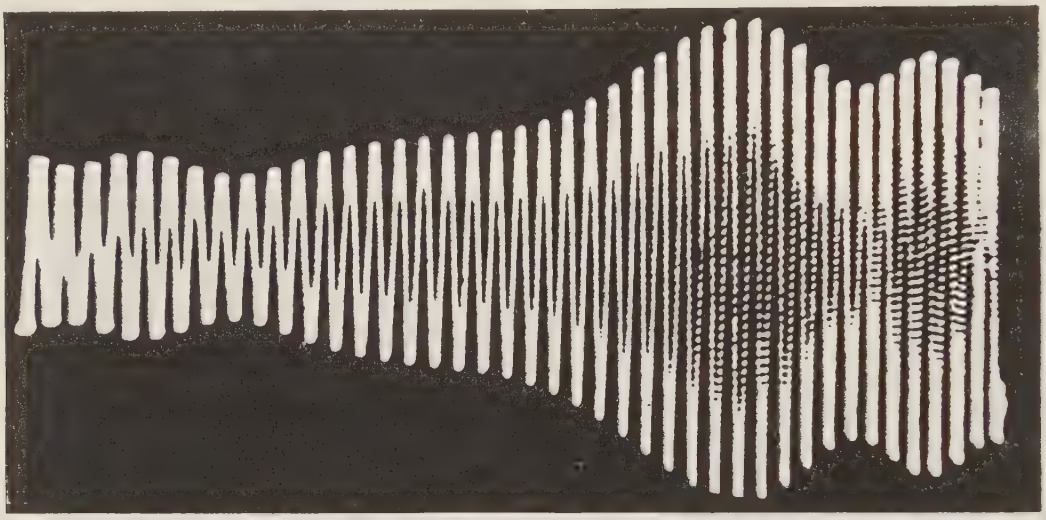

Fig. 4. Process of passing through the resonant zone for a phasotron with $E_k = 57$ Mev for $\epsilon_1 = 3 \cdot 10^{-4}$.

From the theoretical consideration of the excitation of oscillations resulting from the coupling with forced oscillations in the zone of nonlinear resonances of higher order, it is seen that for mirror-symmetry of the magnetic field structures the resonance $Q_z = 1/3$ does not appear, and resonances beginning with $Q_z = 1/4$ are not harmful. The resonance excitation of the vertical oscillations caused by the second and higher harmonics in the magnetic-field structure are also practically not harmful.

The investigations of the process of the passage of ions through the resonance of the oscillation coupling in the zone $n \simeq 0.25$ shows that this resonance determines the limiting radius to which ions are accelerated in large phasotrons. In phasotrons of small radius ($R < 100$ cm), the passage of particles through the zone of this resonance is possible, since the rate of change of the characteristic frequency of the oscillations close to $n \simeq 0.25$ in such phasotrons is considerably higher.

The authors express their gratitude to V. P. Dzhelepov for valuable comments during the discussion of the results of this work.

LITERATURE CITED

1. D. Hamilton and H. Lipkin, Rev. Sci. Instr. 22, 783 (1951).
2. L. Henrich, D. Sewell, and J. Vale, Rev. Sci Instr. 20, 887 (1949).
3. N. N. Bogolyubov and Yu. A. Mitropol'skii, Asymptotic Methods in the Theory of Nonlinear Oscillations [in Russian] (Moscow, Physical and Mathematical Press, 1958).

COMPARISON OF CASCADE CIRCUITS FOR PRODUCING LARGE CURRENTS WITH LITTLE RIPPLE

A. A. Vorob'ev and S. F. Pokrovskii

Translated from Atomnaya Énergiya, Vol. 9, No. 4, pp. 305-308, October, 1960
Original letter submitted March 4, 1960

In order to carry out accurate measurements on large targets in the 2-3 Mev energy region, it is necessary that the particle energy oscillate no more than 0.1-0.5% for a beam current of the order of 5-10 ma. It is interesting to consider the possibility of using for this purpose an electrostatic accelerator employing a cascade generator with a power up to 30 kw.

The operation of cascade generator circuits under various conditions has been considered by the authors of [1-3], who proposed various computational formulas for describing the action of these circuits under identical conditions. In the present work, we compare the results of calculations of the operating conditions of cascade generator circuits with various theories and confront them with the experimental data.

TABLE 1

Formulas for the Calculation of Various Cascade Generator Circuits

Characteristics	Type of circuit					
	Cockcroft-Walton		with a decreasing stage capacity	symmetrical		three-phase
	after Vorob'ev and Melikhov	after Bouwers	after Vorob'ev and Melikhov	after Novikovskii	after Pokrovskii	after Pokrovskii
Ripple voltage	$\frac{(n+1)n}{4}\frac{i_L}{fC}$	$\frac{(n+1)n}{4}\frac{i_L}{fC}$	$\frac{n}{2}\frac{i_L}{fC}$	$\frac{n}{4}\frac{i_L}{fC}$	$\frac{n}{4}\frac{i_L}{fC}-\frac{ni_L}{4C}t_1$	$\frac{(n+1)n}{12}\times\frac{i_L}{fC}-\frac{n}{6}\times\frac{i_L}{C}t_1$
Voltage drop	$\frac{i_L}{6fC}(4n^3+3n^2+2n)$	$\frac{i_L}{12fC}(8n^3+9n^2+n)$	$\frac{i_L}{fC}\left(n^2+\sum_1^n\frac{1}{2k}\right)$	$\frac{i_L}{12fC}(2n^3+3n^2+4n)$	$\frac{i_L}{12fC}(2n^3+3n^2+4n)$	$\frac{i_L}{18fC}(4n^3+3n^2+2n)$
Optimum number of stages	$\sqrt{\frac{fC}{i_L}U_{max}}$	$\sqrt{\frac{fC}{i_L}U_{max}}$	$1\sqrt{\frac{fC}{i_L}U_{max}}$	$2\sqrt{\frac{fC}{i_L}U_{max}}$	$2\sqrt{\frac{fC}{i_L}U_{max}}$	$\sqrt{3\frac{fC}{i_L}U_{max}}$

Note. i_L is the mean load current; f is the source-voltage frequency; n is the number of stages; C is the capacitance of one condenser; U_{max} is the voltage to which the capacitance of each stage is charged; t_1 is the time during which the condenser of one column charges the condenser of the second column.

Computational formulas for four cascade generator circuits recommended by various authors are listed in Table 1.

Figure 1 shows the variation of the output ripple voltage δU with the number of stages n for a cascade generator with selenium rectifiers for a load current $i_L = 1$ ma. The number of stages was varied from two to seven for a supply frequency of 50 cps. The capacitance of each cascade was 1 μf.

In calculating the ripple for the three-phase circuit, we neglected the term $\frac{niL}{6C} t_1$.

Figure 2 shows the variation of the voltage drop at the output ΔU_{min} with the number of stages n for a load current $i_L = 2$ ma for the same cascade generator.

From a comparison of the experimental and theoretical results, we conclude the following:

1. For the Cockraft-Walton circuit, better agreement between the experimental data and the calculations is obtained with the use of Vorob'ev and Melikhov's formula.

2. For the symmetrical circuit, Novikovskii's formula for the calculation of the ripple voltage gives an increased value. More accurate results are obtained from Pokrovskii's formula; for the calculation of the voltage drop, the formulas of Novikovskii and Pokrovskii are recommended.

3. The calculation of the voltage drop from Pokrovskii's formula for the three-phase circuit gives an increased value.

TABLE 2

Comparison of the Properties of Cascade Generators for Various Circuits

Characteristics	Type of circuit			
	Cockroft-Walton (Vorob'ev and Melikhov)	with decreasing stage capacitances (Vorob'ev and Melikhov)	Symmetrical (Pokrovskii)	Three-phase (Pokrovskii)
Ripple voltage, kv	4,0	0,313	0,154	0,25
Voltage drop, kv	267	15,7	69,3	89
Total capacitance μf	5,0	65,0	7,50	10,0
Maximum allowable average load current I, rel. units	1	1	2	3
Optimum number of stages, n	31	31	62	55
Output voltage, kv	2233	2484,3	2430,7	2411
Voltage drop ratio $\frac{\Delta U_1}{\Delta U}$	1	17	3,85	3
Voltage drop for total capacitance of 5 μf, %	100	130	258	150

In Table 2, the properties of the four types of cascade generator circuits, determined from the recommended formulas, are compared for $i_L = 5$ ma, $f = 2$ kc, $U_{max} = 50$ kv, $n = 52$, $C = 0.1$ μf, $2nU_{max} = 2500$ kv. Comparing the data of Table 2, we conclude the following:

1. The Cockroft-Walton circuit is the simplest, but it has the largest ripple voltage and voltage drop; the maximum allowable mean load current is not greater than the rectifier current.

2. The circuit of the cascade generator with capacitances linearly decreasing with the distance from the voltage source has values of the ripple voltage and the voltage drop $^1/_{13}$ and $^1/_{17}$, respectively, of the values for the Cockroft-Walton circuit. The circuit with increasing capacitances is not more complicated than the Cockroft-Walton circuit, but the nonstandard stages of condensers require the construction of condensers with calculated characteristics. The total capacity of the circuit with decreasing capacitances for the same number of stages is thirteen times the total capacitance of the Cockroft-Walton circuit.

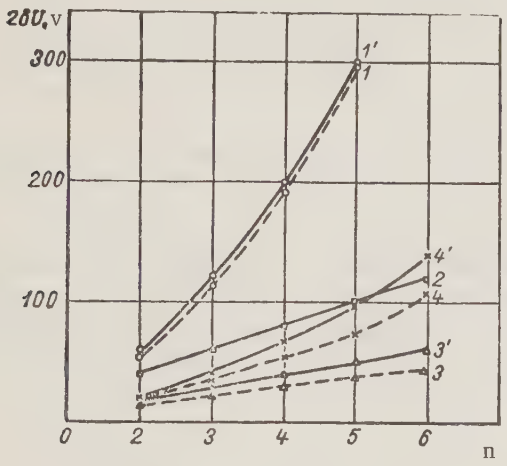

Fig. 1. Variation of the output ripple voltage with the number of stages. Cockroft-Walton circuit: 1) experiment [2]; 1') calculation according to formula of Vorob'ev and Melikhov. Circuit with decreasing stage capacity: 2) calculated according to the formula of Vorob'ev and Melikhov. Symmetrical circuit: 3) experiment [2]; 3') calculated according to the formula of Novikovskii. Three-phase circuit: 4) experiment [2]; 4') calculated according to the formula of Pokrovskii.

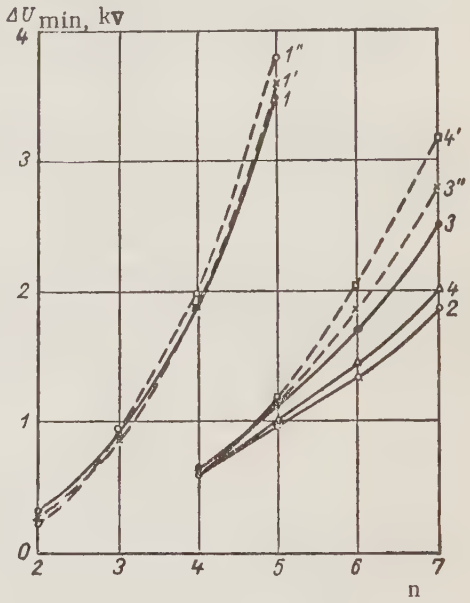

Fig. 2. Dependence of the voltage drop at the generator output on the number of stages. Cockroft-Walton circuit: 1) experiment [2]; 1') calculated according to Vorob'ev and Melikhov's formula; 1") calculated according to Bouwers' formula. Circuit with decreasing stage capacitances; 2) calculated according to Vorob'ev and Melikhov's formula. Symmetrical circuits: 3) experiment [2]; 3') calculated according to Novikovskii's formula; 3") calculated according to Pokrovskii's formula. Three-phase circuit: 4) experiment [2]; 4') calculated according to Pokrovskii's formula.

3. With the symmetrical circuit, the values of the ripple voltage and voltage drop are $^1/_{26}$ and almost $^1/_4$, respectively, of those of the Cockroft-Walton circuit. A shortcoming of the symmetrical circuit in comparison with the Cockroft-Walton circuit is the fact that it requires twice the number of rectifiers and one and a half times the number of condensers.

4. The three-phase circuit is more complex than the symmetrical circuit, and with a smaller voltage stability has a greater number of condensers and rectifiers. The basic advantage of the three-phase circuit is the possibility of obtaining a maximum average load current three times that of the Cockroft-Walton circuit.

LITERATURE CITED

1. A. A. Vorob'ev and V. S. Melikhov, Izvest. TPI 70, 2, 139 (1951).
2. B. S. Novikovskii, Atomnaya Énergiya 4, 2, 175 (1958).*
3. A. Bouwers, Elektrische Hochstspannungen (Berlin, 1939).

*Original Russian pagination. See CB translation.

HYDRAULIC RESISTANCE TO THE FLOW OF A LIQUID ALONG A BUNDLE OF RODS

V. I. Subbotin, P. A. Ushakov, and B. N Gabrianovich

Translated from Atomnaya Énergiya, Vol. 9, No. 4, pp. 308-310, October, 1960
Original article submitted March 25, 1960

In an attempt to extend the ideas on the hydrodynamics of channels of complex shape, the authors investigated the hydraulic resistance to the flow of a liquid along staggered bundles of densely (s/d = 1.0) and semidensely (s/d = 1.13) packed rods.

The bundles consisted of 7 rods and 12 spacers. The spacers ensured that the liquid flowed with a uniformly distributed velocity past the bundle cross section. The experiment was carried out for water whose flow was measured by graduated Venturi tubes. Mercury differential manometers and water pressure gauges were used to measure the pressure drop. The water temperature was controlled by means of a thermocouple. The resistance coefficients were calculated from the formula

$$\lambda = 2\frac{d_h}{l}\frac{\Delta P}{\rho\omega^2},$$

where d_h is the hydraulic diameter of the bundle, equal to the ratio of four times the cross section past which the liquid flowed to the total wetted perimeter.

In Fig. 1, the results of the present work are compared with the results of the study of staggered bundles obtained by various authors. Also shown are curves corresponding to the formulas for round tubes (Blazius' formula [1] and Frenkel's formula [2]):

$$\lambda = \frac{0{,}3164}{Re^{0{,}25}}, \tag{1}$$

$$\frac{1}{\sqrt{\lambda}} = -2\lg\left[\frac{\Delta}{3{,}7\,d_h} + \left(\frac{6{,}81}{Re}\right)^{0{,}9}\right]. \tag{2}$$

Our experimental points for the densely packed bundle lie approximately 40% above curves 1 and 2, and the results of the experiment on the bundle with s/d = 1.13 lie 10-15% above these curves. The experimental data of [3] and [4] agree with one another and lie considerably above the curves for circular tubes. The data of [5] lie close to curves 1 and 2. The experimental results are in satisfactory agreement with the approximate analytical calculations of Buleev and Pyshin. They solved the problem by a numerical method. In the calculations, they used the following approximation for the turbulent viscosity coefficient: in the laminar sublayer, $\nu_T = 0$, and in the turbulent nucleus,

$$1 + \frac{\nu_T}{\nu} \simeq \frac{x\left[1 - \left(\frac{r_0 + x - r}{x}\right)^2\right]u}{2\nu c^2} \tag{3}$$

where r_0 is the rod radius; x is the distance from the center of the mesh of the bundle to the rod surface; c = = 7.1 is an empirical coefficient found by comparing the calculated velocity profile in a circular tube with the experimental data of Nikuradze.

In our experiments, we found a weaker dependence of λ on Re for the bundle with s/d = 1.13 than in the experiments for a smooth circular tube. If the cause for this is the roughness, then the absolute value of the roughness found from formula (2) should fall within the limits 0.005-0.01 mm. However, in complex channels, the influence of roughness may be different from that in a tube.

It should be noted that the resistance coefficient increases with the relative spacing of the rods in the bundle. This is not unexpected. In fact, with the use of a hydraulic diameter as a "universal" dimension, it is assumed that the mean dimensionless tangential stress $\frac{\tau}{\rho w^2}$ depends only on the Re number and the roughness of the channel. It is difficult to expect that this assumption is valid for any channel. In narrow parts of the mesh of a densely packed bundle, a stagnant zone may be created. As a result, the basic flow of the liquid will take place only through parts of the mesh cross section. From this it follows that the friction resistance coefficient calculated from d_h will be smaller than for a circular tube.

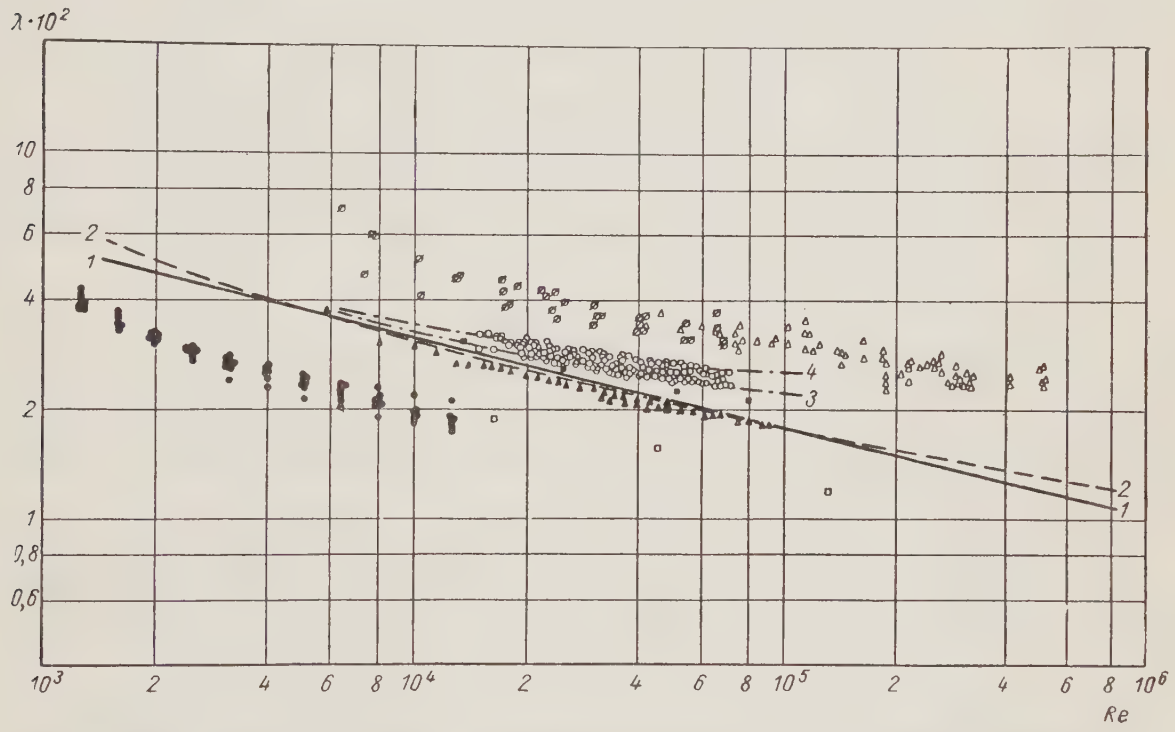

Fig. 1. Friction resistance coefficient of staggered bundles (the hydraulic diameter is taken as the characteristic dimension). ●, ○) Data of the present work for $\frac{s}{d} = 1.0$ and $\frac{s}{d} = 1.13$, respectively; ⌀) data of [3] for $\frac{s}{d} = 1.76 - 2.37$; Δ) data of [4] for $\frac{s}{d} = 1.46$; ▲) data of [5] for $\frac{s}{d} = 1.12$; □, ■) data found from the calculations of Buleev and Pyshin for $\frac{s}{d} = 1.0$ and $\frac{s}{d} = 1.2$, respectively. 1) Data calculated from formula (1); 2-4) data calculated from formula (2) for $d_h = 4.8$ mm with Δ equal to 0, 0.005, 0.010 mm, respectively.

In some channels, the resistance coefficient can prove to be larger than for a circular tube, owing to secondary currents arising in the liquid (secondary currents are observed in the experiments of Nikuradze).

The data obtained for a densely packed bundle were recalculated under the assumption of the existence of stagnant zones. As the characteristic dimension, we used the diameter of a circle inscribed in the bundle mesh. For such an analysis, these data are in agreement with formula (2) for a circular tube (Fig. 2). Apparently, such good agreement is accidental, since by means of the inscribed circle one can only characterize qualitatively the stagnant zones.

With an increase in the velocity of the liquid, the stagnant zones in a densely packed bundle should probably decrease. Therefore, it is logical to assume that at very large Re numbers the characteristic dimension of the densely packed bundle will practically coincide with the equivalent hydraulic diameter.

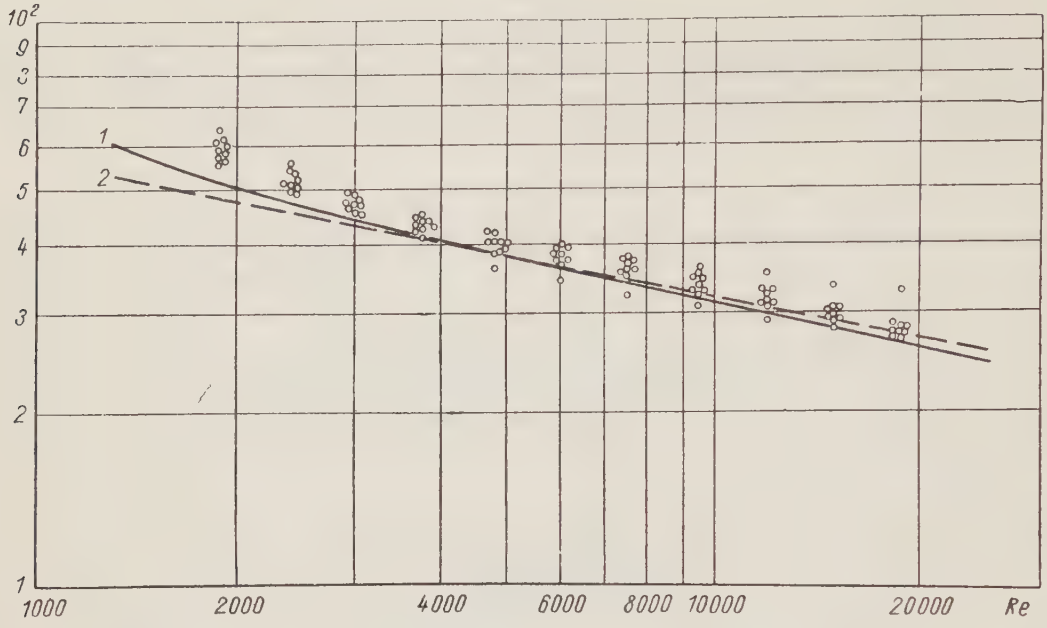

Fig. 2. Data for a densely packed bundle analyzed from the diameter of the circle inscribed in the bundle mesh. ○) experimental data. 1) Data calculated from formula (1); 2) data calculated from formula (2) for $\Delta = 0$.

On the basis of the experiments and analysis of the data of other authors, it was established that the use of the hydraulic diameter as a characteristic dimension in the generalization of experimental data from the hydraulic resistance of bundles does not lead automatically to the taking into account of the spacing of the rods in the bundle.

The obtained data are recommended for practical calculations of the resistance of bundles in the axial flow of a liquid.

LITERATURE CITED

1. H. Schlichting, Boundary Layer Theory [Russian translation] (Moscow, IL, 1956) p. 394.
2. I. I Agroskin, G. T. Dmitriev, and F. I. Pikalov, Hydraulics [in Russian] (Moscow, State Energetics Press, 1954).
3. A. P. Salikov, Ya. L. Polynovskii, and K. I. Belyakov, Teploénergetika 8, 48 (1954).
4. P. Miller, J. Byrnes, and D. Benforado, Am. J. Chem. Eng. 2, 226 (June, 1956).
5. B. LeTourneau, R. Grimble, and J. Zerbe, Trans. Am. Soc. Mech. Engr. 79, 8, 1751 (1957).

INVESTIGATION OF HEAT EXCHANGE IN CONNECTION WITH A TURBULENT FLOW OF MERCURY IN AN ANNULAR DUCT

V. I. Subbotin, P. A. Ushakov, and I. P. Sviridenko

Translated from Atomnaya Énergiya, Vol. 9, No. 4, pp. 310-312, October, 1960
Original article submitted October 28, 1959

For the purpose of obtaining data that has not appeared heretofore in the literature and for studying the effect of two-way heat elimination on heat transmission, in 1958, the authors of the present paper investigated the heat exchange involved in a turbulent flow of mercury in narrow annular ducts.

The experimental ducts, which were made of carbon steel, had the following dimensions. First duct: $l = 1000$ mm, $d_2/d_1 = 1.05$, width of the annular space 1 mm; second duct: $l = 400$ mm, $d_2/d_1 = 1.09$, width of the annulus 2 mm. Uniform heat elimination was realized with electrical heating units. There were no sections for preliminary hydrodynamic stabilization. The mercury was filtered beforehand through chamois. To protect the mercury against oxidation, the free space of the sections was filled with argon.

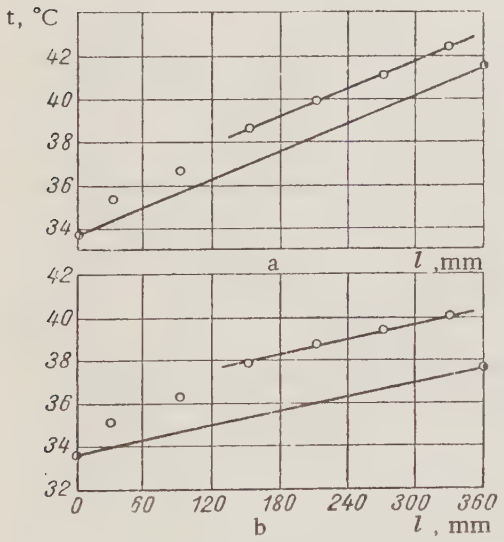

Fig. 1. Temperature variation along the annulus of the second duct for $q = 50 \cdot 10^3$ kcal/m²·hr: a) two-way heating; b) one-way heating; ○, ◐) temperature of the wall and mercury, respectively.

The temperature of the heat-exchange surface was measured by twelve thermocouples having diameters of 0.2 mm; these were embedded at uniform spacing along the length of the outer tube. The effective temperature correction for depth of insertion of the thermocouples was estimated from the results of measurements in water of the heat transfer in a circular tube in which the thermocouples had been inserted in the same manner as in the annular ducts, as well as by electrosimulation of the thermocouple weld. This correction was insignificant (approximately 0.05° C for a flow of approximately $5 \cdot 10^4$ Cal/m²·hr).

In the tests the heat transfer coefficients, stabilized along the length of the ducts, were determined. The hydraulic diameter d_h, equal to twice the width of the annulus, was taken as the characteristic dimension in the similarity criteria. The physical parameters were calculated according to the mean temperature of the mercury. The tests were performed in a mercury flow velocity interval of 0.3-3.8 m/sec at a temperature of 30-40° C and heat flow q ranging from $25 \cdot 10^3$ to $75 \cdot 10^3$ kcal/m²·hr.

The limiting analytic errors in measuring heat transfer in the second duct was no greater than 16 and 30% for one-way and two-way heating, respectively. The measurement accuracy on the first duct was somewhat lower.

Experimental Results

In carrying out the preliminary preparations and adjustments for the first duct, bending of the inner tube was noted to exert considerable influence on the temperature field of the heat-exchange surface. With a crimp in the tube of approximately 0.3 mm and $q \approx 40 \cdot 10^3$ kcal/m²·hr, the temperature nonuniformity in the heat-transferring wall reached 50-60° C. This indicates that in designing for the heat-exchange properties, it is important to take into account the effect of deformation of the ducts.

The heat transfer was measured on the first duct only after careful checking of the duct. The main results were obtained on the second experimental duct, where deformation of the channel was almost entirely avoided.

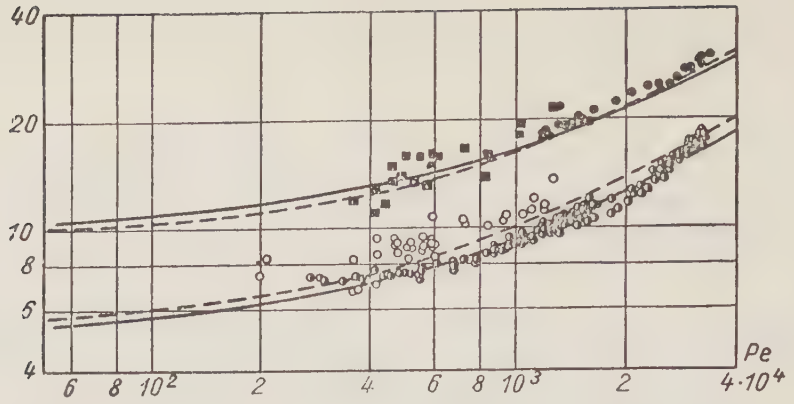

Fig. 2. Comparison of results of the present paper with those calculated on the basis of semiempirical equations: ■, ●) Experimental data, obtained with two-way heating on the first and second ducts, respectively; ○, ◐) experimental data, obtained with one-way heating; ———) calculation according to Eqs. (1) and (2); -----) calculation according to Eqs. (3) and (4).

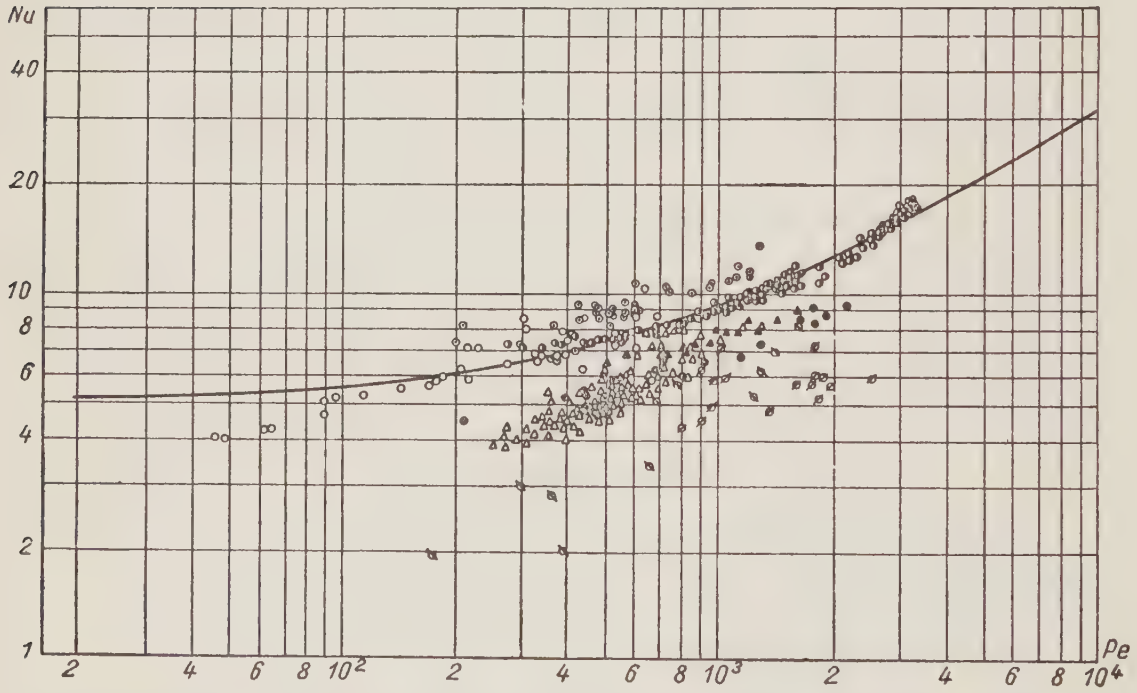

Fig. 3. Comparison of data of the present paper with the data of other authors (one-way heating): for mercury: ⊙, ◑) data of present paper for the first and second ducts, respectively; ●, Ø, ◊, ○) data from [4-7] for d_2/d_1 equal to 1.54; 1.71; 1.85; 1.17 - 1.75, respectively; for Pb-Bi alloy: ▲, △) data from [8] and [9] for d_2/d_1 equal to 1.74 and 1.25, respectively; ———) calculation according to Eq. (2).

The temperature distribution over length of the duct is shown in Fig. 1. The heat stabilization length was approximately $30\,d_h$, which corresponds with the data for a circular tube [1]. The results of the tests, processed on the basis of the dimensionless criteria, are shown in Fig. 2. The slight disparity in points is explained by errors of measurement. The solid lines in the figure correspond to the semiempirical equations of Harrison and Menke for a plane-parallel duct [2]:

$$Nu_2 = 10 + 0{,}025\,Pe^{0{,}8}, \quad (1)$$

$$Nu_1 = 4{,}9 + 0{,}0175\,Pe^{0{,}8*}. \quad (2)$$

The dashed lines are constructed from equations given by Buleev for one-way heat elimination outward from the outer wall of the duct, $d_2/d_1 \leq 2$:

$$Nu_1 = 5{,}1 + 0{,}02\,Pe^{0{,}8} \quad (3)$$

and for symmetrically heated plane-parallel ducts:

$$Nu_2 = 9 + (1{,}41 - 0{,}12 \lg 100\,Pr)(Nu_1 - 5). \quad (4)$$

Equations (3) and (4) were derived on the basis of the methods outlined in [3].

The satisfactory agreement between the experimental data and those calculated from semiempirical equations indicates that either the contact thermal resistance on the heat-exchange surface is small, or that the assertions of the polyempirical theories are not precisely correct.

From Fig. 2, it is evident that heat transfer with two-way heating is about twice as great as with one-way heating.

In Fig. 3 the data of various authors on heat transfer in gaps for mercury [4-7] and Pb-Bi alloy [8, 9] are compared. Such a comparison is valid, since the contact resistances of the mercury and of the Pb-Bi alloy are of the same order [10].

The effect of the curvature of the surfaces generating the annulus are often accounted for with the correction $(d_2/d_1)^{0.3}$. But the introduction of this factor only aggravates the disparity of the experimental points.

Consequently, it has been experimentally established that:

1. With two-way heating of an annular duct having $d_2/d_1 \leq 1.09$, and under the condition that the heat fluxes on both surfaces, the heat transfer to the mercury is about twice as great as with one-way heating. The application of the hydraulic diameter as a characteristic dimension does not therefore imply automatic allowance for the characteristics of heat transfer to liquid metals with one-way and two-way heating of the annular duct.

2. In a narrow annular duct, with no preliminary hydrodynamic stabilization, the thermal stabilization length for mercury comes to approximately $30\,d_h$.

3. Disturbing the geometry of the annular duct has a substantial effect on heat transfer to liquid metals.

In addition to the authors themselves, B. N. Gabrianovich and A. V. Zhukov took part in the testing.

LITERATURE CITED

1. H. Johnson, W. Clabaugh, and J. Hartnett, Trans. ASME 76, 4, 505 (1954).
2. W. Harrison and J. Menke, Trans. ASME 71, 797 (1949).
3. N. I. Buleev, Collection: Heat-Exchange Problems [in Russian] (Izd-vo AN SSSR, Moscow, 1959), p. 208.

* Nu_1 corresponds to one-way, Nu_2 to two-way heat elimination.

4. S. S. Kutateladze et al., Liquid Metal Heat-Transfer Media (Supplement No. 2 to the journal Atomnaya Énergiya) [in Russian] (Atomizdat, Moscow, 1958) p. 57.*
5. M. A. Styrikovich, I. E. Semenovker, and A. R. Sorin, Sovetskoe Kotloturbostroenie 9, 316 (1940); Zhur. Tekhn. Fiz. 16, 10, 1324 (1940).
6. M. I. Korneev, Teploénergetika 7, 30 (1955).
7. L. Trefethen, General Discussion on Heat Transfer (1951) p. 436.
8. R. Seban and D. Casey, Trans. ASME 79, 7, 1541 (1957).
9. B. Lubarsky and S. Kaufman, Rept. Nat. Advis. Comm. Aeronaut. 1270 (1956).
10. V. I. Subbotin, M. Kh. Ibragimov, and P. A. Ushakov, Atomnaya Énergiya 8, 1, 54 (1960).*

ON THE SEPARATION OF BORON ISOTOPES BY CHEMICAL INTERCHANGE

B. P. Kiselev

Translated from Atomnaya Énergiya, Vol. 9, No. 4, pp. 312-313, October, 1960
Original article submitted May 16, 1960

A method of rectification is applied for the concentrated isotope B^{10}. BF_3, BCl_3, and BBr_3 were employed as the working liquids.

From approximate calculations [1] the separation factor α for the system $B^{10}Cl_3 - B^{11}Cl_3$ should be equal to 1.013. Experiments [2] have shown that the separation factor for boron isotopes with rectification of BCl_3 is less than the calculated value by nearly one order of magnitude, and the light isotope of boron is concentrated in the liquid phase. In the literature [3], investigations of the temperature dependence of the separation factor are described. At temperatures above 61.7° C the isotope B^{11} is highly volatile, and at temperatures below 61.7° C this is the case for B^{10}; the separation factor for the system $B^{10}Cl_3$ - $B^{11}Cl_3$ varies, depending on the temperature (from − 85 to + 13° C) from 0.998 to 1.003 [3].

Data on Separation of the Boron Isotopes

Stage of enrichment	B^{11}/B^{10}	α
Initial	4,49±0,02	
First deg.	4,35±0,02	1,031±0,008
Initial	4,45±0,02	
First deg.	4,33±0,02	1,028±0,008
Initial	4,60±0,03	
Second deg.	4,39±0,04	1,025±0,01
Initial	4,63±0,03	
Second deg.	4,38±0,02	1,028±0,008
Average	—	1,028±0,008

In addition to the rectification method for separating the boron isotopes, the reaction of chemical isotope interchange is of considerable interest. It has been shown [4, 5] that in chemical interchange between gaseous BF_3 and a liquid complex compound of anisol with boron fluoride the light isotope B^{10} is concentrated in the liquid phase. The separation factor for this reaction is equal to 1.013 ± 0.005.

The interchange reaction between the gas molecule BF_3 and ion BF_4^- has also been suggested. The interchange between hydrofluoroboric acid† and gaseous BF_3 can be written as follows:

$$B^{10}F_4^- + B^{11}F_3 \rightleftarrows B^{11}F_4^- + B^{10}F_3.$$

*Original Russian pagination. See CB translation.

† Saturated 18.5 N aqueous solution of hydrofluoroboric acid.

Experiments have shown that in bringing about the given reaction, separation of the boron isotopes is observed, where the light isotope B^{10} is concentrated in the gaseous phase. In the table are shown data from some tests for one and two degrees of interchange. Isotope analysis was performed on the MS-2 M mass spectrometer. The separation factor for interchange between hydrofluoroboric acid and gaseous BF_3 is almost one order of magnitude greater than in the case of distillation of BF_3 and is equal to 1.028 ± 0.008. These tests were performed at a temperature of 20-30° C.

The author expresses his indebtedness to B. P. Konstantinov for suggestion of the topic and advice during the work.

Taking part in the experiments and measurements were Yu. P. Batakov, O. N. Shuvalov, and Yu. G. Basargin.

LITERATURE CITED

1. H. Urey, Chemistry of Isotopes, Collection 1 [Russian translation] (IL, 1948) p. 86.
2. M. Green and G. Martin, Trans. Faraday Soc. 48, 5 (1952).
3. N. N. Sevryugova, O. V. Uvarov, and N. M. Zhavoronkov, Atomnaya Énergiya 4, 113 (1956).*
4. G. M. Panchenkov, V. D. Moiseev, and A. V. Makarov, Zhur. Fiz. Khim. 31, 1851 (1957).
5. G. M. Panchenkov, V. D. Moiseev, and A. V. Makarov, Doklady Akad. Nauk SSSR 112, 4, 659 (1957).

DEMARCATION OF PETROLEUM-BEARING AND WATER-BEARING STRATA WITH THE APPLICATION OF ELECTRON AND PHOTON BEAMS

V. I. Gomonai, I. Yu. Krivskii, N. V. Ryzhkina,

V. A. Shkoda-Ul'yanov, and A. M. Parlag

Translated from Atomnaya Énergiya, Vol. 9, No. 4, pp. 313-315, October, 1960
Original article submitted February 10, 1960

The demarcation of petroleum- and water-bearing strata in oil wells is a very complex problem because of the similarity of certain properties of water and petroleum. The solution to this problem is currently based on the presence in the water- and petroleum-bearing strata of various concomitant chemical elements [1, 2].

A direct method for solving this problem can be based on the application of various nuclear properties of the isotopes intering into the composition of the water- and petroleum-bearing strata. For example, these isotopes are distinguished by energy thresholds of the (γ, n) reaction (see table).

From the table, it is evident that in the water and petroleum there exist isotopes with different (γ, n) thresholds. If the water and petroleum could be irradiated with electrons or photons with energies of 2.23 Mev, as a result of the (γ, n) reaction on deuterium, photoneutrons would be formed in the body of the water and petroleum; with higher energies photoneutrons are formed as the result of isotopes whose (γ, n) reaction threshold is equal to or less than the energy of the incident electrons.

The number of photoelectrons formed in an infinite layer of water or petroleum upon irradiation by electrons can be determined with a high degree of precision, as shown in [11], by means of the equilibrium

*Original Russian pagination. See CB translation.

photon spectrum. In the case of irradiation by electrons this number of photoneutrons, as the result of fully developed photon showers, can be calculated from the following equation [11, 12]:

$$Q(\varepsilon_0) = \int_{\varepsilon}^{\varepsilon_0} \frac{\sigma_{\gamma n}(\varepsilon)}{\sigma_{\text{tot}}(\varepsilon)} \varphi_p(\varepsilon_0, \varepsilon)\, d\varepsilon.$$

Here $Q(\epsilon_0)$ is the number of photoneutrons formed by a single electron with energy E_0; $\varphi_p(\epsilon_0, \epsilon) = e^{\varepsilon} \int_{\varepsilon}^{\varepsilon_0} \frac{e^{-x}}{x^2} dx$; $\varepsilon = \frac{2,29E}{\beta}$; $\varepsilon_0 = \frac{2,29E_0}{\beta}$ (E is the photon energy in the interval where $\sigma_{\gamma n}(\varepsilon) \neq 0$; β is the critical energy); $\sigma_{\gamma n}(\epsilon)$ is the (γ, n) reaction cross section; $\sigma_{\text{tot}}(\epsilon)$ is the total photon absorption cross section, which was calculated from the equation [12]

$$\sigma_{\text{tot}}(\epsilon) = \sigma_{\text{comp}}(\epsilon) + \sigma_{\text{par}}(\epsilon).$$

In the calculation of $\sigma_{\text{comp}}(\epsilon)$ for water, the fraction of electrons borne by oxygen and hydrogen atoms was considered; in the calculation of $\sigma_{\text{comp}}(\epsilon)$ for petroleum, those borne by carbon and hydrogen were considered. In the determination of $\sigma_{\text{par}}(\epsilon)$ the fraction of nuclei of each element in the corresponding molecules was considered.

(γ, n) Reaction Thresholds for Various Isotopes Occurring in the Composition of Water and Oil

Isotope	Content of isotope, mol.%		γ, n-reaction threshold, Mev
	in water	in petroleum	
	0,0147 [3]	0,0147 [3]	2,23 [4, 5]
C^{12}	—	98,892 [6]	18,75 [7]
C^{13}	—	1,108 [6]	4,95 [8, 9]
O^{16}	99,760 [10]	—	15,63 [7]
O^{17}	0,042 [10]		4,14 [8]
O^{18}	0,198 [10]	—	8,0 [8]

The value of the critical energy for water is equal to 66.92 Mev, for petroleum 84.03 Mev [12]. A calculation of β and $\sigma_{\text{tot}}(\epsilon)$ was made for petroleum having a density ρ = 0.9 g/cm^3, molecular weight of 256, and containing 87.01% carbon and 12.15% hydrogen, which corresponds to 31.4 atoms of hydrogen and 18.7 atoms of carbon belonging to a single average petroleum molecule [13]. The density of electrons in the petroleum was $3.05 \cdot 10^{23}$ per cm^3.

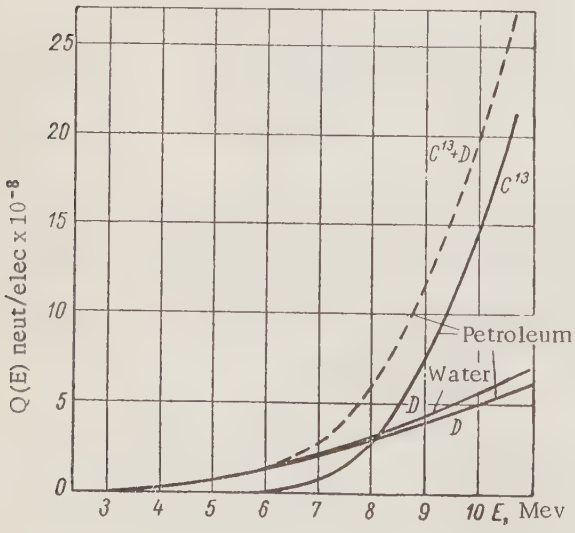

Fig. 1. Photoneutron emissions from water and petroleum due to the (γ, n) reaction on deuterium and the isotope C^{13}.

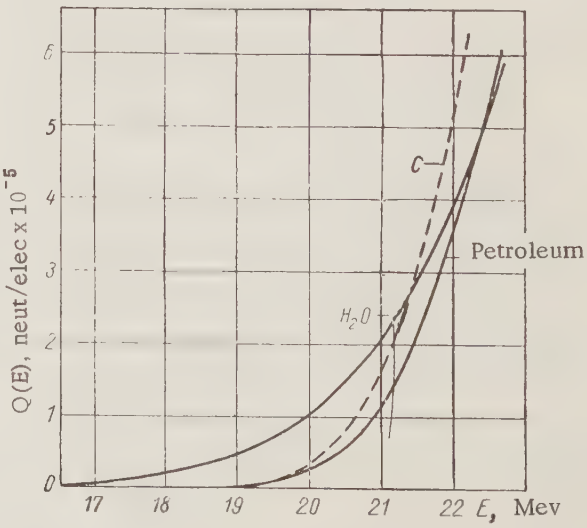

Fig. 2. Photoneutron emissions from water and petroleum due to the (γ, n) reaction on the isotopes O^{16} and C^{12}.

In order to explain the reason for using the (γ, n) reaction on deuterium for the separation of petroleum from water in wells, calculations of $Q(\epsilon)$ for petroleum and water were made; it was assumed in so doing that photoneutrons were formed exclusively as the result of photofission of the deuterium, the content of which in the petroleum and water was assumed to be the same.

The results of calculating Q(E), as obtained by numerical integration with the aid of Simpson's equations, show (Fig. 1) that the number of photoneutrons formed in water and petroleum having the same energy is almost the same. However, in the literature [14-16] there are indications of an increased deuterium content in the hydrogen of the petroleum by 50% or more. Consequently, taking into account the true deuterium content in petroleum, one can obtain a marked difference in the number of photoelectrons formed in water and petroleum.

From the table it is clear that in the petroleum, in addition to deuterium, there is found the isotope C^{13} with a rather low (γ, n)-reaction threshold (4.95 Mev). From the corresponding calculations of Q(E) given in Fig. 1, it follows that the number of photoneutrons formed in the petroleum as the result of C^{13}, when the energy of the incident electrons is 7.6 Mev, is 10^5 neutrons/μa of the electron current. The total number of photoelectrons formed due to C^{13} and deuterium for this same energy is $2.75 \cdot 10^5$ neutrons/μa. The total number of photoneutrons of the isotope C^{13} and deuterium in the petroleum is shown in Fig. 1 by a broken line. In the water, with an electron energy of 7.6 Mev, the photoneutrons are formed only due to deuterium.

The water also contains the isotope O^{17}, whose (γ, n) reaction threshold is equal to 4.14 Mev. In the literature there are no data giving information on the (γ, n) reaction for this isotope, so that an accurate determination of its contribution to the formation of photoneutrons in water is impossible. If we assume that the cross section $\sigma_{\gamma n}(\epsilon)$ of the isotope O^{17} is equal to the cross section for the isotope C^{13} and take into account the low content of the isotope O^{17} in water (0.042% [10]), then it is possible to obtain the number of photoneutrons in water (due to O^{17}), which is approximately $^1/_{40}$ times the number of photoneutrons formed in petroleum due to C^{13}.

As evident from Fig. 2, in the case when the principal isotopes of carbon (C^{12}) and oxygen (O^{16}) are used with higher energies of the incident electron beam – of the order 19 Mev [higher than the (γ, n) reaction threshold for O^{16}] – in water, about $3 \cdot 10^7$ neutrons/μa are formed, whereas in petroleum considerably fewer neutrons are formed for this energy. The photoneutrons formed due to C^{13} and deuterium may be neglected because of the low percentage content of these isotopes in comparison with the percentage content of O^{16} and C^{12}. Consequently, in the energy interval 17-21 Mev, favorable conditions are created for solution of the problem in question.

Therefore, resting on the formation of different numbers of photoneutrons in water and in petroleum, the problem of segregating petroleum- and water-bearing strata can be solved by application of electron beams with energies of the order 8 Mev and higher. For this purpose, it will be necessary to develop physically small electron accelerators with high intensities.

The authors express their appreciation to G. Z. Borukhovich and V. M. Vorobeichik for assisting in the numerical calculations.

LITERATURE CITED

1. A. I. Kholin, Session of the Acad. of Sci. of the USSR on the Peaceful Uses of Atomic Energy (meetings of the technical science divisions) [in Russian] (Izd-vo AN SSSR, Moscow, 1955) p. 267.
2. N. K. Kukharenko, Yu. S. Shimilevich, D. F. Bespalov, and V. A. Odinokov, Heft. Kh-vo 3, 43 (1956).
3. A. M. Brodskii, Chemistry of Isotopes [in Russian] (Izd-vo AN SSSR, Moscow, 1957).
4. R. Sher, J. Halpern, and A. Mann. Phys. Rev. 84, 387 (1951).
5. J. Blatt and V. Weisskopf, Theoretical Nuclear Physics [Russian translation] (IL, Moscow, 1954).
6. D. Strominger and J. Hollander, Rev. Mod. Phys. 30 (2) 2 (1958).
7. R. Montalbetti, L. Katz, and J. Goldemberg, Phys. Rev. 91, 659 (1953).
8. N. A. Vlasov, Neutrons [in Russian] (Gostekhteorizdat, Moscow, 1955).
9. B. Cook, Phys. Rev. 106, 300 (1957).
10. I. Kirschenbaum, Heavy Water [Russian translation] (IL, Moscow, 1953).

11. V. I. Gol'danskii and V. A. Shkoda-Ul'yanov, Zhur. Éksp. i Teoret. Fiz. 28, 629 (1955).
12. C. Z. Belen'kii, Shower Processes in Cosmic Rays [in Russian] (Gostekhteorizdat, Moscow, 1948).
13. M. M. Kusakov, Methods for Determining the Physical-Chemical Characteristics of Petroleum Products [in Russian] (ONTI, Moscow, 1936).
14. N. S. Filipova, Doklady Akad. Nauk SSSR 3, 29 (1935).
15. V. I. Vernadskii, A. P. Vinogradov, and R. V. Teis, Doklady Akad. Nauk SSSR 31, 573 (1941).
16. I. V. Grinberg and M. E. Petrikovskaya, Geologicheskii Zhurnal 17, 4 (1957).

INVESTIGATION OF ATTENUATION FUNCTIONS IN WATER FOR NEUTRONS FROM ISOTROPIC AND ONE-DIRECTIONAL FISSION SOURCES

V. A. Dulin, Yu. A. Kazanskii, V. P. Mashkovich,

E. A. Panov, and S. G. Tsypin

Translated from Atomnaya Énergiya, Vol. 9, No. 4, pp. 315-317, October, 1960
Original article submitted April 27, 1960

In the literature, functions are given for the attenuation in water of neutrons from isotropic sources; for example, point [1] and disk [2] sources. However, in a number of instances it is required to know the attenuation function for neutrons from plane one-directional sources; for instance, when the source is located at a large distance from the shield, and when it may be assumed that the radiation is incident normal to its surface.

In the present paper an experimental investigation is made on the spatial distribution in water of fission neutrons. As a neutron source we used a BR-5 reactor [3, 4]. The neutrons entered the concrete shield through a channel with diameter of approximately 250 mm and impinged on a tank filled with bi-distilled water (dimensions of the tank 137 × 139 × 217 cm).

A neutron beam with total angular divergence of approximately 5° entered the tank through the middle of a 137 × 139 cm wall. For neutron detectors we used proportional boron counters. The applied apparatus permitted us to run measurements at any point in the tank, fixing the position of the detector with an accuracy of 1 mm in the horizontal and vertical directions.

The proportional counter was situated at various distances r from the source and was moved in the direction h perpendicular to the beam (Fig. 1).

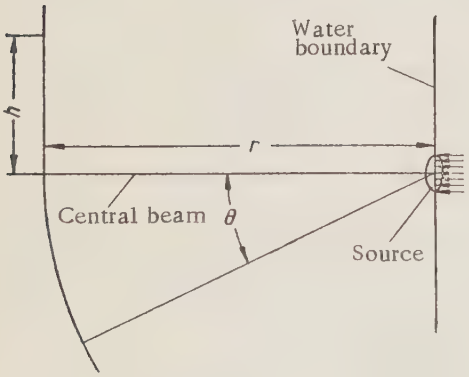

Fig. 1. Geometry of the experiment.

The measured neutron distribution is shown in Figs. 2 and 3.

In Fig. 4 is shown the attenuation function for neutron from an isotropic point source, the function being multiplied by r^2 (curve a), along with the attenuation function for neutrons from a plane one-directional source (curve b). These functions were obtained on the basis of the experimental data with the aid of the transformations for an isotropic point source

$$G_p(r) = C_1 \int_0^{\pi/2} N(r, \theta) \sin\theta \, d\theta, \quad (1)$$

and for a plane one-directional source

$$G_{pl}(r) = C_2 \int_0^{\infty} N(r, h) \, h \, dh. \quad (2)$$

In these equations, N(r, θ) and N(r, h) are the distributions given in Figs. 2 and 3; C_1 and C_2 are constants. In calculating G_T (r) a correction for the finiteness of the source is introduced.

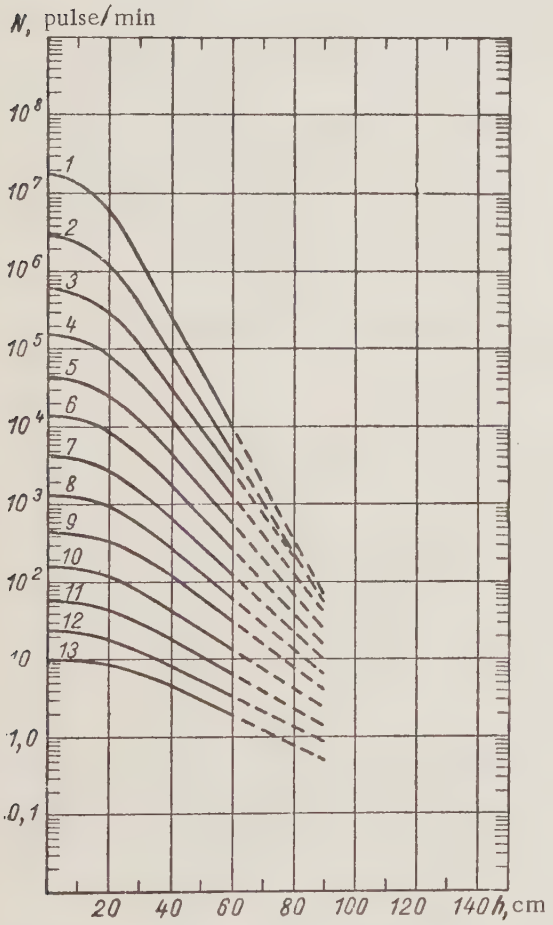

Fig. 2. Measured neutron distribution for the following values of r (cm): 1) 33.4; 2) 43.4; 3) 53.4; 4) 63.4; 5) 73.4; 6) 83.4; 7) 93.4; 8) 103.4; 9) 113.4; 10) 123.4; 11) 133.4; 12) 143.4; 13) 153.4.

The maximum error for curve a occurs for small r attaining a value of approximately 20% for r = = 40 cm. The minimum error (approximately 5%) is observed for large r. The error for curve b varies from approximately 5% for r = 40 cm to approximately 20% for r = 140 cm.

In examining the curves a and b (Fig. 4), we see that the attenuation functions represented by these curves (for an attenuation of approximately 10^5) differ by approximately 20%, which lies practically within the limits of probable error.

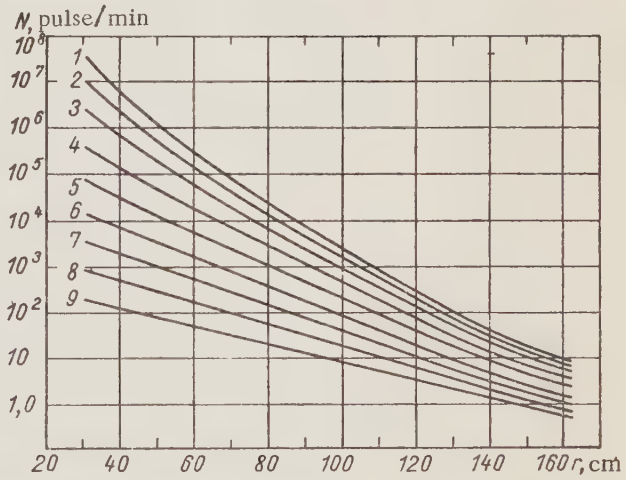

Fig. 3. Measured neutron distribution for the following values of h (cm): 1) 0; 2) 20; 3) 30; 4) 40; 5) 50; 6) 60; 7) 70; 8) 80; 9) 90.

Consequently, for practical problems in calculating the shielding for water thicknesses greater than 40 cm, these attenuation functions may be assumed identical. This conclusion confirms the assumption expressed by Goldstein [1].

For the purpose of comparison with the attenuation functions determined experimentally in [2] for neutrons from an isotropic disk source 71.2 cm in diameter (curve b), in Fig. 5 is shown the attenuation function for neutrons from an isotropic disk source of the same diameter (curve a), but now calculated according to the equation

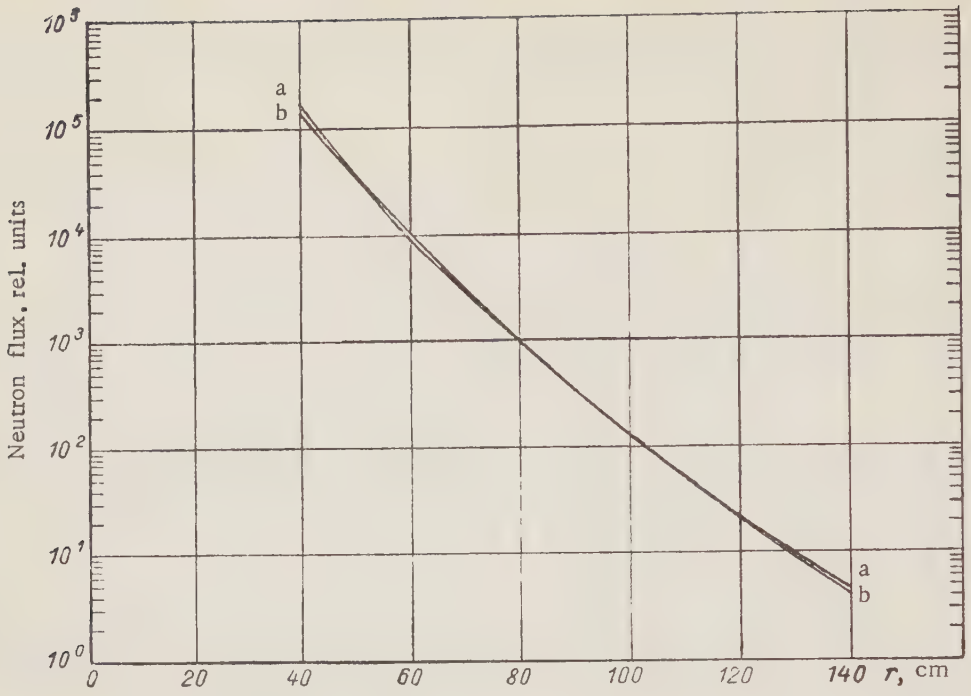

Fig. 4. Attenuation function for neutrons from an isotropic point source, multiplied by r^2 (curve a), and a plane one-directional source (curve b).

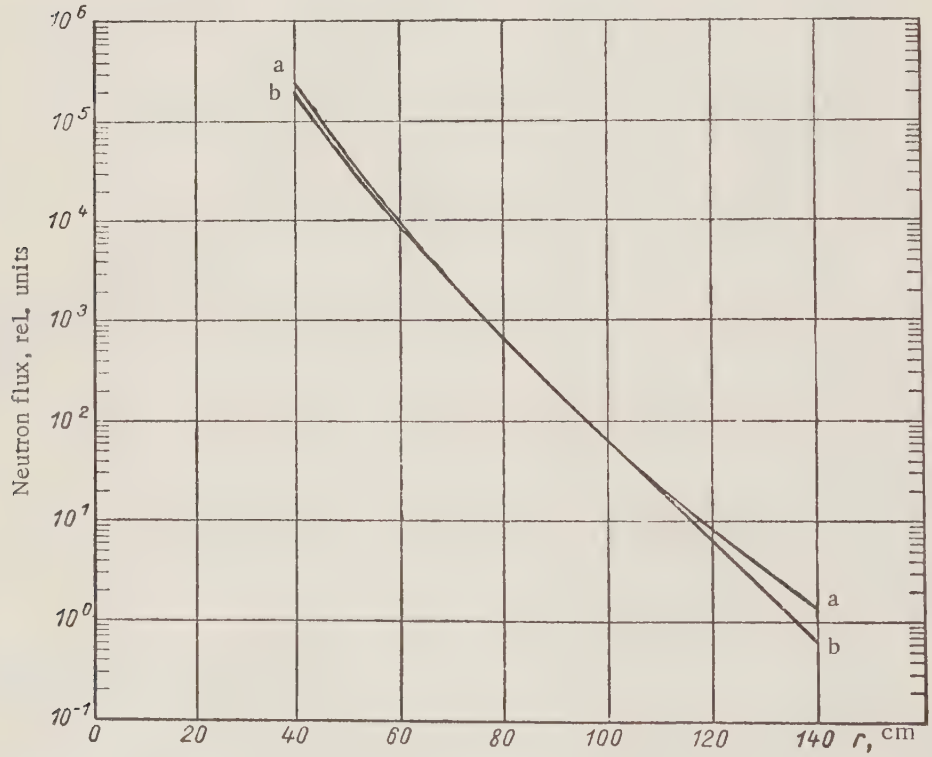

Fig. 5. Attenuation function for neutrons from an isotropic disk source 71.2 cm in diameter. a) Results of the present paper; b) experimental curve from [2].

$$G_{\text{disk}}(r, a) = 2\pi \int_{r}^{\sqrt{r^2+a^2}} G_p(R)\, R\, dR, \qquad (3)$$

where $G_p(R)$ is the attenuation function for neutrons from an isotropic point source; a is the radius of the disk.

Comparison of these curves for r > 40 cm for an attenuation of $3 \cdot 10^5$ exhibits maximum divergence by a factor of two.

The authors express their gratitude to O. I. Leipunskii and V. V. Orlov for valuable remarks in a discussion of the work.

LITERATURE CITED

1. H. Goldstein, The Attenuation of Gamma-Rays and Neutrons in Reactor Shields. U. S. AEC, Washington, 1957.
2. G. Chapman and C. Storrs, Effective, Neutron Removal Cross Sections for Shielding U. S. AEC, Report AECD-3978 (1958).
3. A. I. Leipunskii et al., Atomnaya Énergiya 5, 3, 277 (1958).*
4. Atomnaya Énergiya 7, 2, 192 (1959).*

ENERGY DISTRIBUTION IN WATER OF FAST FISSION NEUTRONS

V. A. Dulin, V. P. Mashkovich, E. A. Panov, and S. G. Tsypin

Translated from Atomnaya Énergiya, Vol. 9, No. 4, pp. 318-319, October, 1960
Original article submitted April 27, 1960

In [1] the method of moments was used to obtain the energy spectrum of neutrons in water at various distances from an isotropic point source of fission neutrons. The experimental determination of the neutron spectrum in water at depths down to 30 cm from the reactor was the subject of [2]. However, in view of a difference in geometries, it is impossible to compare directly the results of these papers.

Characteristics of the Threshold Indicators, in Order of Increasing Threshold Energy

Reaction	Decay half life	Energy threshold, Mev	Indicator material	Indicator height, mm
$P^{31}(n, p)\,Si^{31}$	155 min	~1,5	Solution of chemically pure phosphor in paraffin	3,5
$S^{32}(n, p)\,P^{32}$	14,3 days	~1,5	Melted or pressed chemically pure sulfur	6,0
$Al^{27}(n, p)\,Mg^{27}$	9,8 min	~2,1	Metallic aluminum	4,0
$Al^{27}(n, \alpha)\,Na^{24}$	15 hr	~6,0	The same	4,0

*Original Russian pagination. See CB translation.

In the present investigation, the energy distribution in water of fission neutrons was studied experimentally. As a neutron source we used a BR-5 reactor [3, 4]. A description of the experimental setup is given in [5].

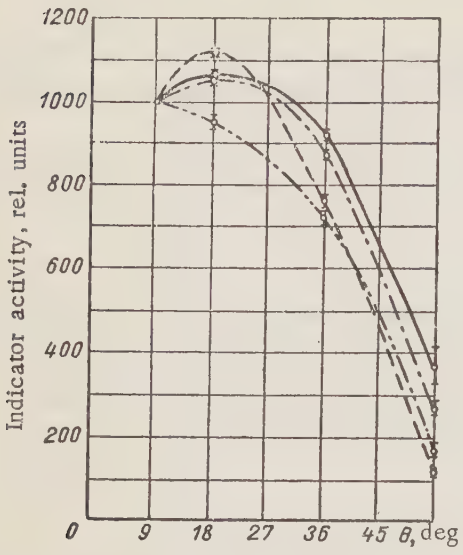

Fig. 1. Activity of threshold indicators as a function of the angle θ for r = 30 cm: ———) P^{31} (n, p) Si^{31}; — · — · — ·) S^{32} (n, p) P^{32}; — · · — · · — · · —) Al^{27} (n, p) Mg^{27}; - - - -) Al^{27} (n, α) Na^{24}.

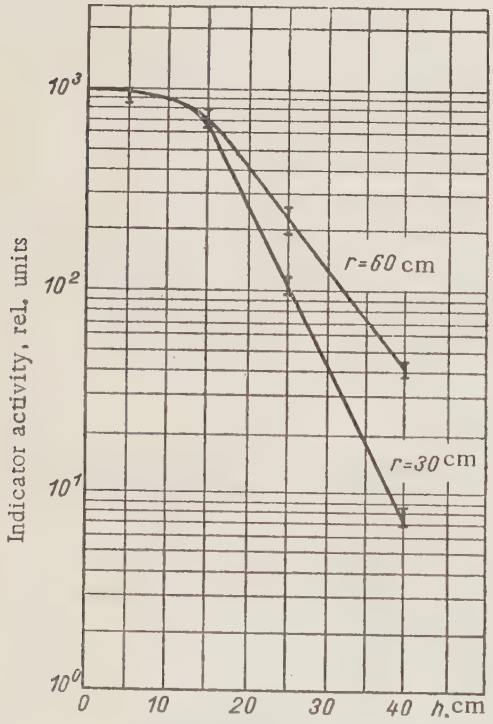

Fig. 2. Activity of phosphor threshold indicators as a function of h for r = 30 cm and r = 60 cm.

For detectors of the fast neutrons we used threshold indicators in the form of disks 35 mm in diameter and of different heights. The data for these indicators are shown in the table.

The threshold indicators (in the form of three-indicator assemblies) were placed in the water at various angles θ with the direction of the incoming neutron beam and at various distances h perpendicular to the beam (see [5], Fig. 1). All threshold indicators in the assembly were activated simultaneously. The absence of an effect was established experimentally by the mutual shielding of the detectors in the assembly within the limits of experimental error. The induced activity of the indicators was determined by constructing the decay curves, which made it possible to exclude the influence of foreign impurities.

The activities of the indicators, normalized to θ = = 9°, are shown in Fig. 1 as a function of θ for r = 30 cm.

The activities of the phosphor indicators, normalized to h = 0, are given in Fig. 2 as a function of h for r = = 30 cm and r = 60 cm.

The energy distribution of neutrons in water at distances of 30 and 60 cm, recalculated from the geometry of the experiment for a point source, is shown in Fig. 3.

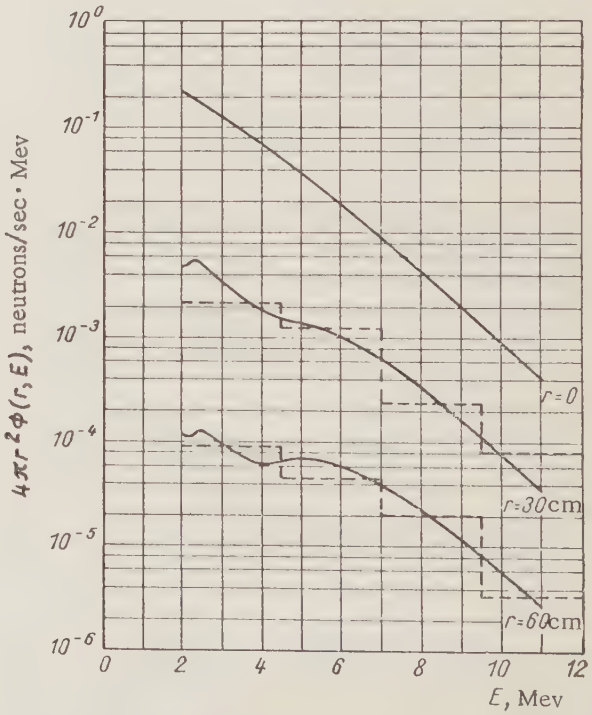

Fig. 3. Spectral distribution in water of neutrons from an isotropic point fission source: ———) analytic spectrum [1]; - - - -) spectrum obtained in the present paper.

The neutron spectral distribution was determined in the solution of the following set of equations by the method of successive approximations:

$$N_i(r) = c\varepsilon_i (1 - e^{-\lambda_i T}) e^{-\lambda_i t} \int_{E_{t_i}}^{\infty} \Phi(r, E)\, \sigma_i(E)\, dE = c\varepsilon_i (1 - e^{-\lambda_i T}) e^{-\lambda_i t} \sum_{j=1}^{n} \Phi_j(r, \bar{E})\, \sigma_{ij}(\bar{E})\, \Delta E_j, \quad (1)$$

where $N_i(r)$ is the activity of the ith threshold indicator, located at a distance r from the source, after irradiation for a period of time T and waiting for a period of time t; ϵ_i is the efficiency of recording of the indicator activity, including corrections for absorption and scattering in the sample, air and the inlet window of the counter, the geometry, resolving time, etc.; $\sigma_i(E)$ is the cross section of the given reaction for an energy E [6]; $\Phi(r, E)$ is the differential flux of neutrons with energy E at a distance r from the source; c is a constant; i is the indicator index ($i = 1, 2, \ldots, n$); j is the energy interval index. The quantities $N_i(r)$ are determined from the equation

$$N_i(r) = c_1 \int_0^{\pi/2} N_i(r, \theta) \sin\theta\, d\theta, \quad (2)$$

where $N_i(r, \theta)$ is the activity of the ith threshold indicator, situated at a distance r from the source at an angle θ with the direction of the neutron beam; c_1 is a constant.

The relative value of the quantity ϵ_i for each indicator was determined experimentally by activating the threshold detectors with a beam of monoenergetic 14.1 Mev neutrons and a flow of fission neutrons.

The set of equations (1) was solved by the matrix method.

In Fig. 3, the data obtained are compared with an analytic neutron spectrum [1]. The experimental spectral histograms are normalized to the analytic spectrum at r = 30 cm. The discrepancy, determined relative to the area beneath the corresponding portions of the curves, is 30-50%, which is almost entirely within the limits of probable error of the spectral distributions obtained, which is estimated at 30%. The error due to finiteness of the source is included in the experimental error.

The authors express their deep appreciation to O. I. Leipunskii and V. V. Orlov for valuable remarks in a discussion of the work.

LITERATURE CITED

1. R. Aronson et al., Penetration of Neutrons from a Point Isotropic Fission Source in Water, U. S. AEC, Report NYO-6267 (1954).
2. R. Cochran and K. Henry, Fast Neutron Spectra of the BSF Reactor, U. S. AEC, Report AECD-3720 (1953).
3. A. I. Leipunskii et al., Atomnaya Énergiya 5, 3, 277 (1958).*
4. Atomnaya Énergiya 7, 2, 193 (1959).*
5. V. A. Dulin et al., Atomnaya Énergiya 9, 4, 315 (1960).*
6. D. Hughes and R. Schwartz, Neutron Cross Sections, Second edition (New York, 1958).

*Original Russian pagination. See CB translation.

CALCULATION OF THE DOSE CREATED IN AN IRRADIATED OBJECT MOVING IN THE RADIATION FIELD OF A LINE SOURCE

U. Ya. Margulis, S. M. Stepanov, and V. G. Khrushchev

Translated from Atomnaya Énergiya, Vol. 9, No. 4, p. 320, October, 1960
Original article submitted March 18, 1960

The existing methods for calculating the dose field generated by sources of different configurations are referred, as a rule, to the case when the object is fixed relative to the source [1-4]. However, in industrial γ-ray equipment it would be more sensible to use a continuous method of irradiation. In this connection, it would seem desirable to come up with a method for calculating the total radiation dose created inside the irradiated object during its motion in the radiation field of the source.

The most functional form of radiator in industrial γ-ray equipment is an activated rod or plane, which can be considered as a system of line sources. Thus, under definite conditions, the analysis can be reduced to a determination of the dose created by a line source.

A line source of length L is placed on the Z axis, one of its ends being located at the origin. The irradiated object is moved with constant velocity $\underline{v}$ (cm/min)* along a straight line parallel to the Y axis (see the figure).

We determine the radiation dose created at some point A inside the irradiated object during the time of its motion along a linear segment of length S_0:

$$D=\frac{2k_\gamma m}{v}\left[A_1\int_0^{\psi_0}\int_0^{\varphi_0} e^{-\mu h(\alpha_1+1)\sec\psi\sec\varphi}\sec\psi\,d\psi\,d\varphi+A_2\int_0^{\psi_0}\int_0^{\varphi_0} e^{-\mu h(\alpha_2+1)\sec\psi\sec\varphi}\sec\psi\,d\psi\,d\varphi\right],$$

where

$$\varphi_0=\operatorname{arctg}\frac{L}{H\sec\psi};\quad \psi_0=\operatorname{arctg}\frac{S_0}{2H};$$

$\underline{m}$ is the linear activity of the source (μC/cm); μ is the linear attenuation factor of a narrow γ-ray beam in the irradiated object; A_1, A_2, α_1, α_2 are constants appearing in the analytic expression for the accumulation factor, which takes into account the role of multiple scattering. The value of the dose is given for a point located on the perpendicular erected from the end point of the rod (in our case the origin). The radiation dose at any other point of the object will be equal to the sum or difference of doses obtained from the corresponding line sources.

The formula given is valid if the irradiated objects are placed on a conveyor belt near enough to one another, so that the distances between them may be neglected and so that we may assume the conveyor belt to be filled in

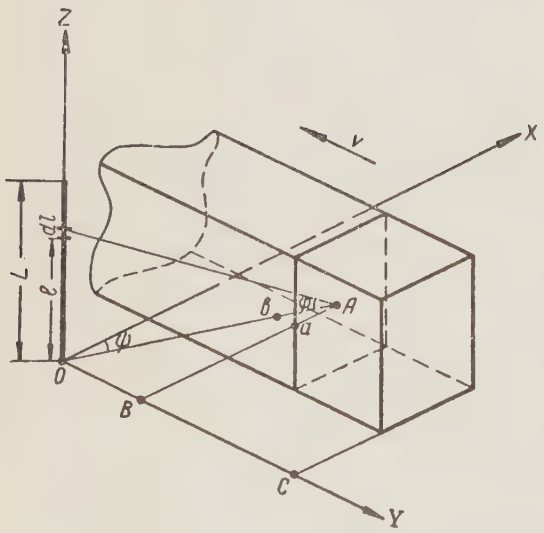

Diagram for calculating the dose of an object while moving in the field of a line source: AB = H is the shortest distance between the point A and the rod; Aa = h is the thickness of the absorbent layer along the X-axis; AO = H'; Ab = h'; H' = H sec ψ; h' = h sec ψ.

* If the velocity is expressed in cm/min, the γ constant of the source k_γ will be expressed in r/min.

solidly with the substance to be irradiated. This same equation is valid for calculating the dose generated by a source in the form of a rectangular plane, which may be regarded as a system consisting of n line sources. If S_0 is large enough, so that the dose created at some point A at the end of the path of each line source becomes sufficiently small, then the total dose acquired by the object upon moving in the field of the plane source will be equal on the path S_0 to nD, where D is the dose generated by one line source, n is the number of line sources composing the active plane.

In those instances when it is necessary to determine the dose power generated by an active plane with stationary irradiation, the equation given may also be used, assuming half the path length $S_0/2$ to be equal to the linear dimension of the plane in the direction of the Y axis. In this case the dose is determined at a point located on the perpendicular erected from a corner of the rectangular plane.

LITERATURE CITED

1. G. V. Gorshkov, Gamma Radiation of Radioactive Bodies [in Russian] (Izd. LGU, 1956).
2. Nuclear Reactor Shields (edited by T. Rockwell) [Russian translation] (IL, Moscow, 1958).
3. D. P. Osanov and E. E. Kovalev, Atomnaya Énergiya 6, 6, 670 (1959).*
4. A. V. Bibergal', Atomnaya Énergiya 7, 3, 244 (1959).*

SIMPLE CALORIMETRIC METHOD OF MEASURING THE ABSOLUTE ENERGY DOSE RECEIVED FROM POWERFUL SOURCES OF IONIZING RADIATION

M. B. Fiveiskii, Yu. S. Lazurkin, and M. A. Mokul'skii

Translated from Atomnaya Énergiya, Vol. 9, No. 4, pp. 321-323, October, 1960
Original article submitted April 14, 1960

The energy dose is an important characteristic condition of irradiation in all radiochemical, radiobiological, and material-testing studies involving nuclear reactors and other sources of powerful penetrating radiation.

In order to determine the energy dose, one usually uses a calorimetric method which gives directly the amount of radiation energy absorbed by the sample under the condition that the release or absorption of energy as a result of other processes taking place in the substance can be neglected.† In this procedure, a stationary calorimetric method is used. For the cases of intensive irradiation (high dose rate) this method is not convenient, since it has basic shortcomings, the main one being the considerable time for the establishment of thermal equilibrium. The dosimetric sample can then heat up considerably, even to the temperature of melting or decomposition; moreover, it receives a large integral dose, which can essentially change its structure and properties. In this connection, we developed, in 1957, a simple nonstationary calorimetric method that is suitable for a nuclear reactor and other strong sources of radiation. The practical application of this method during three years has established its suitability, reliability, and sufficient accuracy.

*Original Russian pagination. See CB translation.

†This is valid in many cases (to an accuracy of several percent). An exception is the triggering of chemical chain reactions, intensive luminescence, phase transitions, etc. by radiation.

The method is based on the following. If a dosimetric sample, at the instant t = 0, is placed in a constant radiation field which is homogeneous within the boundaries of the sample, then, if shielding and side effects are neglected, the temperature at the center of the sample will increase for a certain time τ in accordance with a linear law, independently of the temperature of the surrounding medium. This can be shown by solving the equation of thermal conduction [1] for any sample of simpler shape with uniformly distributed heat sources. The time τ proves to be proportional to the square of the characteristic dimension of the sample d and inversely proportional to the diffusivity χ (this can also be obtained from dimensional analysis). The heating rate $\frac{dT}{dt}$ of a linear segment is determined only by the capacity of the heat sources (dose rate) and the specific heat of the material of the dosimetric sample. The dose rate can be calculated from the formula

$$P = 0{,}417\, c \left(\frac{dT}{dt}\right)_0,$$

where c is the specific heat of the substance (cal/g · deg); $\left(\frac{dT}{dt}\right)_0$ is measured in deg/hr and P in Mrad/hr.

In the practical application of this method, it is necessary to decide on the material and size of the sample, the method of measuring the temperature at the center of the sample, and the design of the entire apparatus. The method was applied to the determination of the dose rate in vertical experimental channels of a reactor operating on ordinary water and enriched uranium [2].

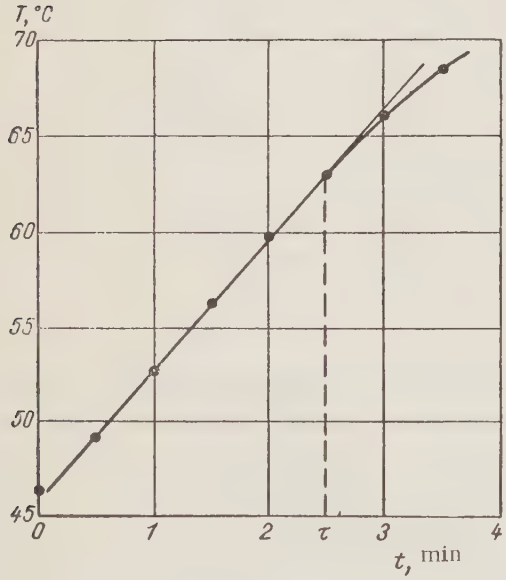

Fig. 1. Time variation of the temperature at the center of the dosimetric sample (polyethylene) in the reactor channel (dT/dt) = = 420 deg/hr; τ = 2.5 min.

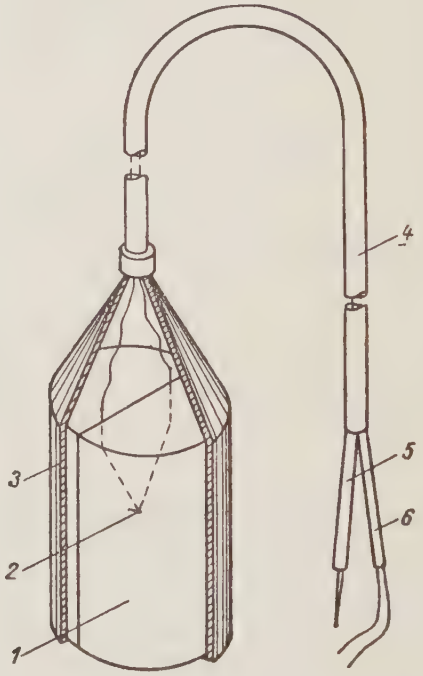

Fig. 2. Dosimetric apparatus. 1) Sample; 2) thermal junction of thermocouple; 3) aluminum foil; 4) flexible support- insulator; 5) cold junction of thermocouple; 6) leads to the measuring instrument.

With regard to choice of material for the dosimetric samples, they were chosen to simulate (in chemical composition) the substances subject to irradiation. In our dosimetric experiments we used polystyrene, polyethylene, slicone rubber, teflon, fused quartz, and others.

The basic samples simulating substances containing hydrogen are polystyrene and polyethylene; for simulating glass (apart from that containing borium), we used quartz. All three substances are convenient, owing to their high radiation stability and small activation.

The samples consisted of cylinders 30 mm in diameter and 50 mm in height. Such a sample size is sufficiently large so that the time constant τ was 2-3 min, which is necessary for a reliable measurement of the heating rate (Fig. 1). At the same time, for such dimensions, the shielding of one part of the sample by another can still be neglected, and the dose field could be investigated over the channel height and diameter.

For the measurement of the temperature, we used a copper–constantan thermocouple introduced between two halves of the cylinder, which was split vertically in two. Special control experiments indicated that for a sufficiently small wire thickness (0.15 mm), the temperature at the thermal junction did not differ, in practice, from the temperature of the sample. The thermocouple's emf was measured on a portable potentiometer (for dose rates of 30-200 Mrad/hr) or on a galvanometer (for dose rates of 0.5-30 Mrad/hr). In the latter case, an auxiliary scale was used. Telemetric measurements were made.

The design of the dosimetric apparatus is extremely simple, and is shown in Fig. 2. Except for the thermocouples, all parts were made from nonactive materials. Sometimes, instead of a flexible hose, we used a flexible aluminum tube. When the dosimetric sample was a liquid, it was placed in a thin-walled container (for example, one made from polystyrene) and an additional cylindrical shield was introduced to prevent convective mixing. In order to increase the time τ for samples of high thermal conductivity, a thermal-insulating jacket was provided, which somewhat increased the size of the apparatus . When it was necessary to measure the dose in the channel filled with water, the entire dosimetric sample was placed in a thin, water-tight case. The position of the sample in the channel was accurately established by means of centering and measuring instruments.

The following procedure was used for the measurements. Before the measurement, the sample was conditioned in the channel outside the irradiation zone, and then lowered to the proper point. The temperature was read for three to six minutes, after which the sample was again raised. We determined the dose rate in this way for various substances in a number of the channels of the VVR reactor. The error in the measurements was 5-10%.* As an example, Fig. 3 gives the curves for the dose-rate distribution over the height along the axis of one of the channels of the VVR reactor for two materials, polyethylene and quartz glass. The difference in the size

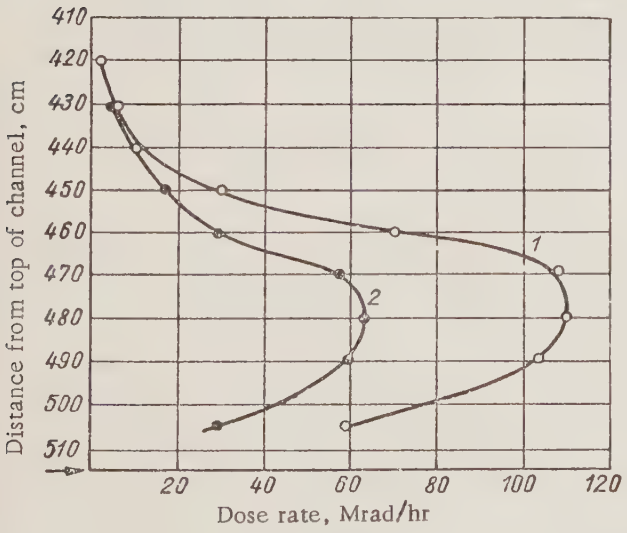

Fig. 3. Distribution of the absorbed-dose rate along the height of channel "65" for polyethylene (1) and quartz (2). The arrow marks the bottom of the channel. The ordinate 480 corresponds to the center of the active zone. The reactor power is 2000 kw.

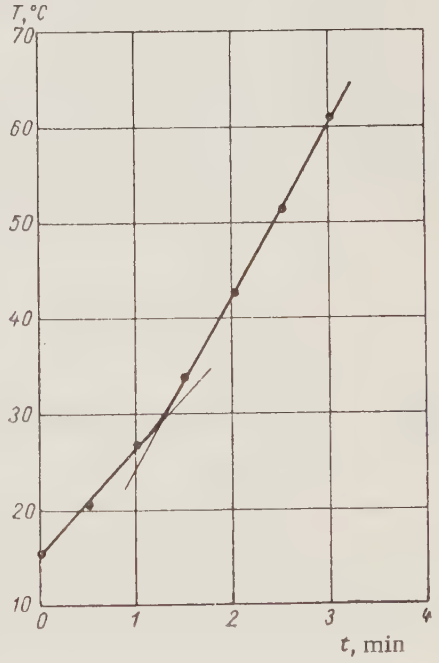

Fig. 4. Heating curve of polytetrofluoroethylene under irradiation.

* As a rule, we used the tabulated values of the specific heat of the materials; in some cases we made additional measurements of the specific heat.

of the dose between these two substances results from the fact that the former receives a dose not only from γ rays, but also from the moderating of fast neutrons, while the latter receives a dose almost exclusively from γ rays. The values of the dose for other substances containing smaller amounts of hydrogen than polyethylene lie between curves 1 and 2 of Fig. 3.

When the character of the neutron spectrum in the irradiation zone was known, even if only approximately, it was possible to divide the absorbed energy into parts resulting from the absorption of γ radiation and from the slowing down of fast neutrons. To do this, one can use the method of variation of the sample composition (mainly the hydrogen content) [3]. We carried out such a separation for a number of substances.

In conclusion, it should be noted that the nonstationary calorimetric method makes it possible to discover certain additional phenomena caused by irradiation if it is accompanied by considerable thermal effects. Thus, for example, with the use of polytetrofluoroethylene as a dosimetric sample, we observed on the heating curve an abrupt change in slope corresponding to a sharp acceleration in the heating of the sample (Fig. 4). It was suggested that this was the result of additional crystallization of the material facilitated by the destruction of the macromolecules under irradiation. This hypothesis was confirmed by measurements carried out by us, by the authors of [4], and by calculation of the thermal effect of the phase transition.

It follows from the above that the nonstationary calorimetric method can be suitable for determining the absolute energy dose in studies connected with the irradiation of organic substances, polymers, water and aqueous solutions, glass, biological objects, etc. in reactors and by powerful γ sources and x-ray tubes.

LITERATURE CITED

1. A. N. Tikhonov and A. A. Samarskii, Equations of Mathematical Physics [in Russian] (Moscow, State Technical and Theoretical Press, 1953).
2. Yu. G. Nikolaev, Reactor Design and Reactor Theory [in Russian], Reports of the Soviet Delegation to the International Conference on the Peaceful Uses of Atomic Energy (Geneva, 1955) [in Russian] (Moscow, Acad. Sci. USSR Press, 1955) p. 265.
3. D. M. Richardson, A. O. Allen, and G. W. Boyle, Dosimetry of Ionizing Radiation, Reports of foreign scientists at the International Conference on the Peaceful Uses of Atomic Energy (Geneva, 1955) [Russian translation] (Moscow, Acad. Sci. USSR Press, 1955) p. 265.
4. A. Nishioka, M. Tajima, and M. Owaki, J. Polymer Sci. 28, 118, 617 (1958).

THE DOSAGE OF OUTDOOR γ RADIATION FROM RADIOACTIVE FALLOUT DURING 1959

V. P. Shvedov, G. V. Yakovleva, and M. I. Zhilkina

Translated from Atomnaya Énergiya, Vol. 9, No. 4, pp. 323-324, October, 1960
Original article submitted March 15, 1960

Radioactive fallout, gathered monthly during 1958-1959 in the vicinity of Leningrad, was subjected to analysis on a scintillation γ-ray spectrometer. The method of investigation was similar to the method used in [1]. The figure presents the results of the γ-spectrometric analysis of radioactive fallout. Two factors affect the amount of radioactive fallout: contamination level of the troposphere by radioactive fission products and the amount of precipitation. The effect of contamination level of the troposphere must be regarded as the main factor. In fact, despite relatively slight fluctuations in the quantity of precipitation, the amount of radioactive

fallout during the period of greatest contamination of the troposphere has characteristic, well-defined maxima as the result of recent nuclear weapons tests or the magnified interchange of the radioactive masses of the stratosphere and troposphere. The maximum fallout in April – June of 1959 was caused precisely by the effect of such an interchange between masses of the stratosphere and troposphere. Despite heavy rains, the fallout in the second half of 1959 had a very low activity due to the absence of any appreciable contamination of the troposphere.

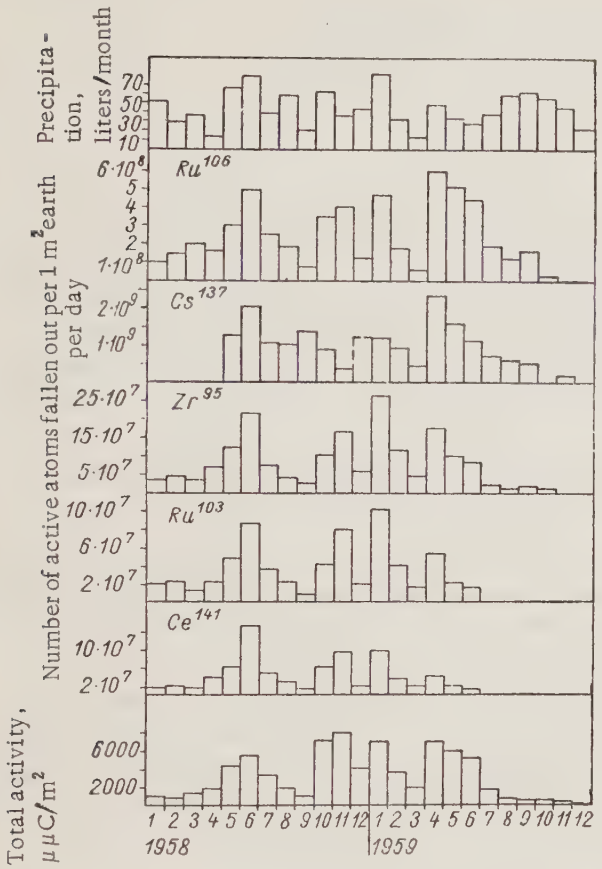

30-Year Dosage of Outdoor γ Radiation from Radioactive Fallout in 1959

Isotope	Dosage, mr
Nb^{95}	1,34
$(Zr+Nb)^{95}$	5,26
Ru^{103}	0,49
Rh^{106}	1,76
Ce^{141}	0,04
Cs^{137}	10,25
Total	19,2

The data given in the figure provides us with the opportunity of determining the 30-year dosage of outdoor γ radiation from radioactive fallout during 1959. The method of analysis was similar to the method used in [1]. The results of this determination are shown in the table.

The 30-year dosage of fallout from 1954 to 1956, 1957, and 1958, according to [1, 2], comes to 16, 18, and 40.1 mr, respectively. Hence, it is clear that the 30-year dosage caused by fallout in 1959 will be considerably less than the fallout dosage for 1958. This fact is due to the absence of nuclear explosions in the year 1959.

LITERATURE CITED

1. V. P. Shvedov, G. V. Yakovleva, M. I. Zhilkina, and T. P. Makarova, Atomnaya Énergiya 7, 6, 544 (1959).*
2. L. I. Gedeonov, V. P. Shvedov, and G. V. Yakovleva, Atomnaya Énergiya 7, 6, 545 (1959).*

* Original Russian pagination. See CB translation.

THE INCREASE IN RADIOACTIVE FALLOUT IN GRADETS KRALOVE (CZECHOSLOVAKIA) AS THE CONSEQUENCE OF NUCLEAR TESTS IN SAKHAR*

V. Santgolzer

Physics Department, Medical Faculty, Karlov University, Gradets Kralove, Czechoslovakia

Translated from Atomnaya Énergiya, Vol. 9, No. 4, pp. 324-326, October, 1960
Original article submitted May 17, 1960

As the result of a temporary cessation of nuclear testing from November 1 of 1958 until the end of 1959, a considerable reduction in the amount of radioactive fallout was observed [1]. In October of 1959, the average daily activity was 0.07 μ C/km^2. In November it dropped to 0.03 μ C/km^2, and this level was maintained until the end of February, 1960. The increase in fallout activity due to rains in these months was relatively mild (maximum of 0.06 μ C/km^2 per day). It may be assumed that during this period, tropospheric fallout was curtailed almost altogether and only the stratospheric variety remained, its source being the stratospheric reservoir [2].

As a result of the first nuclear test in Sakhar (February 13, 1960), an increase in fallout activity was observed in Czechoslovakia from March 1 to 21, 1960.

The results of systematic measurements of rainfall activity from November 1, 1956 until March 31, 1960 are shown in Fig. 1 (in mμC/liter). The strongest radioactivity of rain was observed on March 1, 1960 and was 25.9 mμC/liter. The drop in this activity with passage of time is evidence that it originated on February 13, 1960.

As shown in Fig. 1, even before June of 1959, radioactive rains were noted. The strongest radioactive rain during this time was noted on April 6, 1959, i.e., half a year after the temporary curtailment of nuclear testing. The rain activity on March 1, 1960 was 2.5 times greater than on April 6. One reason for this appears to be that the distance from Czechoslovakia to the test site in Sakhar (4000 km) is less in comparison with the distance from the Nevada desert (11,000 km). Prior to the nuclear tests in Sakhar, Nevada was considered the prime source of radioactive aerosols for Central Europe [3].

The activity that accumulated during March of 1960 was 23.38 mC/km^2, as contrasted with an activity of 0.91 mC/km^2 in February and 0.55 mC/km^2 in January. The accumulated radioactivity was determined by measurements of fallout samples for one month, gathered in a special container, and by calculation of the daily quantities of radioactivity with allowance for the drop in its activity.

Figure 2 shows the activity of daily fallout (in mC/km^2) from February 1 until April 28, 1960. In comparison with the mean fallout of 0.03 mC/km^2 per day that was observed in February, the fallout by March 1 had stepped up to 17 65 mC/km^2 per day, i.e., almost 600 times. After three weeks, the quantity of radioactive fallout diminished and stabilized to an average level of 0.04 mC/km^2 per day. The source of this fallout is also the stratospheric reservoir. About a week later this situation was once again upset by a second nuclear test in Sakhar, taking place on April 1, 1960. An increase in activity was noted in a specimen taken on April 9, when the activity was 0.70 mC/km^2 per day, i.e., approximately 20 times greater than the reading for the end of March and beginning of April, 1960.

* The paper was written for our journal.

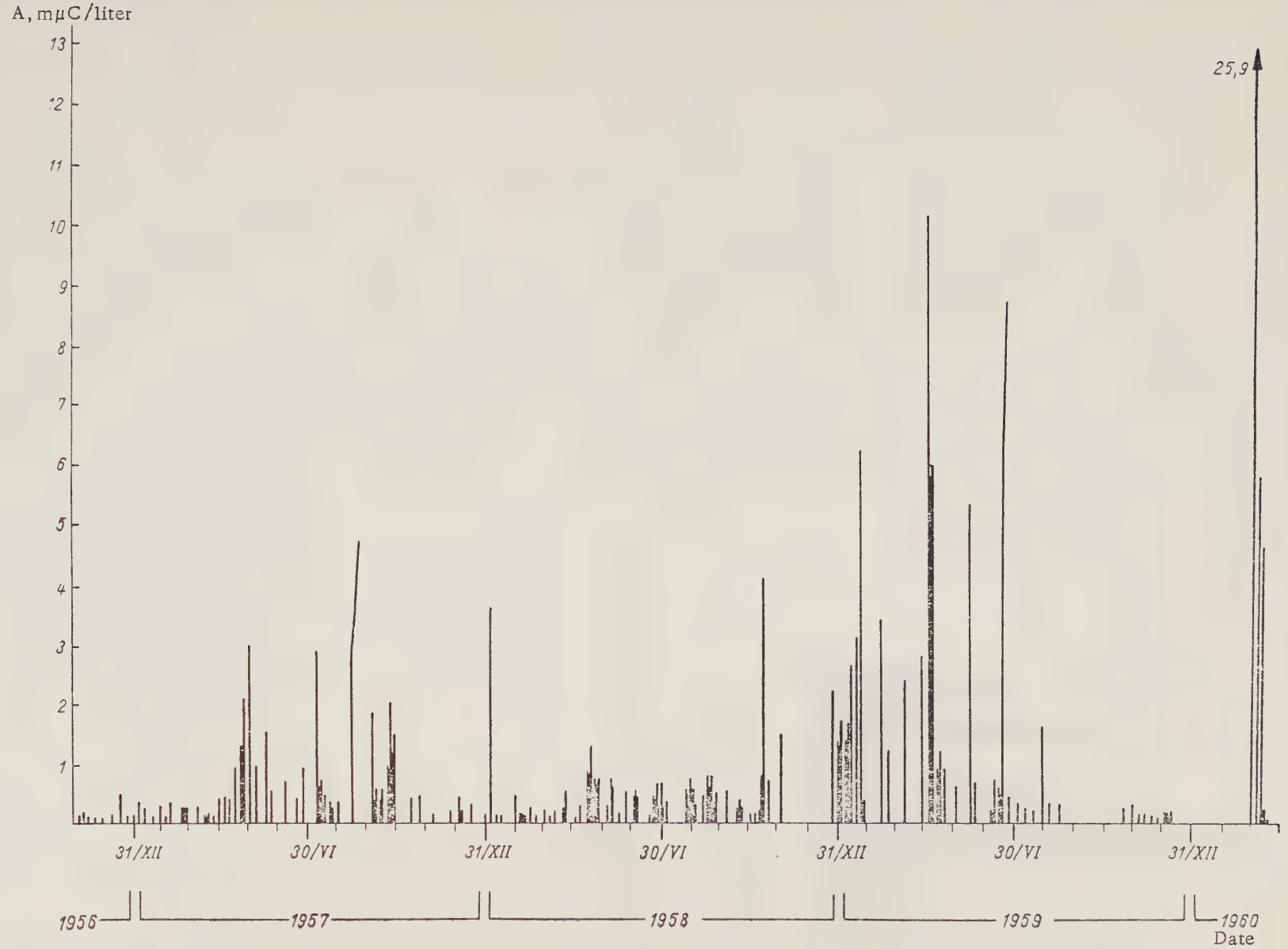

Fig. 1. Radioactivity of precipitation due to radioactive fallout from November 1, 1956 until March 31, 1960.

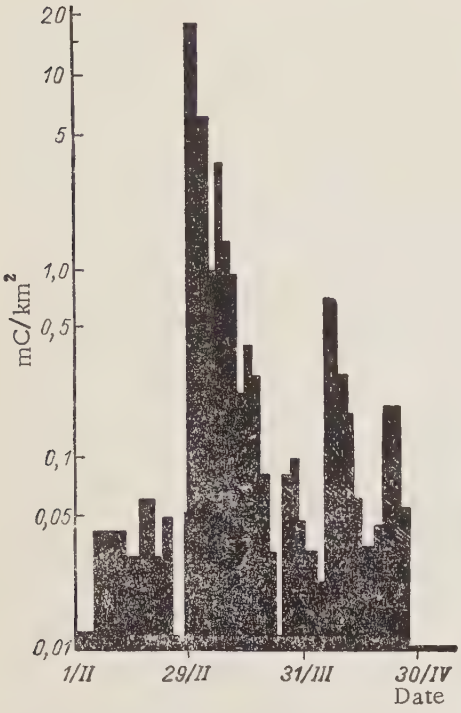

Fig. 2. Increase in radioactive fallout activity in March and April, 1960.

Extrapolation of the activity decay curves for the samples gathered at the beginning of March and in April confirms the dates of nuclear testing on February 13 and April 1, 1960. The behavior of the activity curves can be described by the expression $A = at^{-n}$, where $n = 1,2$.

It should be pointed out that the activity decay for rain samples followed the law $A = at^{-n}$, where $n = 1,2$, whereas for active dry fallout $n = 1,3$.

As a standard preparation for measuring the activity, we adopted $Sr^{90} + Y^{90}$.

We extend our gratitude to Academician F. Begounek for so kindly furnishing us with this preparation and for all the counsel he gave us in this work. We express our appreciation also to I. Matsek for designing and building the automatic apparatus for measuring the radioactivity with a record of the number of pulses.

LITERATURE CITED

1. V. Santgol'zer, Atomnaya Énergiya 7, 5, 480 (1959)*; 9, 1, 60 (1960)*.
2. V. P. Shvedov and L. I. Gedeonov, Collection: Soviet Scientists on the Danger of Nuclear Weapons Testing [in Russian] (Atomizdat, Moscow, 1959) p. 45.
3. M Hinzpeter, F. Becker, and H. Refferscheid, Atomtechnisches Aerosol und atmosphärische Radioaktivität (Strahlenschutz Vol. 7) Braunschweig, 1959.

*Original Russian pagination. See CB translation.

THE PM-2A NUCLEAR PACKAGE POWER FACILITY

Development plans in power reactor design in the USA have been concentrated in recent years more and more on low-power reactors, i.e., reactors producing electric power up to 10 Mw. The results of the development plan heading in this direction include a project of a transportable packaged power plant named PM-24, designed for installation in Greenland [2, 3].

The PM-2A system utilizes a pressurized-water reactor designed by the Alco Products firm. In addition to generation of electric power, the plant will provide steam for space heating.

The basic data of the PM-2A facility are the following:

Reactor thermal power, Mw	10
Minimum energy output for a single loading of core, Mw/yr	8
Available electric power, kw	1560
Amount of heat made available for space heating, kcal/hr	~ 250,000
Operating pressure, atmos	123
Coolant temperature, ° C:	
at reactor inlet	260
at reactor exit	270
Number of fuel assemblies	32
Core:	
diameter, cm	51.3
height, cm	55.2
composition:	
U^{235}, kg	19.5
B^{10}, g	17
stainless steel, kg	172
H_2O, kg	91.5
Number of fuel elements in each assembly	18
Number of control rod bundles	5
Steam generator:	
operating pressure, atmos	38
steam temperature, ° C	240

The fuel elements contain enriched uranium oxide dispersed in stainless steel.

The entire PM-24 package plant will be housed in a tunnel dug out in the ice or snow (Fig. 1). It will be delivered to the assembly site in 27 package shipments totaling 300 tons in weight, the heaviest shipment weighing 13.6 tons. A 10-girder support will facilitate assembly and servicing of the entire installation; the reactor and steam generating unit will be resting on the first girder or supporting skid, while the equipment for feedwater heating will rest on the second. The third skid will support the heat exchanger, and the next three will accomodate air blowers. The turbogenerator unit will rest on the seventh skid, switchgear on the eighth, motors on the ninth, and the steam condenser on the last. Each of the skids consists of two H-frames linked by crossties and matting (Fig. 2). The rigid girder-skids on which the operating units will be mounted provide an adequate substitute for a rigid foundation.

It takes a team of 36 engineers and technicians six weeks to assemble the installation on the operating site. Seventeen men are sufficient for running the plant.

The PM-2A is the third packaged power plant designed by Alco Products. Its first job was the SM-1, now known under the designation APPR-1 [4], which was built in 1957 at Fort Belvoir (Virginia, USA); the second was the SM-1A, now known as APPR-1A, now under construction at Fort Keeley (Alaska). It has double the power rating of the SM-1 for the same core dimensions. The experience accumulated by Alco Products has paid off in plant weight reduction from 2,500 tons (SM-1 and SM-1A) to 300 tons (PM-2A), with the assembly and run-in and testing time telescoped from 18 to 3 months.

The reactors used in all three plants feature the same design, but the heat removal systems are of different design: the PM-2A uses air and ethylene glycol to cool the condenser, while the SM-1 and SM-1A use water for the same purpose.

The experience acquired in operating the SM-1 facility was fully utilized in the design of the PM-2A; the only additional feature incorporated was a study of the distribution of coolant flow through the core. To compute the physical, thermal, and transient processes, the problem was run on a computer. The core of the PM-2A reactor uses eight less fuel assemblies than the SM-1 to achieve the same thermal power output. This means 26 cm less in the girth of the reactor pressure vessel.

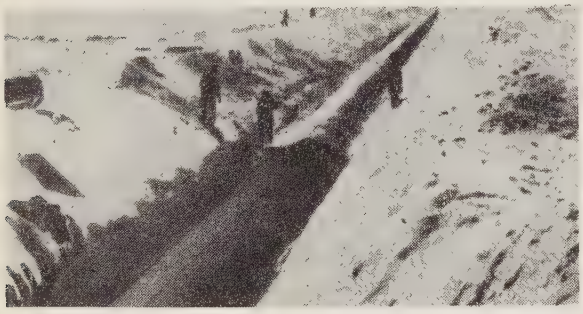

Fig. 1. Driving and lining the reactor tunnel, in Greenland. A similar tunnel will be prepared for the PM-2A facility.

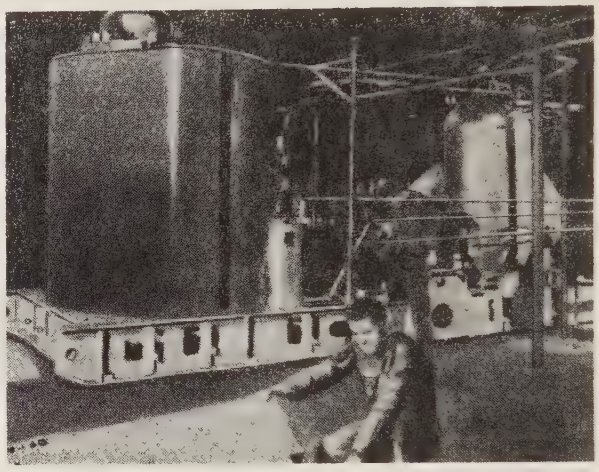

Fig. 2. A support skid with the reactor and steam generator in place.

The cost of the entire PM-2A plant, including the assembly job, is 4.1 million dollars, and operational costs are expected to run in the neighborhood of 800 thousand dollars yearly. By way of comparison, a diesel power plant yielding the same power output costs 400 thousand dollars, but the operational costs (not counting fuel transportation costs) are 1.1 million dollars yearly. The nuclear power plant displays an indisputable superiority over its diesel competitor in this application.

LITERATURE CITED

1. Atomwirtschaft 5, 5, 242 (1960).
2. Nuclear Energy 14, 145, 257 (1960).
3. Nucleonics 18, 6, 120 (1960).
4. Atomnaya Énergiya 2, 6, 574 (1957).*

Yu. K.

*Original Russian pagination. See CB translation.

BERYLLIUM

(Present Status of Beryllium Technology and Research)

N. Mironov and S. Kostogarov

Beryllium has a small thermal absorption cross section and high moderating power. It is therefore found very useful as material for reflectors, displacement rods, and fuel element jackets (in gas-cooled reactors). Beryllium boasts among its exclusive advantages: high modulus of elasticity ranging $(3.1\text{-}3.2) \cdot 10^4$ kg/cm^2, high specific heat and thermal conductivity (when heat-absorbing structures are used), and high ratio of tensile strength to specific weight [1].

However, beryllium's low plasticity at room temperature is a hindrance to its use on a broad scale. The defect in its plastic behavior, affecting beryllium of even the highest grade purity, is explained either by the unfavorable geometry of the metal's hexagonal close-packed lattice which impedes slip flow, or by the possible effect of trace impurities. If it were possible to produce the metal free from any impurities, it would obviously display a certain degree of plasticity, as is the case with impurity-free titanium and zirconium, which have hexagonal lattices with constants close to those of beryllium.

Production of higher-purity beryllium is, therefore, a task meriting close attention. The work is proceeding in the following directions:

1) superhigh-vacuum distillation (residual pressure down to 10^{-7} to 10^{-9} mm Hg) in a vacuum furnace with high-frequency heating [2] and a condenser in the form of a flat rotatable plate. The vacuum system is enclosed in a chamber filled with purified argon. To avoid contamination of the metal by carbon, the system is outgassed by a mercury diffusion pump, and provided with a liquid-nitrogen cold trap. The chamber walls are outgassed by means of a coronal discharge;

2) zone melting in vacuum (residual pressure down to 10^{-5} mm Hg) or in the protective atmosphere of an induction furnace, vertically in a suspended state [3];

3) reduction of beryllium halides by gaseous alkali metals at a temperature of approximately 1000° C. Silver is used for the lines bringing in beryllium chloride into the system; the reaction chamber is made of molybdenum [4].

The purest beryllium metal was made [4] from high-purity beryllia converted to beryllium chloride; the metal was further purified by subsequent distillation. Beryllium buttons obtained by electrolysis of beryllium chloride had the same degree of purity prior to vacuum remelting as found in ordinary beryllium prior to remelting.

The electrolytic process results in beryllium much purer with respect to metallic impurities than that obtained by the magnesium thermal-reduction process, but the electrolytic metal contains a high quantity of sodium and chloride [5], which is diminished in subsequent vacuum remelting.

The plasticity of the most brittle cast beryllium at room temperature is practically null; beryllium obtained by powder metallurgy techniques shows somewhat greater plasticity; cast beryllium has been virtually completely displaced by metal fabricated by powder metallurgical techniques, since 1950.

The beryllium pebbles are remelted in a vacuum, and the resulting ingots are then converted to beryllium flakes. The flakes are comminuted in beryllium-lined pulverizers in a nitrogen or helium atmosphere and passed through a 200 mesh sieve. In a more sophisticated method for fabricating beryllium powder [6], process control is much tighter and the flakes are pulverized in high-speed centrifugal mills,and the powder charge is inserted into dies with all contact with air avoided. The standard powder has the following granulometric make-up [4]: 12% > 100 μ; 15% for both 80-100 μ and 60-80 μ ; 22% for 40-60 μ ; 14% for 30-40 μ ; 10% for 20-30 μ ; about 12% for < 20 μ (beryllium oxide content ranging from 0.5 to 1.5%). The finer powders

are more liable to contamination, by oxygen for the most part. Oxygen content may be minimized by carrying out the pulverization step in dry helium at a temperature of − 64° C.

Beryllium powder items are fabricated by cold pressing (specific pressure 8-25 tons/cm^2) and subsequent sintering in vacuum at a temperature of 1100-1200° C, hot pressing in vacuum (residual pressure of 10^{-1} to 10^{-2} mm Hg) at a specific pressure of 4-20 kg/cm^2 and temperature of 1050-1100° C, warm and hot extrusion of cold-pressed and hot-pressed items, rolling over a temperature range of 455-1100° C for items obtained by various methods.

Vacuum hot pressing is also resorted to in industry. Beryllium ingots weighing as much as 147 kg and measuring 100 by 610 by 1300 mm in size have been fabricated by such methods, while cylindrical, conical, and spherical ingots surpassing 1220 mm in diameter and weighing up to 910 kg are also a matter of record [7].

Recent years have seen more and more frequent recourse to the extrusion of small ingots (up to 60 mm) without cladding at temperatures of 400-450° C (known as warm extrusion) [7]. In this case, the reduction was 4:1, the specific pressure ranged from 6.5 to 16.0 tons/cm^2, the extrusion speed seldom exceeded 2.5 meter/hr [5]. The lubricant used was graphite backed up by molybdenum disulfide [5, 7].

Hot extrusion is carried out in the 900-1150° C range in mild steel jackets covered with copper foil. The specific pressure at 1150° C temperature is 2.2 tons/cm^2. 40:1 reduction is used. Hot extrusion imparts optimum mechanical properties to the metal [5].

A "bare" extrusion practiced in an intermediate temperature range (730-820° C) is also resorted to. The beryllium in this case is covered by a glass or salt lubricant. The reduction used is 9:1.

Extrusion involving the use of a floating core [5] is employed to fabricate tubing of diameter ranging from 63.5 (at a wall thickness of 19 mm) to 12.7 mm (at a wall thickness of 1.5 mm). According to recent data [8], tubes of wall thickness down to 0.25 mm have been fabricated for the AGR reactor, and the tubes are capable of taking a radial flexure of 125 mm in the cold, as well as tubing 8 mm in diameter and 610-680 mm long at a wall thickness of 0.1 mm.

There are some reports in the literature on the use of silver cladding as a lubricant in extrusion, and as protection against oxidation [8].

One report [9] provides a description of hydrostatic pressing of beryllium powder tubing at a temperature of approximately 800° C and pressures up to 31 kg/mm^2. The beryllium powder was charged into a space between a segmental die of Nimonic-80 alloy and a concentrically placed thin-walled steel tube. After being warmed up, the beryllium powder is compacted under radially applied compression (transmitted via an extensible steel tube through molten lead).

Rolling of beryllium on an industrial scale [7] (rolled sheet up to 750 by 1520 mm) is carried out over the range of recrystallization temperatures (455-845° C) [5, 7]. To avert a rupture in the direction of the base plane, to minimize oxidation and level out the temperature distribution, the metal is inserted within heavy steel jackets. After rolling to a thickness of 3.2 mm, the jackets are removed, and the metal sheets, baled into packs, are given an additional rolling.

Reports are available [10] on beryllium rolling studies carried out at temperatures 1040° and 870° C. At 1040° C, the reduction of extruded specimens was 5:1 to 15:1 in transverse rolling (reduction including extrusion to 108:1). The sheet metal obtained showed an elongation of about 30-40%, tensile strength of 40-45 kg/mm^2, and true ultimate strength of 63-70 kg/mm^2. Lowering of the rolling temperature to 870° C resulted in a metal showing a wide spread in elongation and strength data. Temperature effect was negligible over the 870-1040° C for hot rolling in two directions, and the properties of the beryllium transverse to and in the rolling direction were about the same. Sheet rolled with 14:1 reduction (3.75:1 in each direction) showed approximately 25% elongation, tensile strength of 45-49 kg/mm^2 with a true ultimate strength of 60-65 kg/mm^2. The absence of plasticity in the third direction in rolling imposes important limitations on the material, from an engineering standpoint. The property of two-dimensional plasticity is unsuitable for combined stresses, and does not favor the use of rolled beryllium as a really plastic material.

Beryllium is forged over the 730-845° C temperature range [7], but beryllium-forging technology is still at a rudimentary stage of development. It has been reported [11] that vacuum forging of beryllium enclosed

in a crucible has been successfully carried out. It is assumed that this technology will lead to an isotropic metal of much greater plasticity, and equal in this respect to hard aluminum alloys, while retaining the desirable properties inherent in beryllium.

A beryllium ingot 1572 mm in diameter and jacketed in steel was pressed to a diameter of 2030 mm and a height of 76.2 mm at a temperature 1094° C, on a 50,000 ton press [12]. The quality of the ingot was monitored by ultrasonic flaw detection techniques.

Rotary swaging of beryllium and beryllium wire drawing are rarely resorted to, but may be performed at 400° C on beryllium rods [5] extruded from a jacket.

A method has been developed for sintering beryllium blanks, in pressure working of beryllium powder compacts to densities of 1.8 - 1.83 g/cm^3, without applying pressure [6]. Powders of 200 mesh were comminuted in an atmosphere of purified argon, and charged into molds. Sintering proceeded for 6 hours in vacuum induction furnaces at temperatures of 1200-1220° C, in graphite molds. This method was also used on a laboratory scale to produce beryllium cladding for uranium oxide fuel elements [6]. Among the drawbacks encountered in this technique, we might mention the need for strict maintenance of the granulometric make-up of the powders, which must be kept to a minimum of oxidation, and the impossibility of controlling sinter size.

A technique for argon vapor arc welding of beryllium has been developed to overcome the formation of welding cracks, oxidation, and gas formation. The general disadvantage inherent in welding techniques, where a liquid phase is present, is the coarse-grained structure of the cast metal seam and the deterioration in mechanical properties. To reduce thermal shock, it is recommended to preheat the metal prior to welding to 540° C or higher. In diffusion bonding of beryllium, the mechanical properties of the seam are almost indistinguishable from the mechanical properties of the bulk metal. Diffusion bonding is possible over a broad temperature and pressure range. Good results are had by welding for two hours at a temperature of 1200° C [5, 13].

Brazing of beryllium parts to beryllium or to other metals yields satisfactory results. The best brazing alloy for work in an inert atmosphere is an alloy of aluminum and silicon (12%). For furnace-brazing parts of simple geometry, aluminum and silver brazing alloys and aluminum-silver and silver-copper alloys are also used. Highly encouraging results have been obtained from electron-beam welding in a high vacuum [5, 7].

Machining of beryllium is a difficult proposition in view of its brittleness and hardness, and also because of the formation of toxic beryllium dust in the process. Equipment and tools for beryllium machining must be kept in excellent condition and, as a rule, must be housed within suctioned dust-tight hoods.

The following operating conditions and parameters are recommended [7].

In lathe work, cutting speed is recommended at 50-85 meter/min, rate of speed not greater than 0.4 mm/rev, nose angle about 0°, side clearance about 7°; attacking angle of the cutting-tool edge should be kept within 7-10° and should not exceed 10° in any case (to avoid chipping); radius of curvature of the cutting edges must be kept within 0.4-0.8 mm.

The recommended cutting speed for milling operations is 30-50 meters/min, for rough milling and 50-70 meters/min for finish work, with rate of feed ranging from 75 to 150 mm/min.

The recommended drilling speed is 20-30 meters/min, with rate of feed 0.025-0.05 mm/rev (for drills of ϕ 3.2 mm or less), 0.05 - 0.1 mm/rev (for drills of ϕ 6.35 mm), and 0.125 mm/rev (for drills of ϕ 12.7 mm); the angle of the drill-bit cutting faces should be 90°.

Cutting tolerances can be brought to 0.1 mm. A cutting speed of about 6 cm^2/min is recommended.

Oxidation of beryllium exposed to air is negligible at temperatures below 600° C. The corrosion resistance in water is not constant. Standard powder compacts conforming to USAEC regulations were subjected to corrosive attack tests for 96 hours at 250° C [5].

Beryllium presents a considerable health hazard, and this calls for strict attention to safety procedures in handling the material. A new British beryllium mill (of 7 tons annual capacity, staffed by a crew of 200) is being built in a single-storey building with continuous ventilation of warm filtered air provided for; 3000 air samples will be tested weekly in an in-plant laboratory [8].

USAEC rules which have remained in vigor since 1950 stipulate that the beryllium content in air is not to exceed 2 $\mu g/m^3$. Beryllium content in the air outside the building concerned should not exceed 0.01 $\mu g/m^3$.

New methods for treating of beryllium poisoning are being sought, to supplement the usual work safety rules. Reports have come out on positive results in the introduction of $HAu(COO)_3$ into the organisms of experimental animals. This substance inactivates the beryllium present in the organism [4].

Because of the difficulties encountered in its handling, beryllium products are still quite expensive. The price of sheet rolled from extruded products is $ 250 per kg [4]. The cost of complex shaped products, e.g., thin-walled tubing (0.25 annulus) has gone up to 400 £ sterling [8].

LITERATURE CITED

1. Metal Progr. 74, 4, 96 (1958).
2. A. Martin, Vacuum VII and VIII, 38 (1957-1958).
3. G. Ellis, Metallurgia 58, 348, 349, 350 (1958).
4. H. Weik, Metall. 3, 202 (1959).
5. Y. Williams, Metallurgical Reviews 3, 9, 1 (1958).
6. T. Barrett, G. Ellis, and R. Knight, (Geneva, 1958) Conference on Peaceful Uses of Atomic Energy, P/320.
7. K. Wikle, Metal. Ind. 93, 26, 529 (1958).
8. Nuclear Engn. 5, 44, 31 (1960).
9. A. Blayney, Metal. Progr. 74, 3, 95, 184 (1958).
10. J. Greenspan, Trans. of the Metallurg. Society of ASME, 215 (February, 1959).
11. J. Metals 11, 5, 307 (1959).
12. Metal Progr. 76, 3, 128 (1959).
13. N. Weare and R. Monroe, Light Metal Age (August, 1959) p. 10.

THE SECOND AZERBAIDJAN REPUBLIC-WIDE CONFERENCE ON THE USES OF RADIOACTIVE ISOTOPES AND NUCLEAR RADIATIONS

A. M. Mamedov

At the Second Republic-wide Conference on the Uses of Radioactive Isotopes and Nuclear Radiations held at Baku during March, 1960, 33 papers were presented by various scientific institutions of the Academy of Sciences of the Azerbaidjan SSR, the Council of the National Economy for the Republic, the Health Ministry of the Azerbaidjan SSR, and also by the Academy of Agricultural Sciences of the Azerbaidjan SSR and the N. Narimanov Azerbaidjan State Medical Institute.

The reports presented shed light on some of the results obtained from problems resolved in biology, medicine, agriculture, particularly the petroleum industry, on the study of properties of materials (semiconductors), and other fields.

A discussion of the papers showed that during the period stretching from the first conference (in 1957) to the present one, the number of local scientific research, industrial, agricultural, and other organizations which have used radioactive isotopes and nuclear radiations to advantage for scientific and practical aims has increased measurably.

The use of radioactive isotopes, gamma and neutron sources, has resulted in the successful solution of such problems as the effect of irradiation of seeds prior to sowing on the growth, development, and crop yield of cotton,

the effect of prolonged exposure to a radioactive factor on the state of blood and on several biochemical indices, the effect of phosphorus isotopes on the nature and spread of aseptic inflammation, determination of saturated vapor pressure, the behavior of impurities in the distillation of semiconductors, determination of the diffusion coefficient, determination of water content in petroleum blends, circulation of catalyzer in industrial systems, shielding properties of concrete, etc. Radioactive tracer methods have resulted in notable economic savings in several branches of industry.

The "Azneftegeofizika" (Azerbaidjan geophysical oil exploration) trust has made extensive use of radioactive methods in geophysical drill hole studies.

In order to discover aquifers and gas-bearing strata in cases where electric logging methods fail to yield the desired results, and in old boreholes, successful use has been made of gamma-gamma and neutron-gamma logging techniques. Radioactive isotopes have also been used to determine the position of thief zones, break points of casing strings, flow patterns of water outside the casing string in production oil wells. For a quantitative estimate of the distribution of injection fluid in a well zone, a method of ascertaining the injectivity profile with the aid of an activated slurry is used. A method of quality control of drill-hole cement completions which presents a picture of the distribution of cement over vertical and horizontal sections of the wells has been developed.

New methods for holding back the oil-water contact surface in the case of completed wells have recently been developed and put into practice. A new two-channel set of equipment for radioactive logging designed for deep-hole work has also been developed and introduced into field work.

A line of instruments to protect the safety of field personnel working with radioactive preparations has been developed for insertion into the well during checking of hydraulicking performance, cementing, and for locating thief zones; a special field laboratory-on-wheels has been developed.

At the Petrochemical Process Institute of the Academy of Sciences of the Azerbaidjan SSR, plans have been developed for studying the mechanism of transformation of hydrocarbons, the mechanism of the action of oil additives, and for elaborating isotope control techniques. Labeled-atom techniques have been used in a many-pronged attack on the problem of the catalytic cracking method for alkyl aromatic and paraffinic hydrocarbons usually encountered in crude petroleum. The reaction mechanisms of primary and secondary cracking reactions have been studied. The active role of the alkyl aromatic side chain in the formation of coke has been established. Data have been obtained which are of interest in making a correct choice of catalyst for cracking various types of crude.

The labeled-atom tracer technique was applied to the study of the performance of oil additives AzNII-7 and TsIATIM-339. A new instrument was designed to study the qualities and properties of oil additives, and their performance mechanisms; the instrument may be used either with or without labeled atoms. A comparative estimate of the properties of additives AzNII-7 and TsIATIM-339 has been made. The kinetics of film formation, solubility and stability of additives, anticorrosive properties, conditions of formation of a protective film, the degree of participation of the individual components of the additive in the formation of a film layer, are among the topics investigated.

Moreover, the Institute has elaborated a technique of accurate and rapid determination of water content in oil, and a method of exactly estimating the rate of circulation of alum-silica catalyst in the catalytic cracking process using a catalyst pellet labeled with Co^{60}.

Facilities for studying saturation vapor pressures have been built in the isotopes laboratory of the Physics Institute of the Academy of Sciences of the Azerbaidjan SSR. These facilities are highly accurate in the measurement of vapor pressure, and use radioactive isotopes. The laboratory has carried out measurements of the vapor pressure at saturation of selenides, thallium sulfate, and selenium vapors. It has been found that Tl_2Se_3 decomposes upon vaporization from the solid phase, and is converted to Tl_2Se. Experiments were conducted with the proper isotope to investigate the behavior of several impurities in the vacuum distillation of selenium. It was found that mercury impurities present in the vacuum distillation of selenium volatilize simultaneously with the selenium. The isotope Se^{75} was used to study the effect of bismuth impurities on self-diffusion in selenium. The finding was that the activation energy of self-diffusion is dependent on the content of bismuth impurity.

At the Institute of Soil Science and Agrochemistry of the Academy of Sciences of the Azerbaidjan SSR, experiments were conducted with radioactive phosphorus to study P^{32} uptake in the cotton plant and its effect on the yield of raw cotton both under field conditions and greenhouse conditions (1958-1959). On the basis of these investigations, conclusions were drawn that manuring of the soil with superphosphate fertilizer (dosage of 2.5 and 5 millicuries per square meter) was accompanied by accumulation of the greatest quantity of P^{32} in the leaves, with the least propensity to accumulation shown in the stalks and roots of the plant (the cotton yield increased 10-14%); and that when the plants are sprayed with a radioactive phosphorus solution during the budding stage, flowering stage, and cotton boll formation stage (three times in all), the yield is increased by 9-18%.

In the Plant Physiology department of the Institute of Botany of the Academy of Sciences of the Azerbaidjan SSR, the tracer method was used to study the effect of microfertilizers on the rate of photosynthesis and the outflow of assimilates, as well as on the distribution and translocation of radiophosphorus in the white mulberry.

In addition to these research efforts, the tracer isotope method has been applied to the study of the effect of water supply irrigation and vegetation irrigation on the rate of photosynthesis in the mulberry, honey locust, eldar pine, and the olive tree. These investigations showed that the rate of photosynthesis is measurably favored in these species, along with increased outflow of assimilates, by optimized dosages of copper, zinc, and cobalt. Excess cobalt dressing will have an adverse effect on the efficiency of photosynthesis, if performed during the vegetation period since this will have a toxic effect on the plants. The build-up, translocation, and distribution of radiophosphorus show improvement in response to optimized dosage with these trace elements. Under drought conditions, water supply irrigation techniques increase productivity in various species of trees by improving the rate of photosynthesis.

At the Institute of Genetics and Selective Breeding of the Academy of Sciences of the Azerbaidjan SSR, research has been pursued on a study of the effect of radioactive radiations on the variability of several strains of agricultural plants raised in Azerbaidjan. The acceptable range of critical doses for various crops were arrived at. Application of large doses (30,000-40,000 r) brought about pronounced changes in the external features of several varieties of cotton and wheat plants. These changes were accompanied, in some cases, by chromosomal rearrangements in the first mitoses of the rootlets.

In the physiology department of the Academy of Sciences of the Azerbaidjani SSR, the effect of phosphorus isotope on the nature and spread pattern of aseptic inflammation was investigated. A radioactive phosphorus isotope (P^{32}) introduced 20 hours before and 2 hours following the onset of a burn trauma showed a considerable effectiveness in modifying the spreading pattern of the inflammatory process. It was shown that the magnitude and character of interoceptive exchange reflexes are appreciably altered by x-ray treatment. While no appreciable shifts take place in the blood (at the sugar level) in irradiated animals, significant modifications were detected in the character of the interoceptive exchange reflexes. This is of much practical importance.

During the Conference, an exhibit demonstrating the latest radioactive logging equipment was open to the attending public.

DECONTAMINATING ENCLOSURE

G. N. Lokhanin and V. I. Sinitsyn

The widespread use of radioactive materials in the various branches of the national economy, science, and medicine, has posed the task of developing special shielding equipment and appurtenances.

In working with radioactive materials, contamination of equipment, of various types of laboratory ware, instruments, and other objects occurs, and decontamination is a task which is not always possible under ordinary conditions.

In order to create the conditions for cleaning laboratory ware from radioactive contaminations, special washing hoods had to be developed and fabricated. The ShM washing and decontaminating enclosure is now being manufactured to service Soviet industry.

The hood is designed to facilitate washing laboratory ware, instruments, and other equipment contaminated by α-, β-, and γ-active materials.

The hood (Fig. 1, 2) consists of three separate glove boxes interconnected by coupling flanges. The length of the enclosure is 3580 mm, width 825 mm, height 2320 mm, weight (of the whole assembly) 860 kg. The internal volume of each box is 0.4 m^3.

Each box is a gastight frameless enclosure resting on a supporting base. The boxes are fitted with viewing windows, removable fluorescent lamps, rubber gloves, ventilation ducts (intake and exhaust filters, gate valves), a liquid waste drain, liquid waste receptacle, hot and cold water taps, water pressure gages, etc.

Transfer compartments are built on the left and right hand sides of the glove-box line to facilitate placing and removal of laboratory ware and instruments. The transfer chamber is provided with two access doors (an inner and an outer one). The glove boxes are washed down and deactivated by spraying showers installed in each box. The first box is also provided with leads for bringing special deactivating reagents (acids, lyes, etc.) into play, while the second box has a cold water tap for rinsing laboratory ware.

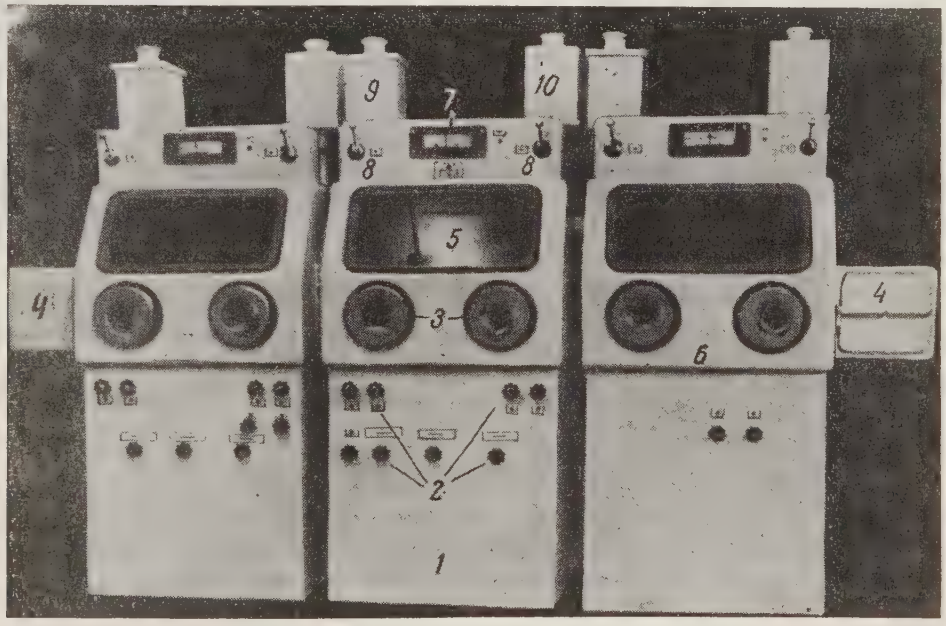

Fig. 1. Decontaminating and washing enclosure, stainless steel fabrication (operator's view): 1) base; 2) hot and cold water and gas valves, etc.; 3) rubber gloves; 4) transfer chambers; 5) viewing windows; 6) body of enclosure; 7) water pressure gauge; 8) gate valves; 9) exhaust filters; 10) intake filters.

All of the ducting is controlled by valves with the valve controls accessible in the front panel. The valve panels are properly labeled to show the function of each valve. The piping arrangement is designed to facilitate unencumbered drainage of the solutions.

A rectangular viewing aperture is built into the enclosure for observation of the insides of each enclosure. One pair of special rubber gloves is installed in the front of each enclosure.

Three baths each (two round and one rectangular) are placed in the first and second enclosures for washing laboratory ware and instruments. The round bath has a capacity of 8 liters, 244 mm diameter, height 190 mm. The rectangular bath has a capacity of 12 liters, height 190 mm, length 390 mm, width 190 mm. Each bath is provided with a small metal basket to hold laboratory ware and instruments during washing. Electric heating is used on the rectangular bath and one of the round baths.

Washing of laboratory ware, instruments, and other objects is attended to in the baths of the first enclosure, using deactivating solutions. After washing, the laboratory ware and instruments are passed through the passage

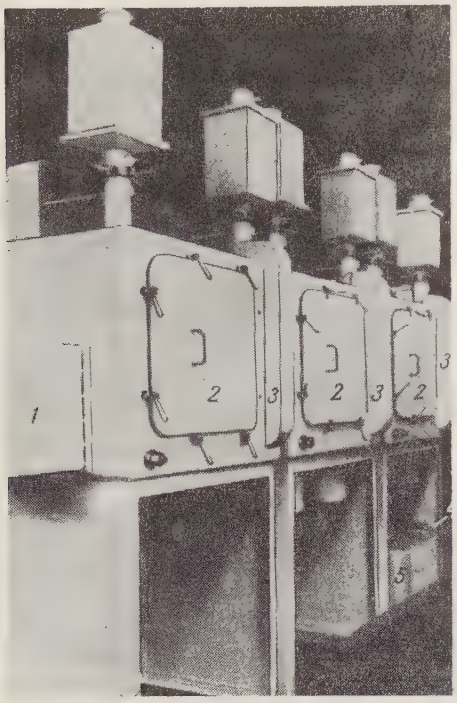

Fig. 2. Stainless steel decontaminating and washing enclosure (view from maintenance access side): 1) transfer compartment; 2) door for placing and removal of equipment and instruments, and for access to inside of glove box; 3) air ducts; 4) rubber hose connecting drain with liquid wastes receptacle; 5) 10KZhO liquid wastes collector, 10 liter capacity.

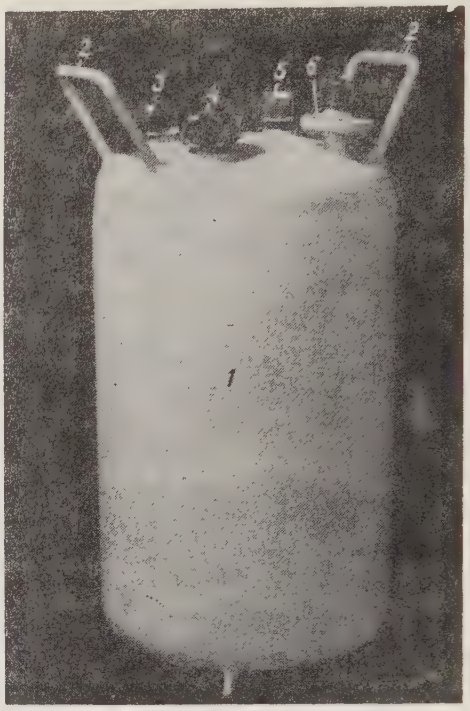

Fig. 3. 10KZhO liquid wastes receptacle: 1) welded gas-tight cylindrical tank; 2) grasping handles; 3) discharge connection; 4) filling and blowdown connection; 5) connection for annunciator device; 6) filter.

from the first enclosure into the second, where the objects are rinsed in water baths. On leaving the second enclosure, the laboratory ware is admitted into the third enclosure, where it is dried off. The degree of radioactive contamination of the laboratory ware is checked with a "Tiss" dosimeter following the drying step. Clean laboratory ware leaves the third enclosure via the transfer chamber at the end of the enclosure line.

To provide removal of contaminated air, the enclosure assembly is outfitted with intake and exhaust ventilation facilities (25 volumes of enclosed air are removed every hour). A rarefaction of 20 mm H_2O is maintained inside each separate glove box; the performance of the ventilation system may be monitored by consulting a TIM-890 water pressure gauge with a 0 ± 125 mm H_2O reading scale. The gate valves are adjusted to control the rarefaction within each glove box separately. Air removed from the glove-box line is subjected to decontamination in a two-stage exhaust filter system prior to being discharged to the stacks; clean air is admitted to the chambers through an intake filter.

The intake and exhaust filters are similarly designed and of similar size. The first and second stage of each filter are included in a common housing and are mounted on the top of each enclosure. The filter system presents a surface of 0.11 m^2. The first filter stage is filled with fiberglass to a layer thickness of 100 mm. The first and second filter stages are equal in cross section. The second filter stage is filled with the high-efficiency FPP filter fabric.

Depending on the extent to which the filters are contaminated, which may be established with a dosimeter, the filters must be replaced at some point. An air duct is positioned on the rear of each enclosure to facilitate removal of contaminated air.

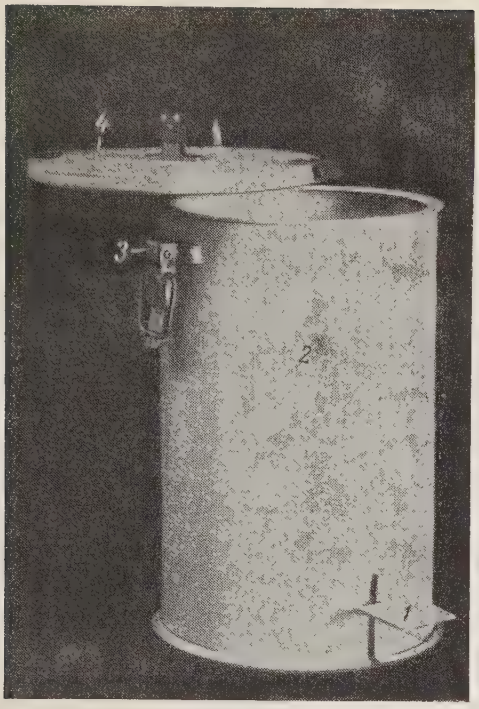

Fig. 4. KTO solid wastes container: 1) foot pedal for raising and lowering container lid; 2) welded cylindrical receptacle body; 3) clamps for leak-tight sealing of lid (hold-down clamps); 4) lid.

Maintenance access doors 600 x 500 mm are present in the rear of each glove box, to facilitate maintenance work and for placing of some types of material to be cleansed.

The removal of the li uid wastes formed furing the washing operation takes place through the drainage system linkec up to each chamber, or directly into the 10-liter-capacity 10KZhO liquid wastes receptable (Fig. 3). Th receptable measures 206 mm in diameter, stands 415 mm high, and weighs 8 kg ; the filter is made from FPP fabric.

A 10-liter-capacity KTO solids wastes receptable is provided for the accumulation of solids (Fig. 4) such as broken laboratory ware, inaccurate instruments, rags, etc. A ten-liter receptable mounted on a 2T dolly may also be used to hold radioactive waste solids.

NEW LEAK-TIGHT GLOVE BOXES FOR HANDLING ALPHA- AND BETA-EMITTING MATERIALS

G. N. Lokhanin and V. I. Sinitsyn

The use of radioactive materials in the various branches of science and the national economy has necessitated research and development work on special-purpose shielding equipment and accessories.

The 1KNZh model glove box, designed for a single operator, has been developed by Soviet industry and is being put on a mass fabrication basis, to service handling of alpha- and beta-active materials (Fig. 1, 2). The box is built for work at high temperature and humidity levels in a corrosive alkaline or acid environment. The box provides adequate shielding of nearby workers from alphas and betas, and prevents contamination of the air in surrounding rooms by aerosols and gases or radioactive and toxic materials.

The dimensions of this glove box model are: height 2320 mm, length with one transfer chamber 1270 mm, width 875 mm. All leads coupled into the glove box enclosure are sealed (with acid-resistant soft rubber packing) and held fast with adhesive. The frameless body of the glove box is welded with stainless steel up to 3 mm thick; the glove-box tables are also welded stainless, to 10 mm thickness. The outer surface of the box is given a prime coating after cleaning from grime and scale, and is then finished with a cream-colored acid-proof enamel. The inner surface of the box frame has a smooth streamlined surface. The leak-tight volume of the box comprises 0.4 m^3. The support base (see Fig. 1) for the 1KNZh box is welded carbon steel.

The 1KNZh glove box is made with either one or two transfer chambers. The function of the transfer chambers is to allow insertion of radioactive materials, withdrawal of finished products, and introduction of clean equipment and other accessories and instruments required inside the box for work. Transfer compartments come with two ports. The outer port (see Fig. 2) is for introducing radioactive materials, laboratory ware, instruments, etc., from the operator's side or the maintenance zone into the transfer chamber. The inner port serves for admitting radioactive materials and other objects inside the box proper. The inner port has a sector which opens up simultaneously with the port. Three-lamp fluorescent fixtures, SDS-45 at 45 watts power, are installed at the top of the box for illumination.

A rectangular viewing window is built into the front of the glove box to facilitate observation of the work (Fig. 1).

A special ventilation arrangement is provided in all rooms where radioactive materials are handled in the open, to protect the air environment of occupied rooms and the atmosphere from contamination by radioactive aerosols.

Radioactive aerosols and other harmful substances and fumes are removed by means of a system of ventilating air ducts (Fig. 2). The air removed from the glove boxes is cleaned prior to venting by passing through a two-stage exhaust filter system. Air entering the glove box passes through a two-stage intake filter.

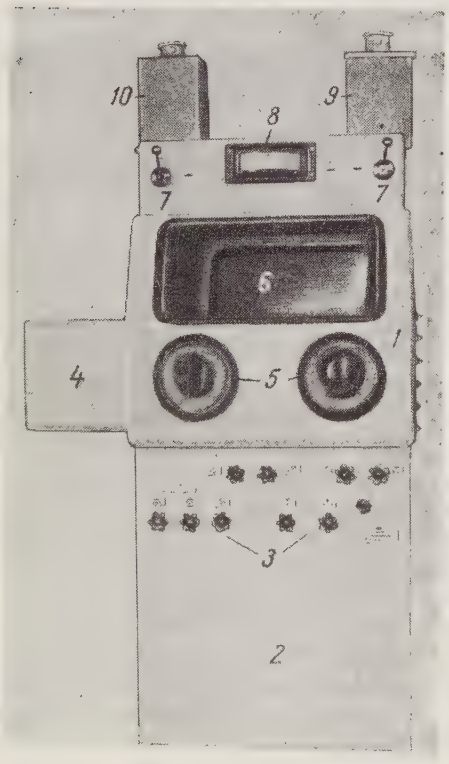

Fig. 1. The 1KNZh glove box (operator's view): 1) glove box frame; 2) support; 3) hot and cold water and gas valves, etc.; 4) transfer compartment; 5) rubber gloves; 6) viewing window; 7) gate valve; 8) water pressure gauge; 9) intake filter; 10) exhaust filter.

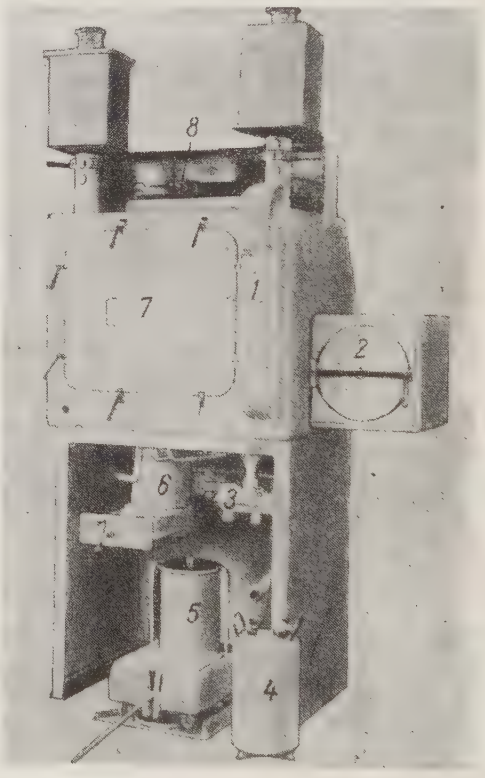

Fig. 2. The 1KNZh glove box (view from maintenance access side): 1) air duct; 2) transfer-chamber port; 3) liquid wastes drain; 4) liquid wastes receptacle; 5) dolly with solid wastes receptacle; 6) solid wastes receptacle; 7) access door to box interior for placing and removing equipment, materials, and instruments, and for maintenance and other work inside the box proper; 8) luminaire.

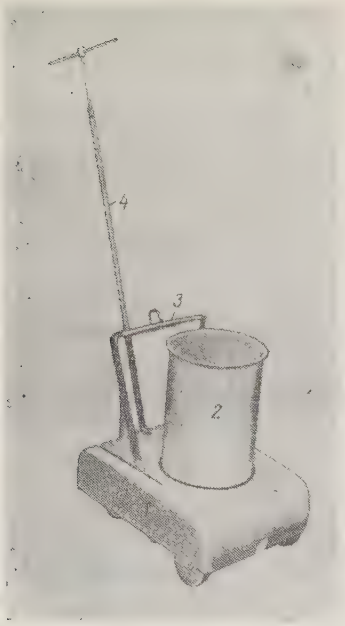

Fig. 3. Solids receptacle on a 2T dolly: 1) dolly; 2) ten-liter-capacity solids container; 3) lid; 4) meter-length steering handle.

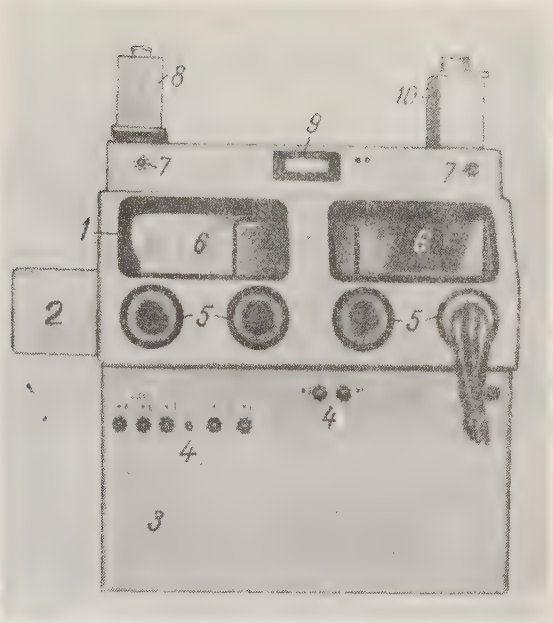

Fig. 4. Two-place stainless steel welded 2KNZh glove box (operator's view): 1) glove-box frame; 2) transfer compartment; 3) base; 4) hot and cold water and gas valves, etc.; 5) rubber gloves; 6) viewing window; 7) gate valve; 8) exhaust filter; 9) water pressure gauge; 10) intake filter.

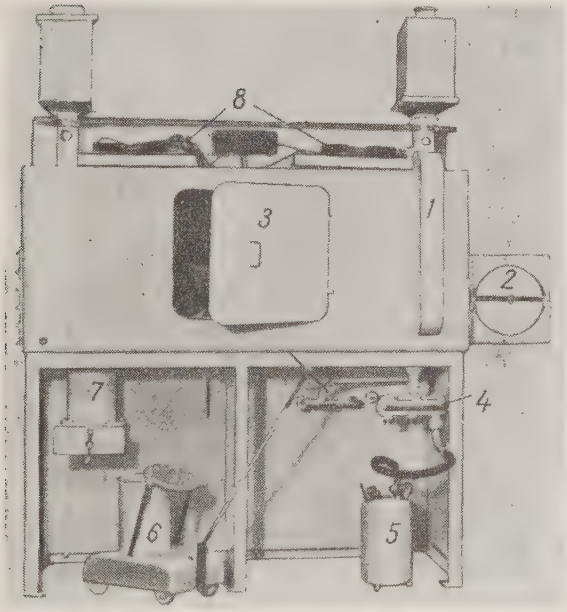

Fig. 5. Two-place stainless steel 2KNZh glove box, seen from behind (maintenance zone view): 1) air duct; 2) transfer compartment vacuum door; 3) access hole to interior of box, for placing and removing equipment and instruments, and also for maintenance and other work in the interior of the box; 4) liquid wastes drain; 5) liquid wastes receptacle; 6) solid wastes dolly; 7) solid wastes receptacle; 8) luminaires.

A rarefaction not less than 20 mm H_2O is maintained inside the glove box while work is in progress.

The intake and exhaust filter systems are similar in dimensions and design. The first and second stage of each filter are mounted integrally on the glove box enclosure frame, at the top of the unit. When a dosimetry check indicates that the filters have reached a certain degree of contamination, they are replaced. The spent filter is discarded in a special waste receptable. Throttle valves controlled from the front panel of the box straddle the intake and exhaust passages.

Radioactive waste solids may form in the course of working with radioactive substances inside the glove box; viz. rags, filter paper, damaged glassware, metal objects, etc. A waste receptable (see Fig. 2) containing a plastic pouch insert is placed beneath the box table level for radioactive solids. This pouch is held by a special device to the discard aperture of the glove-box table, and receives radioactive solid wastes through that hole. The discard aperture is fitted with a lid to seal it hermetically, the lid being opened only inside the box. A pouch completely filled with solids is tied tight inside the box and is later lowered into a valved metal receptacle fastened to the glove-box table. The lid is closed after the pouch is discarded, the

receptacle control valve is opened and the filled pouch is dropped into the solids receptacle resting on the dolly beneath the glove-box table. This procedure for removing radioactive wastes from the box interior eliminates any hazard of hot spills in the area occupied by personnel.

The ten-liter-capacity wastes receptacle (Fig. 3) is designed for temporary storage and hauling of alpha-, beta-, and gamma-active waste solids. The receptacle is carted off on a dolly steerable with a meter-length handle, and constitutes a cylindrical tank with carbon steel lid.

Drainage piping underneath the box table level receives liquid discard, which may also be funneled into the liquid wastes receptacle.

A ten-liter-capacity 10KZhO receptacle (see Fig. 3 in the preceding article) is designed for storage and carrying of liquid alpha-, beta-, and gamma-active wastes. The receptacle is a welded leak-tight vessel made of stainless steel. An air filter and three pipe connections are contained in the receptacle lid. The air filter is a connection sleeve with FPP filter fabric. The connection sleeve is capped by a plug, which is removed when the receptacle is full. The waste receptacle may be moved either by means of the dolly or manually, using the grip handles.

A two-place 2KNZh glove box, similar in design to the 1KNZh, has been developed and is now being manufactured, with a box interior volume of 0.8 m^3, air exchange volume of 25 box volumes per hour, exhaust filter area of 0.25 m^2 and intake filter area of 0.25 m^2 (see Fig. 4, 5).

This two-place glove box is equipped with waste receptacles, two pairs of special rubber gloves, and other accessories. A maintenance access door 600 x 500 mm is built into the rear wall of the box. The entire glove box unit with accessories in place weighs 600 kg.

The 1KNZh and 2KNZh glove boxes are supplemented by viewing windows, rubber gloves, filter systems, fluorescent lighting, plastic waste transfer pouches, ball-joint manipulator (optional), 10KZhO liquid waste receptacles, solid waste containers, rating plate, and instructions for maintenance and operation.

BRIEF COMMUNICATIONS

USSR. A scientific colloquium on heat stress in rods, plates, and shells used in turbomachinery design was held at the Kiev House of Scientists, during June, 1960. The conference was organized by the permanent Commission on Turbomachinery of the State Science and Engineering Committee of the Ukrainian SSR jointly with the Academy of Sciences of the Ukrainian SSR, the Commission on the Strength of Gas Turbines of the Academy of Sciences of the Ukrainian SSR, and was chaired by the Director of the Institute of the Institute of Mechanics of the Academy of Sciences of the Ukrainian SSR, A. D. Kovalenko, a Corresponding Member of that body.

A paper presented by V. I. Danilovskii (Institute of Mechanics of the Academy of Sciences of the USSR) was devoted to applications of the theory of a complex variable in determining temperature fields and thermal stresses in two connected plane regions. A report by S. Ya. Yarema (Institute of Machine Design and Automation of the Academy of Sciences of the Ukrainian SSR) dealt with an investigation of the fundamental solution of the temperature problem for cylindrical shells, based on the familiar solution for a shell subjected to lumped forces. In his report, R. A. Adadurov (Central Aerohydrodynamics Institute, Moscow) discussed flexural and torsional modes of loss of stability of unevenly heated thin, long strips. Lowering of the torsional rigidity of a plate in response to uneven heating was pointed out. A. G. Kostyuk (Moscow Power Engineering Institute) dealt in his report with a method for determining the temperature field and thermal stresses in a gas turbine wheel by replacing the real wheel with a model convention.

A paper submitted by V. I. Savchenko (Kiev University) was based on the use of polarization optical techniques applied to the determination of thermal stresses in planar models with convective heat transfer over

the lateral surfaces by way of a predetermined temperature dependence of the variation of optical and elastic constants of the material comprising the model. D. A. Gokhfel'd (Chelyabinsk Polytechnical Institute) discussed the adaptability of designs to iterated thermal effects. Up to a certain temperature, the adaptability temperature, plastic deformation is caused solely by the first thermal stress cycle and, at the maximum temperature of a cycle which is higher than the adaptability point, plastic flow is caused by each thermal cycle. Calculations take into account yield limit as a function of temperature.

A report delivered by Ya. S. Podstrigach (Institute of Machine Design and Automation of the Academy of Sciences of the Ukrainian SSR) was devoted to a determination of a steady-state temperature field in bounded plates and shells. In a paper by A. D. Kovalenko, the problem of thermoelastic stresses in sloping shells of revolution was discussed, with variability of shell thickness and elastic modulus taken into account.

S. V. Fol'kovskii adduced a solution of the problem of temperature fields and thermoelastic stresses in steam piping A. F. Pronkin suggested a method for calculating the strength of contoured turbine wheels in terms of a limiting state.

In her report, E. D. Pletnikovaya (Central Aerohydrodynamics Institute, Moscow) discussed the problem of steady-state temperature fields in a system of rods converging to a single point, with convective heat transfer over the lateral surfaces.

The conference took note of the need to develop experimental techniques for determining temperature fields and thermal stresses to match performance data, the problem of evolving efficient methods for calculating thermal stresses in elastic and plastic regions affected by the dynamics of a process.

Yugoslavia. An agreement was signed with Indonesia for collaboration in the cause of the peaceful uses of atomic energy. The accord envisages in particular, collaborative efforts in the field of theoretical research, geology, the technology of winning and processing nuclear raw materials, and the study of problems related to the production of nuclear power and shielding against nuclear radiations. Collaboration between the two countries will be developed by an exchange of specialists, documentation, and equipment.

BIBLIOGRAPHY

NEW LITERATURE

Books and Symposia

B. V. Petukhin. Heat Power Engineering in Nuclear Facilities. Moscow, Atomizdat, 1960, 323 pages, 8 rubles, 80 kopeks.

The book outlines available information on nuclear reactors; presents the basic data on design and calculations of nuclear facilities working on steam and gas turbine power cycles; discusses the characteristics of commonly used reactor coolants; describes in detail the flow schemes of the most typical nuclear electric power stations now operating or in construction; cites data needed for the calculation and design of heat exchange equipment and steam raising units for nuclear electric power stations.

The book may be used as a text for students in physics and power engineering departments, and may also prove useful for scientific workers, engineers, and graduate students interested in problems of nuclear power and the design of heat exchange equipment.

G. E. Kaplan, T. A. Uspenskaya, Yu. I. Zarembo, and I. V. Chirkov. Thorium: its Raw Material Resources, Chemistry, and Technology. Moscow, Atomzidat, 1960, 226 pages, 8 rubles, 60 kopeks.

This book presents data on thorium which have appeared in the Soviet or foreign literature during the past 15-20 years. The basic information on the geochemistry and mineralogy of thorium is given, and light is shed on the present state of the raw materials base of thorium abroad. The physicochemical, corrosive, and radioactive properties of thorium, its fields of applications, the processes used in producing thorium metal (both technical-grade and high-purity thorium) are offered, as well as the basic thorium compounds and alloys. Concise information is presented on the analytical chemistry of thorium. The book is well illustrated. Each chapter ends with a pertinent literature reference list.

The book is written for scientific and engineering workers and technicians; it may also be useful to students in chemical and metallurgical advanced vocational schools.

A. M. Rozen. Theory of Isotope Separation in Columns. Moscow, Atomizdat, 1960, 438 pages, 16 rubles, 50 kopeks.

The first section of the book (chapters 1 to 6) deals with the peculiarities of individual methods of countercurrent separation: distillation, isotope exchange, thermodiffusion, mass diffusion, and centrifugation. The second section (chapters 7 to 10) describes the general methods for designing columns and cascades. The theory and methods of column technology are developed. The general theory of separation is applied to the optimization of fundamental column parameters. Attention is focused on optimization of separation conditions using two-phase methods, when a fraction of the losses are proportional not to the work of separation, but to the process stream.

Chapter 11 singles out some comparatively simple formulas for calculating the rate of approximation to equilibrium in various types of columns.

Chapter 12 contains examples of the design of separation facilities and, to a certain extent, compares different techniques of heavy water production and other isotope processes.

The book is written for scientific workers, chemical engineers, and students interested in problems of separation of mixtures, and may also be found useful in designing separation facilities.

A. V. Lebedinskii and Z. N. Nakhil'nitskaya. The Effect of Ionizing Radiations on the Nervous System. Moscow, Atomizdat, 1960, 187 pages, 7 rubles, 60 kopeks.

Material from Soviet and foreign literature on the effect of ionizing radiations on analyzers and on the nervous system. Particular attention is focused on the work of Soviet researchers. On the basis of a generalization of data culled from the literature and their own data, the authors develop a concept of the mechanism involved in the disturbance of functions of the nervous system in response to exposure to ionizing radiations.

The book is written for a broad readership of scientific workers in the field of radiobiology, biophysics, physiology, pathophysiology, and also for practicing physicians.

V. A. Sokolov. The Radiosulfur Isotope S^{35}. Moscow, Atomizdat, 1960, 16 pages, 60 kopeks.

This brochure presents the basic information required on the radioactive sulfur isotope S^{35}. Methods for producing the isotope are described, as well as the properties and field of applications of the isotope; some data are offered on the chemistry and technology of S^{35}-tagged compounds, as well as information on safety techniques.

The book is written for a broad audience.

Articles from the Periodical Literature

I. NUCLEAR POWER PHYSICS

Neutron and reactor physics. Physics of hot plasmas and controlled fusion.
Physics of the acceleration of charged particles.

Zhur. éksptl. i teoret. fiz. 38, 6 (1960)

V. N. Nefedov, pp. 1657-1662. On the mechanism of emission of prompt fission neutrons.

S. E. Grebenshchikov and M. D. Raizer, pp. 1665-1667. The skin effect and shock waves in an inductive gas discharge.

K. A. Petrzhak et al., pp. 1723-1728. Spread of ranges and kinetic energy of fission fragments of U^{233}.

A. B. Kitsenko and K. N. Stepanov, pp. 1840-1846. On the instability of a plasma with an anisotropic distribution of ion and electron velocities.

Pribory i tekhnika éksper. No. 3 (1960)

Yu. G. Abov and D. F. Litvin, pp. 3-15. Experimental neutron diffraction methods (survey article).

N. P. Glazkov, pp. 16-19. Cylindrical fast-neutron spectroscopy camera.

J. Appl. Phys. 31, 6 (1960)

P. Auer and H. Hurwitz, pp. 1007-1009. Space charge neutralization by positive ions in diodes.

Nucleonics 18, 7 (1960)

G. Johnson, pp. 49-53. Status and promise of peaceful nuclear explosions.

D. Hughes, pp. 54-58. Neutron spectroscopy with nuclear explosions.

Nukleonik 2, 4 (1960)

K. Beckurts, pp. 129-131. A simple time-amplitude converter for slow neutron time-of-flight experiments.

A. Kraut, pp. 149-174. Results of physical research on fission of nuclei.

Nukleonika V, 4 (1960)

T. Rzeszot, pp. 191-194. Measurement of the angular distribution of neutrons scattered from a reactor experimental channel.

Progr. Theor. Phys. 23, 3 (1960)

Y. Ichikawa, pp. 512-518. Bremsstrahlung in a high-temperature plasma.

Reactor Science 12, 1-2 (1960)

D. Stupegia, pp. 16-20. Thermal neutron cross sections for the Cs^{137} (n, γ) Cs^{138} reaction.

R. Tattersall et al., pp. 32-46. Measurement of resonance absorption integrals using pile oscillators.

II. NUCLEAR POWER ENGINEERING

Nuclear reactor theory and calculations. Reactor design.
Performance of nuclear reactors and nuclear power stations.

Morskoi flot 7 (1960)

I. Bykhovskii, pp. 15-16. On nuclear-propulsion merchant ships.

Atompraxis 6, 6 (1960)

— — — pp. 231-238. The Hannover industrial fair.

Atomwirtschaft V, 6 (1960)

F. Hoffman et al., pp. 250-253. The U. S. HTGR high-temperature reactor project.

R. Nass, pp. 257-264. Materials and welding operations in reactor design.

— — — pp. 273-276. Nuclear technology at the Hannover fair.

D. Weissbarth, pp. 276-281. On the uses of various research reactors.

Energia Nucl. 7, 6 (1960)

G. Calabria, pp. 385-396. The Latina nuclear electric power station.

L. Biondi, pp. 397-406. On the further development of organic-moderated reactor designs.

A. Cicchitti et al., pp. 407-425. Experimental investigations of cooling with a two-phase fluid coolant. Measurements of pressure drop, heat transfer, and burn-out heat loads.

F. Faldini et al., pp. 426-434. Study of the dynamics of a nuclear power plant steam generator, by analog simulation.

Energia Nucl. 7, 7 (1960)

S. Battaglia and U. Cassinary, pp. 457-462. Applications for organic fluids in nuclear reactors.

G. Casini et al., pp. 488-495. Nuclear composition of natural uranium fuel after prolonged irradiation in a thermal reactor.

Kernenergie 3, 5 (1960)

W. Mai, pp. 407-413. Calculations of temperature field and thermal stresses in a pressurized-water reactor vessel.

Kerntechnik II, 6 (1960)

O. Werner, pp. 192-200. New trends in fuel element development.

K. Kimbel, pp. 208-211. Report on the seventh conference on hot laboratories and associated equipment (Cleveland).

G. Rõbert, pp. 211-212. The French nuclear industry represented at the Hannover fair.

Nucl. Energy No. 146 (1960)

– – – – pp. 305-307. The Windscale AGR reactor, as the prototype for a new type of nuclear power stations.

C. Whelhel and C. Robbins, pp. 321-322. The use of rarefactions in the containment shells of nuclear power reactors.

Nucl. Power 6, 51 (1960)

R. Campbell, pp. 68-72. Power reactor control. 1.

– – – – pp. 73-75. Economic problems in atomic energy.

F. Theunissen, pp. 76-79. Economical uses of conventional and nuclear fuels.

D. Iggulden, pp. 84-87. Design of gas-cooled reactors.

P. Garay, pp. 96-99. Use of hydrogen for reactor cooling.

– – – – p. 101. Fuel elements for the DRAGON reactor.

Nucl. Power 5, 52 (1960)

– – – – – p. 66. The Dungeness nuclear power station.

J. Collier and P. Lacey, pp. 68-73. Two-phase liquid coolant for nuclear reactors.

R. Campbell, pp. 74-77. Control of power reactors. 2.

J. Burkett, pp. 78-82. Nuclear-powered merchant ships.

G. Deleuze and G. Petillat, pp. 98-99. Decladding fuel elements at Marcoule.

G. Wallis, pp. 99-101. Gas-fluid model for bulk boiling.

Nucleonics 18, 7 (1960)

R. Lightle, p. 59. Criticality of MTR-type fuel elements.

W. Brown and C. Bergmann, pp. 60-63. Reducing radioactivity buildup in pressurized-water reactors.

D. Bradley, pp. 84-88. Hydrogen as a power reactor coolant.

W. Lewis and R. Goin, p. 91 and p. 93. Safer packages for shipping fuel.

Nukleonik 2, 4, (1960)

M. Kũchle, pp. 131-139. Measurement of the temperature dependence of neutron diffusion length in water and diphenyl, by the pulsed method.

M. Brose and K. Beckurts, pp. 139-141. Measurements of neutron absorption cross section in aluminum.

G. Blãsser, pp. 141-144. Slowing down of neutrons in a heterogeneous system.

T. Springer, pp. 144-149. Spatial dependence of neutron temperature in a moderator.

Nukleonika V, 3 (1960)

A. Kostyrko, pp. 133-142. Studies of radiolytic decomposition of water in the primary coolant of the Polish EVA reactor (WWR-S).

Reactor Science 12, 1-2 (1960)

A. Takahashi, pp. 1-15. Probability of the "first impact" in periodic systems.

M. Angelopoulos, pp. 21-25. Calculation of attenuation of neutron flux in thin absorbing rods.

H. Takahashi, pp. 26-31. Probability of resonance escape in annular fuel elements.

III. NUCLEAR FUEL AND MATERIALS

Nuclear geology and primary ore technology.
Nuclear metallurgy and secondary ore technology.
Chemistry of nuclear materials.

Radiokhimiya II, 3 (1960)

V. I. Grebenshchikova and R. V. Bryzgalova, pp. 265-273. Study of coprecipitation of Pu(IV) with lanthanum oxalate.

É. I. Moiseenko and A. M. Rozen, pp. 274-280. Distribution of plutonium in extraction with tri-n-butyl phosphate.

V. B. Shevchenko et al., pp. 281-290. On the effect of hydrocarbons of the aliphatic and aromatic series on extraction of U(IV), Pu(IV), Zr(IV), and Ce(III) from nitrate solutions, using tri-n-butyl phosphate.

V. M. Vdovenko and E. A. Smirnova, pp. 291-295. On the hydration of uranyl nitrate in organic solvents in extraction from salt solutions.

V. M. Vdovenko et al., pp. 296-300. Infrared spectra of organic solutions of uranyl nitrate hydrates in the region of bending vibration frequencies of water.

V. M. Vdovenko et al., pp. 301-306. Spectrophotometric investigation of the formation of nitrato complexes of plutonyl compounds in acetone.

V. M. Vdovenko et al., pp. 307-311. Spectrophotometric investigation of the formation of nitrato complexes of plutonyl compounds in aqueous solutions, and extraction of Pu(IV) with dibutyl ether.

V. M. Vdovenko et al., pp. 312-314. On the formation of a complex trinitrate neptunyl compound.

P. I. Kondratov and A. D. Gel'man, pp. 315-319. Oxalate compounds of tetravalent neptunium.

V. D. Nikol'skii et al., pp. 320-329. Properties of plutonyl nitrate solutions. III. Stability of plutonyl in nitrate solutions.

V. P. Nikol'skii et al., pp. 330-338. On the existence of a monoacetate uranyl complex in solution.

A. A. Zaitsev et al., pp. 339-347. Disproportionation of americium (V).

A. A. Zaitsev et al., pp. 348-350. Kinetics of the reduction of americium (V) with hydrogen peroxide.

I. A. Lebedev et al., pp. 351-356. Study of complexing of Am^{+++} with oxalate ions.

V. I. Kuznetsov and T. G. Akimova, pp. 357-363. Organic coprecipitants. XIII. Coprecipitation of tetravalent plutonium.

V. N. Bobrova, pp. 364-368. Determination of solubility of double sulfates of zirconium and plutonium in saturated potassium sulfate solutions, using radioactive tracers.

T. A. Slepyan and S. M. Karpacheva, pp. 369-376. Physicochemical properties of nitrate solutions of uranyl nitrate, and determination of the properties of those solutions (specific weight, electric conductivity, refractive index).

L. E. Drabkina, pp. 377-378. Determination of the solubility of ammonium plutonyl carbonate in various aqueous solutions.

Atomwirtschaft V, 6 (1960)

H. Krauch, pp. 265-268. Radiochemistry from the engineering and economics points of view.

Energia Nucl. 7, 7 (1960)

L. Damiani et al., pp. 463-469. A pulsed column for liquid-liquid extraction. II. Column design.

G. Imarisio, pp. 470-476. Preparation of a UO_2 sinter.

E. Cerrai and C. Testa, pp. 477-487. Use of quercetine-hydrogen peroxide in the calorimetric determination of hafnium in zirconium.

J. Inorg. and Nucl. Chem. 13, 1-2 (1960)

L. Asprey and F. Kruse, pp. 32-35. Bivalent thulium. Thulium di-iodide.

N. Brett et al., pp. 44-53. Investigation of the uranium-thorium-carbon system.

J. Danon, pp. 112-118. Determination of the stability constants of thorium nitrate complex, using anion-exchange resins.

W. Brown et al., pp. 119-124. Extraction of the lanthanides using acetylacetone.

F. Habashi, pp. 125-137. Processes for recovering uranium from phosphoric acid.

D. Peppard et al., pp. 138-150. Extraction of thorium (IV) with diethers of orthophosphoric acid $(GO)_2PO(OH)$.

T. Siddall, pp. 151-155. Effect of various alkyl substituents in trialkylphosphates on extraction of actinides.

E. Hesford and H. McKay, pp. 156-164. Extraction of mineral acids with tri-n-butyl phosphate.

E. Hesford and H. McKay, pp. 165-173. Extraction of uranyl perchlorate with tri-n-butyl phosphate.

C. Hardy and D. Scargill, pp. 174-180. Extraction of niobium (V) from nitrate solution with tri-n-butyl phosphate.

J. Inorg. and Nucl. Chem. 13, 3-4 (1960)

R. Panzer and J. Suttle, pp. 244-247. A new uranium complex compound $5UCl_5 \cdot CCl_2 = CCl - COCl$.

D. Mathews et al., pp. 298-309. Investigation of transference and solvation phenomena. 1. Uranium chloroxide in water, ethanol, and water-alcohol mixtures.

J. Kooi et al., 310-312. Solubility of Cs_2UCl_6, Cs_2UOCl_4, and Cs_2PuCl_6 in hydrochloric acid.

G. Duyckaerts et al., 332-333. Extraction of lanthanides in the form of their di-n-butylorthophosphates.

Kernenergie 3, No. 5 (1960)

D. Naumann and R. Ross, 425-428. Anion exchange of cerium, thorium, and uranium in concentrated electrolytes.

R. Münze, 429-434. Removal of trace amounts of fluorine compounds by coprecipitation with barium sulfate.

Kernenergie 3, No. 6 (1960)

R. Münze, 518-521. A new method for continuous production of carrier-free I^{132} and Te^{132}.

Nucl. Energy No. 146 (1960)

---, 317 ff. Fluorine derivatives and atomic energy. II. Properties and fields of application of fluorine.

Nucleonics 18, No. 7 (1960)

R. Koch and G. Grandy, 76 ff. Xenon-krypton separation by gas chromatography.

Nukleonika V, No. 3 (1960)

J. Minczewski et al., 115-122. Some methods used in the separation and determination of uranium.

W. Korpak and Sz. Deptula, 123-132. Effect of chlorides and sulfates on solvent extraction (using TBP) of uranium and iron.

Nukleonika V, No. 4 (1960)

E. Herczyńska, 195-204. A mechanism effecting precipitation of anions and cations from aqueous solutions.

S. Siekerski and R. Gwóźdź, 205-217. Investigation of the TBP-$HClO_4$-H_2O system.

Z. Zagurski and W. Nej, 219-226. Novel arrangement used for direct investigation of systems in a gamma-radiation field, by physical-chemistry means.

VDI-Zeitschrift 102, No. 11 (1960)

K. Frank, 409-424. Reactor metals. Some metals used in reactor design: thorium, beryllium, zirconium, hafnium, lithium, and others.

IV. NUCLEAR RADIATION SHIELDING

Radiobiology and radiation hygiene. Shielding theory and techniques. Instrumentation

Biofizika 5, No. 3 (1960)

S. A. Valeva, 362-365. On effects of gammas and neutrons on seeds of agricultural plants.

Gigiena i sanitariya No. 5 (1960)

O. S. Andreeva, 77-82. Some data on the effects of exposure to uranium and uranium compounds in the human organism (review paper).

Gigiena truda i prof. zabolevaniya No. 6 (1960)

N. Yu. Tarasenko, 21-27. Note on thorium toxicity.

Izvestiya akad. nauk SSSR, seriya biol. No. 3 (1960)

A. M. Kuzin, 355-363. Modern problems in radiobiology.

Med. radiologiya 5, No. 4 (1960)

I. K. Sokolova, 68-72. Investigation of chloroform in aqueous solution as a possible dosimeter for x radiation and gamma radiation.

Med. radiologiya 5, No. 5 (1960)

V. V. Dmokhovskii, 78-84. Shielding calculations for a 25 Mev betatron.

Pribory i tekhnika éksperimenta No. 3 (1960)

Yu. V. Dukarevich and A. N. Dyumin, 48-50. Effective fast-neutron detector with little sensitivity to gamma rays.

M. Yu. Tissen, 51-53. Note on one possibility of achieving absolute measurements of the activity of C^{14}-labeled and S^{35}-labeled gases.

Teploénergetika 7, No. 7 (1960)

A. V. Surnov, 90-91. On calculations of the size of a gamma source by transmission of a pencil beam of gamma photons.

Atompraxis 6, No. 6 (1960)

W. Flichtbauer and W. Simonis, 217-219. Equipment for beta irradiation of suspended biological objects.

D. Sauerbeck, 221-225. C^{14} labeling of plants.

K. Scharrer and S. Heilenz, 226-227. A simplified technique for using cation exchange to determine strontium in plants.

E. Welte and U. Marckwordt, 228-229. Simplified method of Sr^{90} determinations in plants.

Energia Nucleare 7, No. 7 (1960)

R. Somigliana, 495-496. Determination of spurious counts in coincidence measurements.

Kernenergie 3, No. 5 (1960)

H. Abel and V. Bredel, 414-421. Preparation and study of neutron scintillators.

K. Oertel et al., 422-424. Dissociation of isopentane in Geiger-Müller counters.

Kerntechnik II, No. 6 (1960)

M. Pollermann, 185-191. Low-pressure ionization chamber filled with pure water vapor.

T. Nielsen, 201-202. A device for continuous monitoring of beta and gamma activity in air and gases.

T. Springer and M. Oberhofer, 203-205. Neutron shielding and gammas released in the shielding.

Nucl. Power 5, No. 51 (1960)

D. Taylor, 88-92. Dosimetric instrumentation. 4.

R. Brooks, 94-96. Personnel shielding problems in beryllium reactor applications.

Nucl. Power 5, No. 52 (1960)

W. Loosemore, 84-89. Ionization radiation detectors.

D. Taylor, 91-94. Dosimetric instrumentation. 5.

Nucleonics 18, 7 (1960)

J. Waugh and R. Nicholson, pp. 70-74. Transistor amplifier for fast proportional counting.

Nukleonika V, 3 (1960)

J. Domanus and B. Osuchowski, pp. 143-148. On the concept of the "Gram-equivalent of radium" for nonexact isotopic gamma sources.

A. Mafik and J. Malesa, pp. 149-155. Relative measurements of organic scintillators.

Nukleonika V, 4 (1960)

K. Mikke et al., pp. 181-189. ZnS (Ag) – paraffin type scintillators for detecting fast neutrons.

J. Domanus and L. Halski, pp. 227-238. Film dosimeter measures gamma radiation doses of radioactive isotopes.

V. RADIOACTIVE AND STABLE ISOTOPES

Labeled-atom techniques. Uses of radioactive radiations.
Direct conversion of nuclear energy to electrical energy.

Voprosy ekonomiki No. 5 (1960)

G. Mikheev, pp. 67-76. Economic advantages in the use of radioactive isotopes in industry.

Izvestiya akad. nauk SSSR. Otdel tekhn. nauk. Metallurgiya i toplivo No. 2 (1960)

S. P. Zaitseva et al., pp. 120-132. Applications of radioactive isotopes and nuclear radiations in research on the flotation process.

Izvestiya vyssh. ucheb. zaved. Tsvet. metallurgiya No. 3 (1960)

A. I. Levin and V. I. Falicheva, pp. 62-69. Studies of cathodic processes in electrodeposition of zinc, using tracer techniques.

Koks i khimiya No. 5 (1960)

A. Z. Kulishenko, pp. 17-19. Automation of the flotation shop at the Yasinovka coke and chemicals plant, using radioactive density gauges.

Konserv. i ovoshchesushil'n. prom. No. 7 (1960)

L. V. Metlitskii, pp. 19-22. Uses of nuclear radiations in the food processing industry and in agriculture.

Prom. stroitel'stvo No. 5 (1960)

V. A. Volokhov and Yu. D. Markov, pp. 47-50. Quality control of concrete placing operations, using tracer quality control techniques.

Atomwirtschaft V, 6 (1960).

L. Wiesner, pp. 253-256. Applications of nuclear physics techniques in oil prospecting and exploitation. II.

Nucl. Energy No. 146 (1960)

– – – – pp. 333-337. Radioactive isotope applications in railroad transportation in the USA.

Nucl. Power 5, 51 (1960).

B. Lindley, pp. 80-83. Direct conversion. 2.

Nucleonics 18, 7 (1960).

W. Mayer et al., pp. 64-68. Radioactive gauges for air-cooled turbine blades. Liquid-source gauge for hollow blades and vanes. Scanning beta gauge for cooling-channel walls.

C. Clayton, pp. 96-100. Precise tracer measurements of liquid and gas flows.